Identification of sub-clinical biomarkers that predict the risk of developing diabetic cardiomyopathy

UNIVERSITY *of the*
WESTERN CAPE

Xolisa Nxele

A thesis presented in fulfilment of the requirements for the **Degree Philosophiae Doctor** at the Faculty of Natural Sciences, University of the Western Cape

Supervisor: **Dr Rabia Johnson**

Co-supervisor(s): **Prof. Mongi Benjeddou and Prof. Sandrine Lecour**

ABSTRACT

Cardiovascular disease (CVD) is the leading cause of death of people with obesity and type 2 diabetes (T2DM). According to a statistical report from the World Health Organization (WHO), approximately 17.9 million people die annually because of CVD and diabetic cardiomyopathy (DCM), a disease of the heart muscle occurring in the absence of coronary artery disease or hypertension. Although not fully elucidated, the pathophysiology of DCM includes myocardial left ventricular hypertrophy, impaired calcium handling, energy metabolism, inflammation, apoptosis and myocardial fibrosis. DCM was discovered over 40 years ago, however, its subclinical detection remains a hurdle, especially in resource-poor environments and for unreferred diabetics. To date, there is no effective diagnostic treatment to detect DCM preclinically. Diagnostic biomarkers can be used for the early detection of individuals at risk of developing CVD. Therefore, this study aimed to identify potential diagnostic biomarkers that may detect DCM at the asymptomatic stage.

To achieve this, an *in silico* prediction pipeline was developed to identify biomarkers associated with T2DM and CVDs. To eliminate bias, a $p<6 \times 10^{-6}$ was used to select the top 5 *in silico* predictive genes that were differentially expressed. These included Ubiquitin Specific Peptidase 34 (USP34), Electron Transfer Flavoprotein Subunit Beta (ETFβ), Lysyl oxidase-like 2 (LOXL2), Zinc finger with KRAB and SCAN domains 4 (ZKSCAN4) and Insulin-like growth factor 1(IGF1)) for further analysis. Thereafter, a Leptin receptor-deficient diabetic mouse model ($Lepr^{db/db}$), with a phenotype including obesity, insulin resistance and T2DM, and its homozygous control $Lepr^{db/-}$ were used to evaluate diagnostic biomarkers measured against the known N-terminal-pro B-type Natriuretic Peptide (NT-proBNP), a marker of hypertrophy, and the gold standard Tissue Doppler Imaging (TDI) echocardiography. Gene expression analysis showed significant differences in LOXL2 (role in the regulation of extracellular matrix linked to fibrosis) and IGF1(role in myocardial hypertrophy) when the $Lepr^{db/db}$ were compared to their $Lepr^{db/+}$ counterparts. Serum protein expression showed a significant increase in LOXL2 and a decrease in ETFβ (role in mitochondrial fatty acid oxidation and adenosine triphosphate (ATP) production) protein expression. Serum protein expression data correlated with Tissue Doppler echocardiography showing reduced left ventricular diastolic function in $Lepr^{db/db}$ mice when compared to the $Lepr^{db/-}$. Haematoxylin

and Eosin stain and Masson's Trichrome stain did not show any significant differences in the microanatomy of the heart tissue.

However, marked myocardial derangements were observed following anti-LOXL2 and anti-ETFβ immunostaining. Functional analysis using an *in vitro* H9c2 model allowed for LOXL2 and ETFB knockdown. Messenger ribonucleic acid (mRNA) levels of transforming growth factor-beta (TGFβ), involved in fibrosis signalling and transcriptionally regulated by LOX, and collagen 1a1 (Col1a1), a known marker of fibrosis, were significantly increased compared to the scrambled control. Furthermore, western blotting experiments of knockdown of ETFβ showed a significant decrease in Col1a1 expression, suggesting collagen production requires energy for its execution. The receiver operating characteristic (ROC) curve analysis was used to determine the sensitivity and specificity of the identified markers. LOXL2 and ETFβ had an area under the curve (AUC) of 0.813 with a cutoff value of 0.824, indicating the good predictive power of the model with biomarkers being robust when used together. Altogether, these data suggest that LOXL2 and ETFβ can be potential biomarkers to detect DCM in diabetic patients during the asymptomatic phase.

Declaration

I declare that ***"Identification of sub-clinical biomarkers that predict the risk of developing diabetic cardiomyopathy"*** is my own work, that it has not been submitted for any degree or examination in any other university, and that all the sources I have used or quoted have been indicated and acknowledged by complete references.

Xolisa Nxele

Date

Signed

Dedication

Dedicated to my loving grandmother **Msindose Gladys Duba née Nxele**

(1937-11-13 to 2018-01-10)

List of abbreviations

Alpha	α
Actin-β	Actβ
Activating the enzyme poly	ADP-ribose
Acyl-Coenzyme A dehydrogenase	Acadm
Adenosine triphosphate	ATP
Advanced glycation end products	AGEs
AMP-activated protein kinase	AMPK
Angiotensin-converting enzyme inhibitors	ACE
Apoptotic protease activating factor-1	APAF-1
Applied Biosystem Instrument	ABI
Alanine Transaminase	ALT
Aspartate Transaminase	AST
Atrial natriuretic peptide	ANP
Beta	β
B-cell lymphoma-2	BCL-2
Bcl-2-associated X protein	BAX
Biological Database Network	bioDBnet
Bovine serum albumen	BSA
Brain natriuretic peptide	BNP
Calcium	Ca^{2+}
Ca^{2+}-ATPase sarco-endoplasmic reticulum	SERCA2a
California	CA
Caspase-3-activated DNase	CAD
Cardiac troponin T	cTnT
Cardiotrophin-1	CT-1
Cardiovascular diseases	CVDs
Cardiac output	CO
Carnitine palmitoyltransferase deficiency type 2	*CPT2*
Chitinase-3-like protein 1	CHI3L1 or YKL-40
Chronic kidney disease	CKD

Chronic obstructive pulmonary disease	COPD
Collagen 1a	Col1A
Coronary artery disease	CAD
Complimentary DNA	cDNA
Connective tissue growth factor	CTGF
Cytochrome-c	Cyt-c
Degrees	°
Deoxynucleotide triphosphates	dNTPs
Diabetic cardiomyopathy	DCM
Diabetic ketoacidosis	DKA
Diastole	d
Dipeptidyl peptidase 4	DPP-4
Dimethyl sulfoxide	DMSO
double distilled water	dH2O
Dulbecco's Modified Eagle's Medium	DMEM
Dulbecco's phosphate-buffered saline	DPBS
Dynamin-related protein 1	DRP1
Dynamin-like protein	DLP1
Galectin-3	GAL 3
Get With The Guidelines-Heart Failure	GWTG-HF
Gene Expression Omnibus	GEO
Growth differentiation factor-15	GDF-15
Early passive transmitral inflow velocity	E
Early ventricular filling wave	E wave
Echocardiogram	ECG
Ejection fraction	EF
Endoplasmic reticulum	ER
Endothelial nitric oxide synthase	eNOS
Ethics Committee of the University of the Western Cape	ECUWC
Ethics Committee of Research on Animals	ECRA
Enzyme-linked immunosorbent	ELISA
Empagliflozin Cardiovascular Outcome	EMPA-REG OUTCOME

Electron transport chain	ETC
Electron transfer flavoprotein β	ETFβ
E wave deceleration	E_{DT}
Extracellular matrix	ECM
Fatty acid oxidation	FAO
Fission protein	FIS1
Foetal bovine serum	FBS
Flavin adenine dinucleotide	FAD
Galectin-3	GAL 3
Gated-single photon emission computed tomography	G-SPECT
Glucagon-like peptide 1	GLP-1
Gravitational acceleration	g
Haematoxylin and Eosin	H&E
Heart failure with preserved left ventricular ejection fraction	HFpEF
Heart-type fatty acid-binding protein	H-FABP
Heart rate	HR
Heterozygous control littermate	$Lepr^{db/+}$
Herts	Hz
High-density lipoprotein	HDL
High glucose	HG
Highly sensitive C-reactive protein	hs-CRP
Human epididymis protein 4	HE4
Horseradish peroxidase	HRP
Hydrogen peroxide	H_2O_2
Hypoxanthine phosphoribosyl transferase 1	Hprt1
P38 mitogen-activated protein kinases	p38-MAPK
Palmitic acid	PA
Percent	%
Peroxisome proliferator-activated receptor gamma coactivator 1-alpha	PGC-1α
Phospholamban	PLN
Phosphatidylinositol 3-kinase	PI3K)/Akt
Phosphor anti-mothers against decapentaplegic	Smad

Polyacrylamide gel electrophoresis	PAGE
Polymerase-1	PARP
Polyvinylidene fluoride	PVDF
Principal component analysis	PCA
Primate Unit and Delft Animal Centre	PUDAC
Protein phosphatase 1	PP1
Protein Kinase A	PKA
Protein kinase B	Akt
Protein specificity 1	Sp1
Late ventricular filling wave	A wave
Left bundle branch block	LBBB
left ventricular diastolic dysfunction	LVDD
Left ventricular hypertrophy	LVH
Left ventricle posterior wall	LVPW
Left ventricle internal diameter	LVID
Leptin receptor-deficient homozygous db/db mice	$Lepr^{db/db}$
Low-density lipoprotein cholesterol	LDL-C
Lipoprotein lipase	LPL
L-type calcium channels	LTCC
Lysyl oxidases	LOX
Lysyl like oxidases	LOXL
Sample buffer	SB
Sarcoplasmic reticulum	SR
scramble	scrRNA
Sirtuin 1	SIRT1
Suppression of tumorigenicity 2	ST2
Sub-Saharan Africa	SSA
Sodium-glucose cotransporter	SGLT2
Sodium-glucose cotransporter-2-inhibitors	SGLT2
Sodium-calcium exchanger	NCX
Sodium dodecyl sulfate	SDS
South Africa	SA

South African Medical Research Council	SAMRC
Speckle tracking echocardiography	STE
Spontaneously hypertensive rats	SHR
Store-operated calcium entry	SOCE
Systole	s
Small interfering RNA	siRNA
Identifiers	IDs
Isovolumetric relaxation time	IVRT
Immunoglobulin G	IgG
Incorporated	Inc
Intercellular Adhesion Molecule 1	ICAM-1
Interleukin	IL
Interventricular septum	IVS
Intermediate glucose	IG
Insulin	INS
Insulin-like Growth Factor 1	IGF-1
Janus kinase	JAK
Threshold cycle	Ct
Tumour necrosis factor	TNF
Tissue culture	TC
Tissue Doppler Imaging	TDI
Type 1 diabetes mellitus	T1DM
Type 2 diabetes mellitus	T2DM
Trademark	™
Transforming growth factor β	TGF-β
Tris-buffered saline	TBS
Tris-buffered saline containing Tween-20	TBST-20
Matrix metalloproteinases	MMPs
Mammalian target of rapamycin	mTOR
Maryland	MA
Medial mitral annulus velocity	e’
Metalloproteinases	TIMPs

Membrane-bound Suppression of Tumorigenicity 2	ST2L
Molar	M
Micro liter	μL
Micro molar	μM
Mitochondrial DNA	mtDNA
Mitofusins	MFN1 and MFN2
Mitogen-activated protein kinase	MAPK
Miligrams/mili litre	mg/mL
Multi-slice computed tomography	Multi-slice CT
My Structured Query Language	MySQL
NAD phosphate oxidase	NOX
Nano molar	nM
Natriuretic peptide A	NPPA
Normal glucose	NG
Nicotinamide adenine dinucleotide	NAD
Nicotinic acid adenine dinucleotide phosphate	NADPH
Nuclear factor κβ	NF-κβ
Nuclear receptor subfamily 2 group F member 2	NR2F2
N-terminal prohormone of brain natriuretic peptide	ACYLNT-proBNP
Optic atrophy 1	OPA1
Quantile discretization	QD
Reactive oxygen species	ROS
Reduced cardiorespiratory fitness	CRF
Relaxin for the Treatment of Acute Heart Failure	RELAX-AHF
Renin-angiotensin-aldosterone	RAA
Reverse transcriptase-Plus	RT-Plus
Reverse transcriptase-Minus	RT-Minus
Revolutions Per Minute	rpm
Retinoic acid	RA
Ribonucleic acid	RNA
Receiver operating characteristic curve	ROC
Robust-Multi array Average	RMA

Ryanodine receptor 2	RyR2
Janus kinase	JAK
Signal transducer and activator of transcription	STAT
Soluble Suppression of Tumorigenicity 2	sST2
Square centimetre	cm^2
Ubiquinone oxidoreductase	QO
Ubiquitin-Specific Protease 34	USP34
United States of America	USA
Vascular cell adhesion protein 1	VCAM-1
Volts	V
Weight by volume	w/v
Xanthine oxidase	XO
Zinc finger with KRAB and SCAN domains 4	ZKSCAN4

Table of Contents

Acknowledgements

Dr Rabia Johnson, thank you for your enthusiasm towards my progress and for the privilege to work under your supervision throughout this PhD journey.

Prof. Sandrine Lecour, thank you for allowing me to have access to the state-of-the-art echocardiography facilities at HATTER institute and ensuring this thesis is finalized. I truly appreciate your intervention.

Special thanks to Ruzyda van Aarde, Charna Chapman, Desmond Linden; your assistance was invaluable.

To the cardiometabolism group, I am grateful for the privilege of having had to work with such excellent minds

Akhona Nxele, thank you for your support and prayers.

Bulumko Ondah Awaseh, my wonderful son, thank you for enduring sleeping on the couch waiting for me to come home and bringing me back to life with your interesting stories, contagious laughter and inviting me to play with you.

Shekinah Ondah Awaseh, your arrival finally made me sit down and finish this long-overdue project.

Franklin Ondah Awaseh, I am immensely grateful for your love, support, encouraging words, patience, and strength. Thank you for the various roles you had to play throughout this journey. May God bless you and establish you.

Chapter 1

Literature Review

1.1 Introduction

The current global prevalence of diabetes mellitus (DM) is 537 million. This number is projected to increase to 783 million by 2045 (Figure 1) (Webber, 2021). It is further estimated that 23.% in America people between the ages of 20 to 79 years have diabetes but are unaware of their condition (Centers for Disease Control, 2022). This increased prediction of both known diabetic and undiagnosed diabetic cases is of great concern since failure to address this health issue may lead to harmful complications such as developing cardiovascular diseases (CVDs). Cardiovascular diseases are defined as a group of myocardium and blood vessel disorders and kill 17.9 million individuals annually while contributing to 31% of all global deaths(World Health Organisation, 2021). Furthermore, the risk of developing cardiovascular disease is known to increase with age, with individuals older than 40 years having a 75% greater risk of heart failure (HF) and 2-4 times likelihood of dying due to HF.

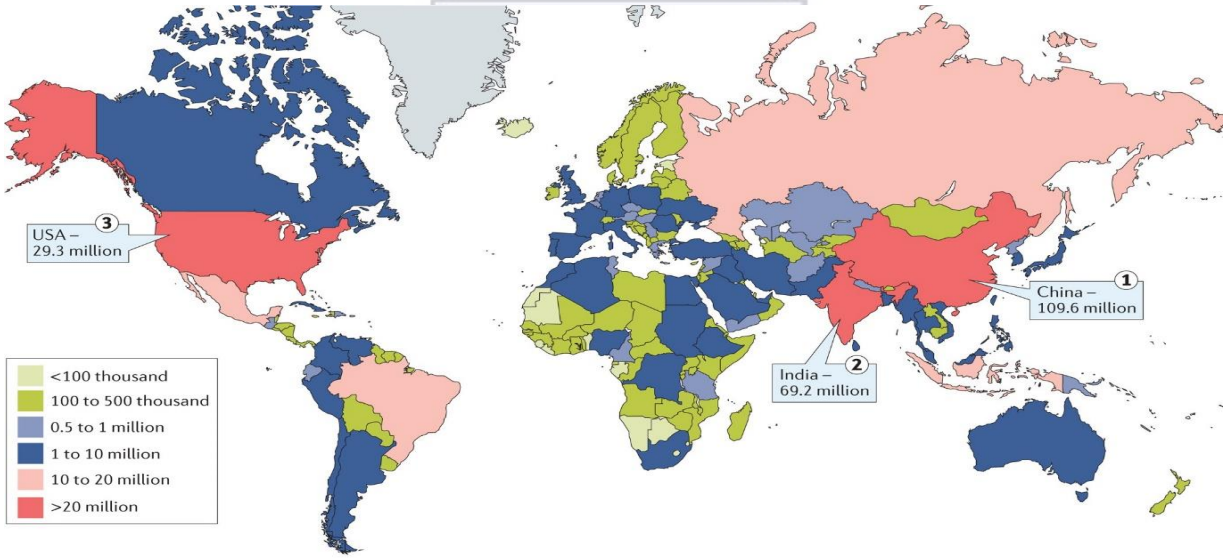

Figure 1.1: Global distribution of adults (20-79) living with diabetes mellitus, also showing the three countries with the highest number of diabetic individuals in 2015. The following countries namely; China, India and the Unites States of America (USA) had the highest number of individuals with diabetes mellitus 109 million, 69.2 million and 29.3 million respectively. The colours show the number people between 20 and 79 with diabetes mellitus in each area/country. (Picture adapted from (Zheng et al., 2018)

In 2016, coronary artery disease (CAD) was the leading cause of death from cardiovascular disease (43.2%) in the United States, followed by stroke (16.9%), high blood pressure (9.8%), HF (9.3%), diseases of the arteries (3.0%), and other cardiovascular diseases (17.7%) (Association, 2019). In sub-Saharan Africa (SSA), the number of deaths from CVD has increased to more than 50% over the past three decades, with ischemic heart disease, stroke and hypertensive heart disease being the leading causes of death in this region (Yuyun et al., 2020).

Any stress on the heart is detrimental as cardiac cells are terminally differentiated and therefore unable to regenerate. As such, diabetes/ischemic heart disease can cause cardiac muscle cells to die, resulting in decreased heart function and an inability to pump blood in the body effectively. This is especially true in diabetic cardiomyopathy (DCM), a unique clinical entity with poor clinical outcomes. DCM is a nebulous CVD complication independent of CAD and hypertension (Lee & Kim, 2017; Lorenzo-Almorós et al., 2017). DCM limits the ability of the heart to effectively circulate blood in the body, causing HF with oedema in the lungs and legs (Boudina et al., 2007, Boudina & Abel, 2010). The latter results from the impairment of normal pump function of the heart over time, causing reduced left ventricular relaxation and impaired filling (Borlaug & Paulus, 2011, Paulus & Dal Canto, 2018). This heart impairment is also referred to as HF with preserved left ventricular ejection fraction (HFpEF, i.e. EjectionFraction≥50%). The pathophysiology of DCM involves hyperglycaemia, hyperlipidaemia, systemic inflammation, fibrosis and apoptosis (Paulus & Dal Canto, 2018). The onset of DCM/HFpEF is asymptomatic, thus making it difficult to diagnose, preventing the implementation of corrective treatment, which will pre-empt HF complications (Asghar et al., 2009).

Other cost-effective methods of detecting DCM at the asymptomatic stage would be advantageous, especially in resource-poor countries. Biomarkers, which are defined as measurable features of an organism that represents a physiological state, are good candidates. However, to date, there are no prognostic marker(s) available to detect asymptomatic onset of DCM, although several imaging techniques to detect this cardiac phenotype, including Tissue Doppler Imaging (TDI) echocardiography, speckle tracking imaging and cardiac magnetic resonance imaging (MRI) are available to individuals who are not referred (León et al., 2016; Lorenzo et al., 2013). These imaging technologies are non-invasive and allow for 'real-time' visualization of the functional and structural properties of the heart. However, not all public health facilities have access to such technologies. In addition, due to financial constraints on the national health system, TDI echocardiography is not routinely performed and is therefore only performed on referred cases of diabetes. Therefore, asymptomatic detection of DCM goes undocumented and unnoticed and will only be detected at an advanced stage.

In the last decade, an increasing body of knowledge came to the forefront associating certain genes with early onset of HF, some of which included N-terminal prohormone of brain natriuretic peptide (NT-

pro-BNP), cardiac troponin T (cTnT), suppression of tumorigenicity 2 (ST2) and left bundle branch block (LBBB) to name a few (Hogas et al., 2017, Piek, Du, de Boer, & Silljé, 2018, Grodin & Tang, 2013). However, none of the markers could detect DCM either in its asymptomatic stage or early enough to implement corrective treatment. As such, all diagnosed T2DM patients are automatically placed on a treatment regime that includes cardioprotective agents such as angiotensin-converting enzyme (ACE)-inhibitors, β-blockers, statins, or sodium-glucose cotransporter-2 (SGLT2)-inhibitors. The Sodium-glucose cotransporter-2 inhibitor is a glucose-lowering drug that acts by preventing glucose reabsorption from the kidneys. The drug has been reported to be the most effective in protecting the diabetic myocardium from a hyperglycaemic insult, thus making it an ideal prescription anti-diabetic drug. Since SGLT2-inhibitors are known to cause dehydration and urinary tract infection (Mordi et al., 2017), medical practitioners will only prescribe the drug to patients with confirmed cardiovascular events.

Since TDI echocardiography analysis is only performed in referred diabetic cases, having a biomarker that can be used routinely to guide clinical decisions on when to initiate treatment using SGLT2-inhibitors would be useful. Highlighting again the importance of identifying such a prognostic marker, which could also aid in identifying this complex disease. In this project, we sought to bridge the gap in understanding the current pathology, pathophysiology, imaging technology and biomarkers used for early detection of DCM to identify a panel of potential biomarkers that could be used routinely for asymptomatic detection of DCM. To achieve this, an *in silico* prediction pipeline was used to identify potential biomarkers described in previous studies conducted in diabetic and CVD patients. Once these putative biomarkers are identified, experimental studies will be conducted in a mouse models to determine whether these biomarkers are associated with the early onset of diabetic cardiomyopathy.

1.2 History and evidence of DCM existence

As early as 1881, Leyden commented on HF being a common and notable complication of diabetes mellitus (DM), while Mayer said that the disease could be traced to abnormalities in cardiac metabolism (Asghar et al., 2009). However, it was not until 1972 that Rubler and co-workers observed a distinct clinical entity where cardiac dysfunction was present in post-mortem tissue of four diabetic patients in the absence of CAD or hypertension, thereby confirming the existence of this nebulous (Murarka & Movahed, 2010, Nunes, Soares, Pereira, & Reis, 2012). Several reports then confirmed the presence of this entity (Toedebusch et al., 2018). Although there is mounting evidence supporting the existence of DCM in the literature, contrasting views on its existence remain (Bugger, 2015). Most of the structural, histological, and mechanical and biochemical features associated with DCM are not unique to the disease state but are common features of most myocardial diseases. Therefore, the nebulous nature and misclassification of the disease continue. However, subsequent studies confirmed that this entity occurs

in different populations (Bertoni et al., 2003; Rodeheffer & Chen, 2008; Shaver et al., 2016). Bonito and co-workers confirmed the presence of DCM in its asymptomatic stage using TDI echocardiography in 40 non-obese normotensive T2DM patients (Di Bonito et al., 2005). A 43-month follow-up study of 2 737 older individuals showed that people with diabetes were 1.3 times more likely to develop HF than those without diabetes (Aronow et al., 1999). Furthermore, diabetic women were five times more likely to develop DCM than their non-diabetic counterparts (Kannel et al., 1974). In a hospital-based study conducted on 837 individuals living in the United States, diabetes was significantly correlated with nonischemic systolic dysfunction. Diabetes-related cardiomyopathy was observed in more cases than they had anticipated (Bertoni et al., 2003).

1.3 Epidemiology and prevalence of DCM population-based studies

The prevalence of DCM varies depending on the population surveyed. The prevalence is currently estimated to be between 12%-60% among people with type 2 diabetes (Fuentes-Antrás et al., 2015). A nationwide study conducted in Olmstead County, Minnesota, showed that the prevalence of DCM was increasing annually at a rate of 1% in relation to HF (which can be termed diastolic/preserved ejection fraction or systolic/reduced ejection fraction), suggesting HFpEF (diastolic) could become the most common type of HF in the future (Owan et al., 2006). A large hospitalisation study in the United States (The Get With The Guidelines-Heart Failure (GWTG-HF)) showed that the proportion of HF patients with HFpEF hospitalised patients increased from 33% to 39% between 2005 and 2010 (Oktay et al., 2013). However, HF was reported to increase by 1.44% in an Italian population while increasing proportionally with age (Savarese & Lund, 2017). In a cross-sectional study of diabetic patients, the authors showed that nearly half of normotensive T2DM patients presented with increased LV hypertrophy compared to the normotensive control population (Oktay et al., 2013). This supports the notion that DCM is asymptomatic and therefore still understudied in most countries and possibly misdiagnosed. Age and sex have also been shown to be risk factors for DCM, with higher incidences of DCM in women and the elderly (Maric, 2010). Older diabetic individuals have also been shown to be 1.3 times more likely to develop congestive heart failure than their nondiabetic counterparts. Owan (2006) confirmed this, showing an increase in DCM prevalence over 15 years, while mortality rates remained unchanged (Owan et al., 2006). Diabetes was projected to affect about 40.7 million people in sub-Saharan Africa by 2015; however, more than two-thirds of these people remain undiagnosed (Mercer et al., 2019). It is estimated that approximately 50% of patients with T2DM have echocardiography detectible abnormalities, but there have not been any appropriate comparisons of these with matched background populations (Huson et al., 2019).

1.4 Normal heart function and cardiac cycle

The heart is a hollow muscular organ about the size of a closed fist. During a typical lifetime, the heart beats about 100,000 times a day and 2,5 billion times overall. The heart has four chambers, two ventricles and two atria. The atria are upper chambers, the right atrium receives venous blood (deoxygenated blood) from the different sources, including the inferior and superior vena cava, anterior cardiac veins and coronary sinus, and the left atrium receives oxygenated blood from the pulmonary veins (Anderson, 1993). After passing through the right atrioventricular orifice (tricuspid valve), blood flows into the right ventricle and is pumped into the lungs via the pulmonary arteries. At the same time, wastes are removed, and oxygen is substituted. The oxygenated blood returns to the left atrium through the pulmonary veins and passes through the left atrioventricular orifice (mitral valve) into the ventricle of the left. During contraction, blood flows into the arterial system. The cardiac cycle is the sum of all the cardiac events occurring from the beginning of one heartbeat to the next. It consists of the following events: ventricular diastole (relaxation) and ventricular systole (contraction). During ventricular diastole blood flows from the atria through the open tricuspid and mitral valves into the relaxed ventricles. During ventricular diastole, the aortic and pulmonic valves are closed. During diastole, about 70-75% of the blood flows by passive diffusion from the atria through the open tricuspid and mitral valves and into the ventricles even before the atria contract. Approximately 25-30% of ventricular filling is from atrial contraction. The mitral and tricuspid valves are shut during ventricular systole, while the relaxed atria are filled with blood. The aortic and pulmonic valves open due to increased ventricular pressure. Effective atrial contraction is lost in myocardial diseases like DCM, resulting in reduced cardiac output (CO) (Figure 1.2).

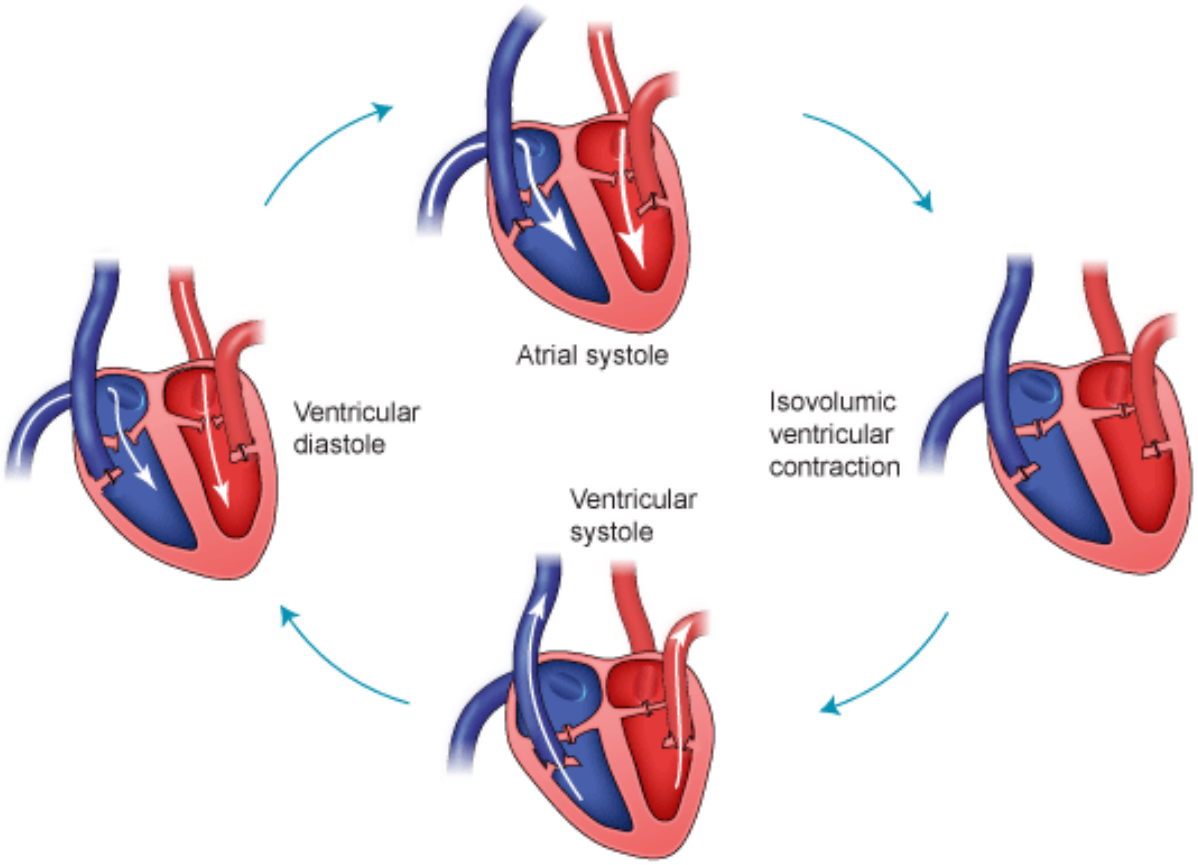

Figure 1.2: The cycle of the heart and cardiac output: the cardiac cycle consists of several phases, including atrial systole, isovolumic contraction, ventricular- systole and diastole. (Adapted from https://thephysiologist.org/study-materials/the-cardiac-cycle-and-cardiac-output/)

1.5 The three stages of diabetic cardiomyopathy

DCM has three stages: the early stage, the middle stage, and the late stage (Figure 1.3). The asymptomatic early stage is characterised by cardiac hypertrophy, diastolic dysfunction, and normal ejection fraction (EF) (Boudina et al., 2007, Battiprolu, Gillette, Wang, Lavandero, & Hill, 2010). Moreover, free fatty acid levels are elevated at the molecular level, calcium homeostasis is distorted, and glucose uptake and oxidation are suppressed. In the middle stage, the LV wall is thickened, and the LV mass is elevated (Boudina & Abel, 2010, Li, Lv, Li, & Yu, 2012). This is intertwined with diastolic and systolic dysfunction with a 50% reduction in EF. As the disease progresses from the middle to the late stage, it is associated with macrovascular alterations and cardiac necrosis that damages both systolic and diastolic functions and culminates in HF (Jia et al., 2018).

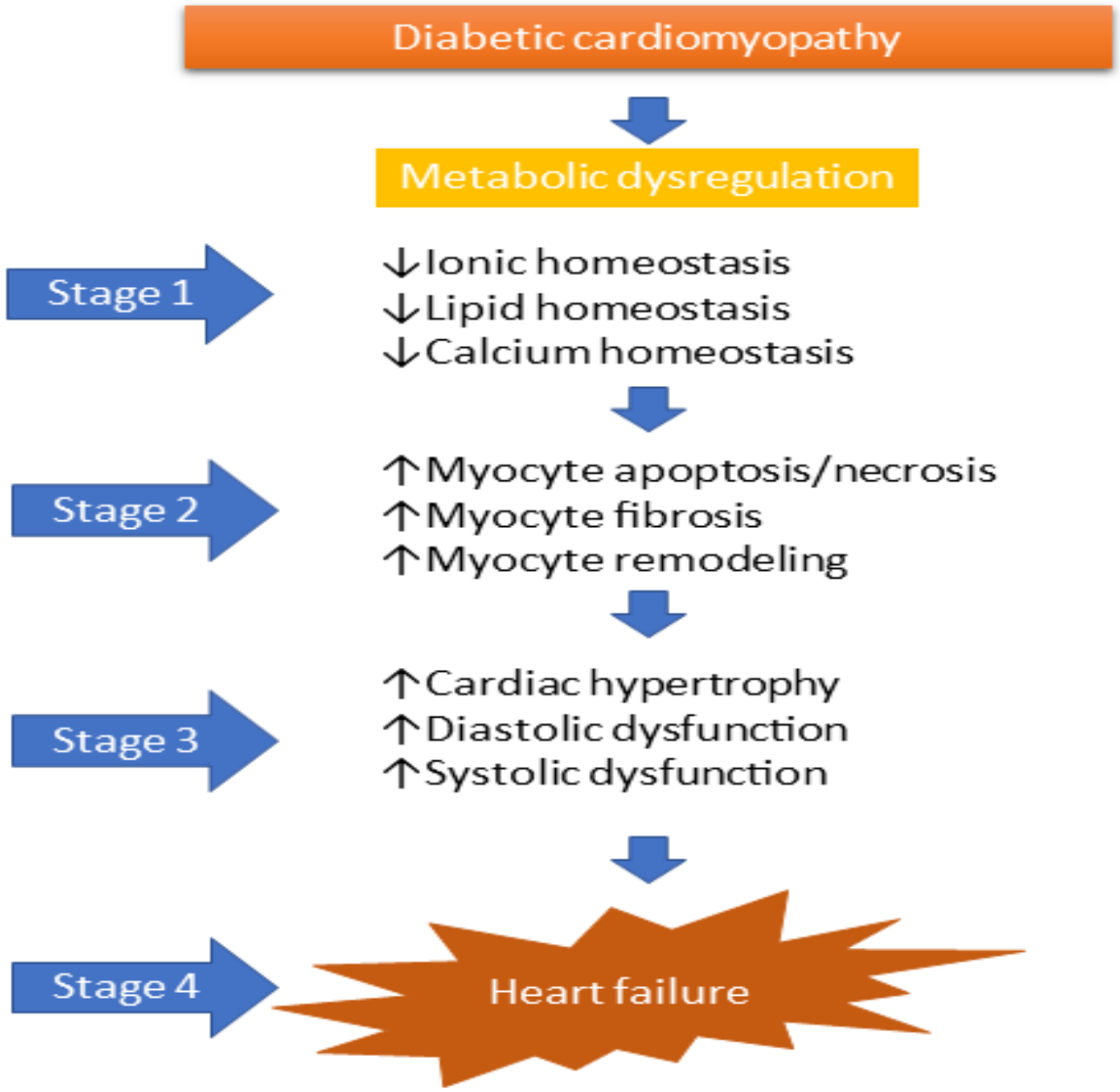

Figure 1.3: Stages of diabetic cardiomyopathy: DCM has four stages: metabolic dysregulation of ions, lipids, and calcium. This is followed by a second stage, where the myocytes have increased apoptosis, fibrosis and remodelling. A third stage is when the heart has hypertrophied, diastolic and systolic dysfunction are increased, and a fourth stage culminates in heart failure.

1.5.1 Stage 1

1.5.1.1 Metabolic disturbances

The heart is a metabolically active organ with high mitochondria content and needs a constant supply of high-energy substrates to maintain normal cardiac function. Seventy per cent of the substrates are triglycerides and long-chain fatty acids in a healthy heart, with approximately 30% derived from glucose and lactate. Interestingly, in the foetal heart, glucose oxidation (90%) is the primary energy source, while in the adult heart, oxidation of fatty acid becomes the preferred energy substrate (70%)

(Stanley et al., 2005). The most notable change during the development of DCM is the hypertrophied heart that almost entirely relies on fatty acid oxidation (70-90%) (Stanley et al., 2005). Indeed, in times of stress, the nondiabetic heart will revert to a foetal state where glucose oxidation will be used as the preferred substrate since glucose as a substrate uses less oxygen per molecule of adenosine triphosphate (ATP) produced (Athéa et al., 2007, Schilling & Mann, 2012). Various studies have reported on the hearts' inability to shift between substrates to adapt to stress conditions, such as chronic hyperglycaemia. In various animal models, this phenomenon prevails with increased gene expression observed in fatty acid oxidation (FAO) and mitochondrial oxidative phosphorylation pathways. As a result, the diabetic heart is more susceptible to glucose and lipid-induced cardiac injury (Saunders et al., 2008). Thus, the observed inflexibility of the metabolism can directly be linked to hyperinsulinemia, hyperlipidaemia, and hyperglycaemia.

1.5.1.2 Glucotoxicity

Glucotoxicity refers to the adverse effects of poor glycaemic control due to impaired β-cell function, leading to increased insulin resistance with worsening glycaemic control. Insulin resistance, with sustained chronic hyperglycaemia, is known to impair cardiac insulin metabolic signalling. Chronic hyperglycaemia can induce a protein glycation reaction that increases advanced glycation end products (AGEs). Increased AGE deposition subsequently contributes to augment connective tissue crosslinking, fibrosis, cardiac stiffness and impaired left ventricular diastolic dysfunction (LVDD) (Leroith, 2002). LVDD is one of the earliest cardiac changes in patients with DCM. In DCM, insulin-stimulated glucose uptake is reduced due to inhibition of glucose transporter type 4 (GLUT4), which is known to facilitate glucose transport across the plasma membrane. Chronic hyperglycaemia promotes the overproduction of reactive oxygen species (ROS) that induce apoptosis while activating the enzyme poly (ADP-ribose) polymerase-1 (PARP). This diverts glucose from the glycolytic pathway towards the hexosamine biosynthesis pathway, the polyol pathway, and protein kinase C, increasing AGEs (Battiprolu et al., 2010). Advanced glycosylation end products formation has been found to form irreversible crosslinks within or between many proteins, including the calcium (Ca^{2+})-ATPase sarco-endoplasmic reticulum (SERCA2a) and the Ca^{2+} release channel, ryanodine receptor 2 (RyR2), causing their inactivation and resulting in abnormal cardiac relaxation and contractility. Increased hexosamine biosynthesis also reduces the expression and function of SERCA2, resulting in impaired excitation-contraction coupling and myocardial relaxation (Schilling & Mann, 2012).

Interestingly, AGEs interact with their receptors, including AGE and galectin-3 (GAL 3), and up-regulate them. This activates transcription factors like nuclear factor κβ (NF-κβ) (Schilling & Mann, 2012), which causes myocardial damage by triggering several gene dependent pathways to induce pro-inflammatory cytokine production such as tumour necrosis factor-alpha (TNFα). Chronic hyperglycaemia also activates the polyol pathway by being converted to sorbitol through aldose

reductase in the presence of nicotinic acid adenine dinucleotide phosphate (NADPH) that is oxidized to $NADP^+$ (Yan, 2014). NADPH is important for the generation of reduced glutathione (an essential ROS scavenger in the body). As the polyol pathway relies on increased NADPH use, the redox balance in the cells is lost. Consequently, increased oxidative stress can result in DNA damage and cardiomyocyte apoptosis. Sorbitol also glycates proteins that leads to AGEs formation, which results in tissue injury in diabetes.

1.5.1.3 Hyperlipidaemia and lipotoxicity

Increased lipolysis in the adipocytes and elevated lipogenesis contributes to increased circulating fatty acids and triglycerides in diabetic patients. Additionally, insulin stimulates the transport of fatty acids to cardiomyocytes. Due to increased intracellular fatty acids, the myocardium quickly adapts by promoting fatty acid use (An & Rodrigues, 2006). However, when the amount of fatty acids is greater than their oxidative capacity in the cardiomyocytes, these are stored as lipids like triglycerides, saturated fatty acids, and ceramide, resulting in lipotoxicity. Aggregation of triglycerides and ceramides triggers oxidative stress and cardiomyocyte apoptosis, leading to cardiac dysfunction and organ failure (Bayeva et al., 2013; Boudina & Abel, 2010). Several studies have confirmed that augmented fatty acids stimulate lipotoxicity and contribute to DCM pathogenesis. A significant increase in fatty acid delivery with elevated lipid storage, lipotoxic cardiomyopathy, and contractile impairment was observed in cardiac-specific overexpression of lipoprotein lipase (LPL) (An & Rodrigues, 2006).

Moreover, elevated fatty acid use by cardiac-specific overexpression of PPAR-α causes cardiomyopathy and impaired cardiac function. Conversely, reduced expression of PPAR-α and PPAR-γ leads to decreased cardiac lipid accumulation and cardiomyopathy in diabetic animals (Van De Weijer et al., 2011). Similarly, in obese ZDF rats, using a PPAR-γ agonist reduced plasma lipids and led to decreased myocardial ceramides and triglycerides and improved cardiac function (Zhou et al., 2000). This has been corroborated by Van de Weijer et al. (2011), who reported that increased ceramides affect cardiac function(Van De Weijer et al., 2011).

1.5.1.4 Mitochondrial energy metabolism

Mitochondria play an important role in the cellular bioenergetics of cardiomyocytes and are essential for normal functioning due to the high energy demands of the beating heart. Mitochondria make up 20–30% of the cell volume of cardiomyocytes, but their number can increase with enhanced myocardial energy requirements. Mitochondria are dynamic organelles that generally meet the energy needs of the tissue. The production of myocardial energy is primarily in the form of mitochondria-generated ATP to bridge nutrient metabolism and oxidative respiration. The heart consumes 6 kg of ATP per day, most of which is produced by mitochondrial oxidative phosphorylation, fed by lipid and carbohydrate catabolism and used for various biological events (Lopaschuk et al., 2018). Although there are

contrasting views on the specific mitochondrial electron transport chain (ETC) site affected by T2DM in human and animal models, cardiac mitochondria are more susceptible to T2DM-induced ETC dysfunction than kidneys and liver (Sivitz & Yorek, 2010). Heart samples of T2DM patients showed decreased mitochondrial palmitoylcarnitine oxidation (Berthiaume et al., 2019).

Significant data support the role of mitochondria in cardiac function, but little information is available on the dynamic regulation of mitochondrial biogenesis in cardiomyocytes. Mitochondria are a major energy source for cells and mediate biological responses, including cell proliferation and death. Changes in mitochondrial biogenesis and function have been documented in metabolic syndrome and diabetes. Clinical and experimental findings suggest a 30–70% reduction in phosphocreatine and total creatine levels in heart failure (Bugger & Abel, 2010). Myofibrillary creatine kinase activity in heart failure drops to approximately 50% of normal levels. In general, cardiac dysfunction is accompanied by defects in all three energy metabolism components in cardiomyocyte mitochondria: substrate metabolism, oxidative phosphorylation, and the transfer and use of energy. These interactions can be further complicated in the metabolic syndrome, exacerbating metabolic dysregulation and mitochondrial dysfunction, reinforcing the other abnormalities (Ventura-Clapier, Garnier, & Veksler, 2008, Athéa et al., 2007).

This is illustrated in metabolic/diabetic cardiomyopathy, wherein the initial manifestations of diastolic dysfunction are more pronounced in the presence of endothelial dysfunction. It is well validated that various components of metabolic syndrome, including insulin resistance, contribute to mitochondrial dysfunction. However, the extent of mitochondrial dysfunction in the metabolic risk constellation associated with metabolic syndrome and the relationship to metabolic cardiomyopathy is not well known. Under routine physiological conditions, the myocardial function depends on the continued recycling of ATP from mitochondrial oxidative phosphorylation (Chong et al., 2017). Maladaptation of mitochondria due to loss and/or reduced efficiency of mitochondria results in a series of events such as decreased ATP synthesis, abnormal accumulation of metabolic intermediates, and ROS production, all of which may contribute to the impaired mechanical functions of the heart.

The results of a wide range of studies support the pivotal role of mitochondrial dysfunction, the reduction of mitochondrial biogenesis in metabolic cardiomyopathy pathogenesis. For example, DCM is associated with the intracellular accumulation of toxic intermediates, such as Acyl-CoA and acylcarnitine, which affect the mitochondrial ATP / ADP ratio and lead to a decreased metabolic function of the mitochondria. Decreased gene expression of the mitochondrial regulatory protein PGC1α was found to be associated with dysfunction of the human heart (Duncan et al., 2007). Mitochondrial alterations may underlie several aspects of the observed metabolic cardiac phenotype, such as altered handling of Ca^{2+}, interstitial fibrosis, cellular and subcellular remodelling and

cardiomyocyte loss. In humans and animals with metabolic syndrome, reduced mitochondrial biogenesis was demonstrated, coinciding with reduced ATP levels and dysfunctional transport of mitochondrial electrons (Duncan, 2011). Mitochondrial quality is controlled through balanced fusion and fission events that continuously alter mitochondrial morphology. By undergoing fission, mitochondria become fragmented while fusion facilitates the formation of an interconnected elongated network (Galloway & Yoon, 2015).

Through the interaction of fusion and division, mitochondria adapt metabolism to the cell's energy requirements, allowing mixing of mitochondrial DNA (mtDNA), lipids, proteins, and metabolites. This enhances communication with the endoplasmic reticulum (ER) or separates dysfunction or depolarized mitochondria away from the healthy network causing its clearance (Nishida & Otsu, 2017). Fusion and fission are controlled by mitochondrial fusion and fission proteins: mitofusins (MFN1 and MFN2) and optic atrophy 1 (OPA1) facilitate mitochondrial fusion while dynamin-related protein 1 (DRP1) facilitates fission by interacting with fission protein (FIS1) (Galloway & Yoon, 2015, Dorn II, 2016). MFN2 expression is decreased in skeletal muscles in obese Zucker rats and obese and diabetic patients (Dorn II, 2016). In diabetic hearts, changes in mitochondrial numbers may reflect mitochondrial fusion/fission. Using isolated cardiac cells, a previous study showed that mitochondrial fission played a role in high glucose-induced apoptosis (Duncan, 2011). Additionally, several cardiac-derived cells exposed to high levels of glucose showed fragmented mitochondria and increased cell death. When a dominant-negative DLP1 (dynamin-like protein) was overexpressed thus inhibiting mitochondrial fission, mitochondrial morphology, ROS and cell death were normalized (T. Yu et al., 2008).

1.5.1.5 Impaired calcium (Ca^{2+}) handling

One of the major abnormalities in diabetes-induced heart failure is the abnormal handling of intracellular Ca^{2+} (Davia et al., 2001). This disruption of Ca^{2+} handling is due to changes in the function of the sarcoplasmic reticulum (SR), a major regulator of myocardial contraction, encoded by sarco/endoplasmic reticulum calcium ATPase cardiac isoform 2a (SERCA2a). Overexpression of SERCA2a has been shown to reduce contractile dysfunction and ventricular arrhythmias in ischaemic/reperfusion injury models, making SERCA2a one of the most promising targets for HF treatment (Davia et al., 2001). As such, Ca^{2+} is crucial during chamber contraction and relaxation. In cardiomyocytes, cytosolic Ca^{2+} influx stimulated by activation of voltage-dependent L-type Ca^{2+} channels on membrane depolarization induces Ca^{2+} release through the Ca^{2+} channels (Ryanodine receptor 2 (RyR2)) of the sarcoplasmic reticulum (SR) (Belke & Dillmann, 2004). Ca^{2+} then diffuses through the cytosolic space to reach the contractile proteins, binding to troponin C's myofilament protein (Boudina & Abel, 2010). As Ca^{2+} binds to the troponin C, the Ca^{2+} starts the sliding of thin and thick filaments, which ends in sarcomeric shortening and muscle contraction. Muscle relaxation is initiated by RyR2 closure accompanied by Ca^{2+} being dissociated from the troponin complex. The

concentration gradient then goes back to diastolic levels through activation of SR and re-uptake of Ca^{2+} into the SR by SERCA2a (Falcão-Pires & Leite-Moreira, 2012). Ca^{2+} and other ion homeostasis are altered in diabetic cardiomyocytes, and the mechanism by which Ca^{2+} is stimulated include; decreased ATPases activity, reduced ability of the SR to take up Ca^{2+} and decreased activities of other exchangers like Na^{+}/Ca^{2+} and the sarcolemmal Ca^{2+} ATPase (M. K. Kim et al., 2010).

In DCM patients, elevated cytosolic Ca^{2+} is mediated either by calcium overload in the cytosol or decreased Ca2+ efflux (Belke & Dillmann, 2004). Increased cytosolic Ca^{2+} entry is due to disruption of voltage-controlled L-type calcium channels (LTCC), sodium-calcium exchanger (NCX) and store-operated calcium entry (SOCE). In human cardiomyocytes, cytosolic Ca^{2+} influx is mainly through the LTCC, while LTCC phosphorylation is increased in DCM. This has been associated with SR Ca^{2+} via RyR2 leak. Store-operated calcium, a mechanism of calcium release-activated calcium channels (Orai-1) in the sarcolemma, detect intracellular Ca^{2+} reduction and open to allow extracellular Ca^{2+} influx. This phenomenon can change in response to pathological cardiac remodelling.

Furthermore, decreased Ca^{2+} efflux through the sarcolemma from the cytosol is mainly due to a defective NCX (Falcão-Pires & Leite-Moreira, 2012). Excess sodium in the cytosol restricts Ca^{2+} efflux from the cell using NCX and can lead to the exchanger working in reverse mode. Conversely, in DCM, NCX is less sensitive to extruding intracellular Ca^{2+} resulting from weakened transmembrane sodium gradient. Several studies have shown upregulation of NCX in HF, which is speculated to be an early adaptive response to compensate for SERCA2a downregulation and subsequent contractile depression (Ottolia et al., 2013; Schillinger et al., 2003). However, sustained NCX induction is dysregulated and gives rise to reduced SR Ca^{2+} content due to elevated Ca^{2+} removal.

A salient feature of DCM is elevated end-diastolic cytosolic Ca^{2+} levels and the lengthening of Ca^{2+} transient during diastole (M. K. Kim et al., 2010). This is primarily due to reduced SR Ca^{2+} resulting in SERCA2a dysfunction. SERCA2a expression is enzymatically regulated by Protein Kinase A (PKA) through serine-16 phosphorylation of Phospholamban (PLN), and DCM patients have been shown to have decreased SERCA2a expression. In it, the dephosphorylated form, PLN, inhibits SERCA2a expression in cardiac tissue, decreasing SR Ca^{2+} influx. To date, no differential PLN protein expression has been observed. However, certain studies have observed reduced levels of PLN mRNA in dilated or ischemic cardiomyopathy (Belke & Dillmann, 2004). Decreased expression of SERCA2a in DCM increases the ratio of PLN to SERCA2a and increases the inhibition of SERCA2a. At the same time, decreased PLN phosphorylation is associated with increased protein phosphatase 1 (PP1), which regulates Ca^{2+} cycling and contractility and cardiac response to β-adrenergic stimulation. PLN mutations have been associated with increased cardiac hypertrophy and reduced EF (Falcão-Pires & Leite-Moreira, 2012).

1.5.2 Stage 2

1.5.2.1Oxidative stress

Oxidative stress leads to the development and progression of myocardial insulin resistance, diabetic cardiomyopathy, and subsequent HF. Mitochondrial ROS occurs through oxygen metabolism in complexes I and II within the ETC (Huynh et al., 2012). The major electrochemical protein gradient is utilised to synthesise ATP under normal physiological conditions. The genes ETFα, ETFβ and ETF-ubiquinone oxidoreductase (QO) play a significant part in shuttling electrons between Acyl-CoA substrates to ubiquinone, connecting fatty acid oxidation and certain amino acids to the mitochondrial respiratory system (Boudina et al., 2007). However, under stress conditions such as hyperglycaemia and insulin resistance, increased nicotinamide adenine dinucleotide (NAD) and flavin adenine dinucleotide (FAD) flux to the mitochondrial respiratory chain causing hyperpolarization of the mitochondrial inner membrane, inhibiting electron transport in the complex III and excessive ROS production (Cai & Kang, 2001, Battiprolu et al., 2010). Additionally, NAD phosphate oxidase (NOX) is another important source of cardiomyocyte ROS (Figure 1.4). High levels of NOX activity have been observed in diet-related obesity and systemic myocardial insulin resistance (Asghar et al., 2009). The elevated renin-angiotensin-aldosterone system (RAAS) – mediated NOX activity may also directly promote cardiac fibrosis by activating profibrotic transforming growth factor β/SMAD 2/3 signalling pathway. Other ROS sources include elevated xanthine oxidase (XO), microsomal P-450 enzyme activity and nitric oxide (NO) synthase uncoupling. Increase cardiac tissue ROS is not limited to the polyol pathway flux, AGE formation, AGE receptor expression and activation of its ligands, PKC signalling, and hexose pathway (Murarka & Movahed, 2010, Duncan, 2011).

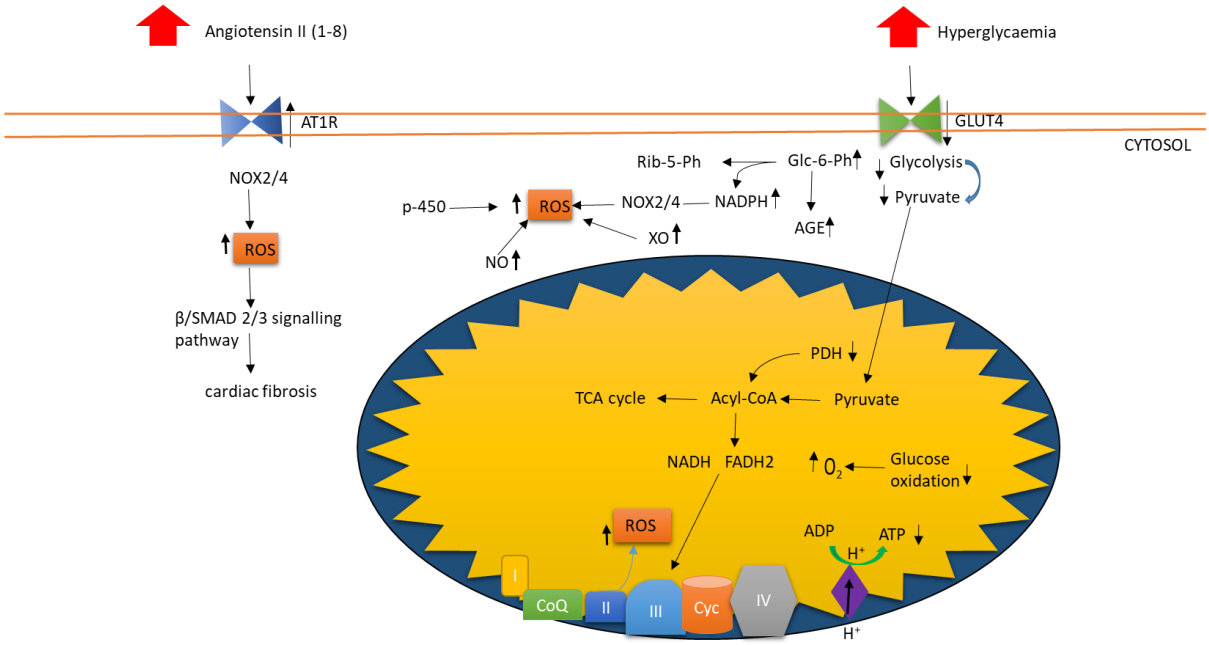

Figure 1.4 Oxidative stress in DCM. In the cytosol, angiotensin II (Ang II) binds to the angiotensin receptor 1 (AT1R) and induces a number of signalling pathways including the protein kinase C (PKC), mitogen-activated protein kinase (MAPK) and NADPH oxidase 2/4 (NOX), increasing the production of reactive oxygen species (ROS). In turn these signalling pathways activate the cascade of hypertrophic and/or fibrotic transcription factor proteins and pathways. Concurrently, Hyperglycaemia leads to reduced Glucose transporter type 4 (GLUT4) translocation, glycolysis, pyruvate dehydrogenase (PDH) and pyruvate. From aerobic respiration, increased glucose-6-phosphate (Glc-6-Ph) causes increased production of advanced glycation end products (AGEs), ribose-5-phosphate (Rib-5-Ph) and is nicotinamide adenine dinucleotide phosphate hydrogen (NADPH). NADPH activates the NOX 2/4 pathway which activates the production of ROS. Similarly, xanthine oxidase (XO), nitric oxide and p-450 cause an increase in ROS production. In the mitochondrion, the pyruvate is used to produce acetyl coenzyme A (Acyl-CoA) and is either fed into the tricarboxylic acid (TCA) cycle while its by-products nicotinamide adenine dinucleotide (NADH) and flavin adenine dinucleotide (FADH2) are use in the electron transport chain (ETC) to produce adenosine 5′-triphosphate (ATP).

1.5.2.2Myocardial interstitial fibrosis

Interstitial/perivascular fibrosis is one of the structural features of DCM. The extracellular matrix (ECM) comprises about 300 proteins involved in tissue homeostasis, organ development, inflammation, and disease. These include fibrous proteins (collagen, elastin, fibronectins and laminins) and proteoglycans (heparan sulphate, hyaluronic acid and keratin sulphate). The main site of secretion and assembly of these proteins are fibroblasts, which form the framework of the mechanical structure of the tissue network (Murarka & Movahed, 2010). The heart is composed primarily of collagen, with fibrillar collagen types I and III found in the interstitium and nonfibrillar collagen types IV and VI, fibronectin and laminin found mainly in the basement membrane. Under normal physiological conditions, the ECM

is regulated through degradation and remodelling by numerous enzymatic proteins such as matrix metalloproteinases (MMPs), tissue inhibitors of metalloproteinases (TIMPs), crosslinking transglutaminases and enzymes like lysyl oxidases (LOX) and lysyl like oxidases (LOXL) (Phillip et al., 2015). In the diabetic heart, increased left ventricular wall rigidity is a distinct feature of myocardial fibrosis, characterised by decreased LV function (Fan et al., 2012), which is attributed to the reduced activity of MMP and TIMPs resulting in ECM accumulation.

Additionally, diabetes increases the insoluble form of collagen, further stiffening the heart (Phillip et al., 2015). Fibrosis-related genes that increase myocardial content and ECM gene, type I, III, and VI expressions, especially collagen deposition, are often observed in human studies and are closely associated with LV diastolic filling disorders (Asbun & Villarreal, 2006). Diabetes-induced myocardial fibrosis coincides with increased levels of transforming growth factor β, which differentiates fibroblasts to myofibroblasts and increases collagen production (TGF-β1), its TGF-β receptor II and its downstream effector connective tissue growth factor (CTGF). A study by Yang et al. (2016) showed that LOX is regulated by TGF-β1, which is in turn interconnected to the phosphatidylinositol 3-kinase (PI3K)/Akt and SMAD pathways since TGF-β1 expression decreased when PI3K was inhibited (Yang et al., 2016).

1.5.2.3 Inflammation

In the diabetic heart, mild chronic inflammation is a common consequence of obesity, and clear evidence suggests that the activated inflammatory responses are a major contributor to DCM pathology (Lorenzo et al., 2013). During this process, several kinases are activated, such as P38 mitogen-activated protein kinases (p38-MAPK), nuclear factor-κB (NF-κB) and c-jun NH2, which mediates the inflammatory response linked to T2D and subsequent development of DCM (Kaneto, Nakatani, Kawamori, Miyatsuka, & Matsuoka, 2004, Nishida & Otsu, 2017). The activation of NF-κB is associated with the increased release of cytokines such as tumour necrosis factor alpha (TNF-α), which is often involved in heart damage, thereby intensifying adverse effects in the diabetic heart (Lorenzo et al., 2013). Apart from the pro-inflammatory response, increased expression of these kinases is further enhanced by increased circulating levels of triglycerides, LDL and VLDL lipoproteins (Nishida & Otsu, 2017). For example, in a study done by Gordillo-Moscoso et al. (2013), it was argued that in diabetic patients, vascular inflammation results from changes in lipid profile and not glycaemia (Gordillo-Moscoso et al., 2013).

In addition, the accumulation of data indicates an important inflammatory component in the pathogenesis of DCM, where plasma concentrations of inflammatory mediators such as TNF-α, IL-6, IL1-β and NF-κB, exacerbate insulin resistance, resulting in muscle cell contractile function. Also, excessive production of IL-6 has been shown to promote LV dysfunction during acute myocardial

infarction (D. Westermann et al., 2006). The inflammatory response appears to be associated with DCM development, but its presence and severity vary between the early and long-term stages of the disease (Ares-Carrasco et al., 2009). Additionally, Ares –Carrasco and co-workers (2009) showed myocardial fibrosis and apoptosis are characteristics of myocardial damage secondary to long-term experimental diabetes using normotensive and spontaneously hypertensive rats (SHR) with T1DM induced by streptozotocin. However, inflammation was modulated by the expression of anti-inflammatory molecules, IL-10, and antioxidants. Moreover, Westermann's study showed that increased cytokines lead to LV dysfunction in diabetic patients. This was observed through an inverse correlation between the maximum ventricular pressure rise (dP/dtmax) and TNF-α. Also, they observed increased cardiac protein levels of TNF-α, IL1-β and other pro-inflammatory cytokines like IL-6 and TGF-β (D. Westermann et al., 2006).

Some typical characteristics of DCM and hypertensive cardiomyopathy include functional and structural changes that contribute to the impairment of heart tissue. In addition, these findings suggest that activation of PPARα as a compensatory response to metabolic, apoptotic and hypertrophic impairment could reduce cardiac hypertrophy at such a stage of diabetes and hypertension. Therapeutics with PPARα agonists may have beneficial anti-hypertrophic effects on hypertensive DCM in this sense (Dirk Westermann et al., 2007). These interesting recent findings, using SHR without T1DM compared to T1DM, strengthen and expand previous suggestions in patients with T2DM, in which the presence of hypertension increased changes in myocardial and vascular cells observed in patients with diabetes. Therefore, DM-induced changes in myocardial cells and capillaries lead to myocardial cell injury, interstitial fibrosis, and impairment of systolic and diastolic ventricular function when diabetes and hypertension coexist.

In a mouse model of streptozotocin-induced DCM, the additive effect of diabetes and hypertension may explain the beneficial effects of antihypertensive drugs such as irbesartan, an antagonist of angiotensin type 1 receptors (Dirk Westermann et al., 2007). Additionally, evidence suggests that the production of monocyte chemotactic protein-1, which provides a molecular link between hyperglycaemia, inflammation and DCM, mediates cardiomyocyte apoptosis induced by hyperglycaemia (Chavali et al., 2013). Yu et al. indicated that diastolic dysfunction caused by hyperglycaemia might be mediated in part by the inhibitory factor of macrophage migration, suggesting that the NF-κB pathway may be involved (X. Y. Yu et al., 2011). In the same study, the authors also demonstrated the inhibitory factor effects of macrophage migration in the abnormal upregulation of G protein-coupled receptor kinase 2, which can be associated with the constant activation of β1-adrenergic receptors and the development of HF. Another critical factor in the modulation of inflammation during DCM development is the activation of RAAS, which augment Ang II expression whilst increasing vasoconstriction and

inflammation. Ang II may induce the release of cytokines, which also stimulate the production of PAI-1 and pro-inflammatory transcription factors, such as NF-κB, which in turn regulate the adhesion molecules (VCAM-1 and ICAM-1) and the expression of several cytokines, as mentioned above (Hernandez-Presa et al., 1997; Schieffer et al., 2000).

1.5.2.4 Apoptosis

Apoptosis, autophagy, and necrosis are three categories of cell death. Apoptosis is a highly controlled and programmed cell death process that causes intracellular suicide. Cell death is essential for proper tissue development, embryonic development, and normal cell turnover (Marín-García, 2016). Apoptosis causes significant cellular morphological, energy-dependent biochemical changes, including cell shrinkage, chromatin condensation, protein cleavage, DNA breakdown, plasma membrane blebbing, and apoptotic body formation. This can be initiated via intrinsic or extrinsic pathways (Blanco & Blanco, 2017). Several mechanisms such as hyperlipidaemia, oxidative stress, and hyperglycaemia may increase the rate of cardiomyocyte apoptosis in diabetics. Hyperglycaemia-induced cardiomyocyte apoptosis occurs through activation of caspase-3 stimulated by mitochondrial cytochrome-c (cyt-c).

Moreover, ROS-induced DNA damage induces p53-dependent apoptosis by inducing pro-apoptotic members such as Bcl-2-associated X protein (Bax) while inhibiting anti-apoptotic members of the Bcl-2 family, thereby stimulating the apoptosis mitochondrial pathway (Schilling & Mann, 2012). The pro-apoptotic protein Bax is induced and inserted into the mitochondrial membrane to form a channel for the release of cyt c / APAF-1/caspase-9 containing apoptosome complex. The caspase-3 effector cleaves cellular proteins and DNA and causes cell death. Activated caspase-3 may result in DNA fragmentation by activating specific nuclease caspase-3-activated DNase (CAD), allowing CAD to enter the nucleus, leading to fragmentation of DNA. As a result, the phosphatidylserine membrane, which is a phospholipid embedded in the cytosol-oriented plasma membrane, is inverted and exposed on the cell surface. Phosphatidylserine plays the role of an ‘eat me‘ signal, attracting the apoptotic cells (Blanco & Blanco, 2017).

1.5.3 Stage 3

1.5.3.1 Diastolic and systolic dysfunction

Left ventricular diastolic dysfunction is a major feature of DCM and occurs before systolic dysfunction. Diastole is the period during which the heart muscle cannot generate enough force to contract, returns to its non-contracted length, and cannot generate another force. Therefore, diastolic dysfunction begins when the heart fails to generate enough force to contract and relax rhythmically, and each cycle becomes long, slow, or incomplete (Zile & Brutsaert, 2002). Left ventricular diastolic function is measured by the transmitral Doppler (measuring mitral valve blood flow using Pulse wave Doppler) and TDI (Borghetti et al., 2018). The following parameters are used to measure the degree of diastolic function:

the early ventricular filling wave (E wave) and late ventricular filling wave (A wave), which are commonly reported as the (E/A) ratio, the isovolumetric relaxation time (IVRT), E-wave deceleration time (EDT) and A wave duration (A-dur) (Aneja et al., 2008). The degree of diastolic dysfunction is then characterised using the parameters mentioned above either as: normal pattern, impaired relaxation (grade I), psuedonormal pattern (grade II) or restrictive pattern (grade III), as shown in Figure 1.4. Patients presenting with grade I diastolic function show reduced E/A ratio <1, caused by decreased early and elevated late diastolic flows. Elevated IVRT and EDT are also observed in these patients. Patients with grade III diastolic dysfunction show an E/A ratio of >1 due to elevated left atrial pressure resulting from defective LV relaxation. Filling pressures are increased to maintain normal cardiac output, resulting in impaired LV relaxation. Additionally, grade III diastolic function is characterised by an E/A ratio of >2, leading to advanced diastolic HF (Gilca et al., 2017). Furthermore, the ratio between the early passive transmitral inflow velocity (E) and medial mitral annulus velocity (e') are used to measure changes in left ventricular filling pressure (Borghetti et al., 2018).

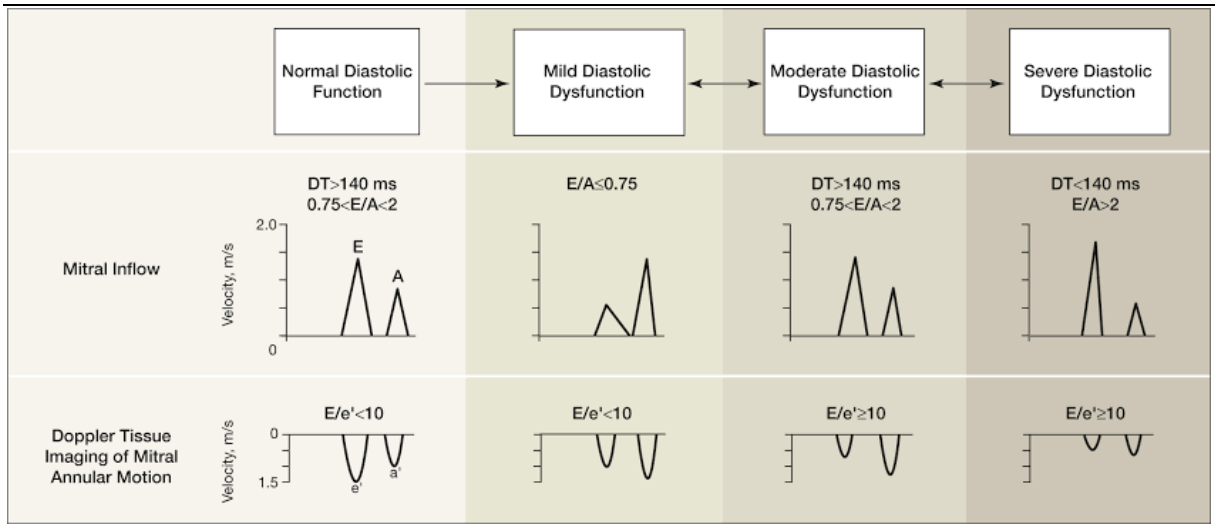

Figure 1.5: Echocardiographic classification of diastolic dysfunction. Showing the progression of diastolic dysfunction, from normal, impaired relaxation (grade I), pseudonormal (grade II), reversible restrictive (grade III), in the mitral inflow and TDI of mitral annular motion. (adapted from Bursi et al., 2017)

1.5.3.2 Left ventricular hypertrophy

Left ventricular hypertrophy (LVH), defined as the thickening and enlargement of the left ventricular muscles of the heart, is an important condition that develops in response to various stresses (Katholi & Couri, 2011). Hypertension is arguably the largest stressor associated with LVH. However, increasing evidence suggests that diabetes induces pathological responses that result in remodelling the left ventricle, leading to LVDD (Levy et al., 1996). LVDD can be detected using echocardiography, and studies conducted on diabetic patients using this technology confirmed a strong correlation between diabetes incidence, increased LV mass and LVH without the co-occurrence of hypertension (Boudina

& Abel, 2010; Murarka & Movahed, 2010; Schilling & Mann, 2012). It has been reported that LV mass indexes above 125 g/m^2 and 110 g/m^2 correlating to increased LVH in men and women, respectively. Moreover, obesity has been shown to increase the risk of LVH in the absence of elevated blood pressure. In line with this, it has been shown that cytokines secreted from adipose tissue tend to increase cardiac hypertrophy in high fat/Western diets(Anthony et al., 2019; Fuster et al., 2016). Furthermore, insulin resistance, accompanied by a compensatory hyperinsulinemic response, is one of the conditions associated with abnormal glucose metabolism and significantly affects the development of LVH (Nkum et al., 2014). As such, diabetes-induced LVH is associated with structural modifications characteristic of DCM. The latter results in an increase in a systemic inflammatory response, which is positively correlated with an increase in serum markers such as; fibrinogen, highly sensitive C-reactive protein (hs-CRP), and microalbuminuria. Increased levels of the inflammatory markers are associated with subclinical LVDD in patients with CVD risk (Masiha et al., 2013; Torun et al., 2012). Apart from inflammation, diabetes-induced oxidative stress can alter the function of the K_{ATP} channels in the myocardium, inducing cardiac hypertrophy by triggering an enzyme S6 kinase involved in myocardial remodelling (Masiha et al., 2013).

1.6. Treatment strategies for HF

1.6.1 Glycaemic control

In many clinical trials, effective glycaemic management is associated with improved outcomes for diabetic microvascular complications. In addition, studies focused on achieving glycemic control in animal models have been shown to delay the progression of DCM. For example, in a prospective study performed by Murarka & Movahed et al. (2010), strict glycaemic control in diabetic patients decreases the onset of ventricular dysfunction.

As such, medications such as glucagon-like peptide 1 (GLP-1) are used to manage glycaemic levels in people with diabetes. This drug has both biological and synthetic mimetic agents that have short and longer half-lives, respectively. The synthetic GLP-1 medications used for obese T2DM patients are linked to weight loss and glycemic control advances. These medications promote insulin secretion, increase nitric oxide-induced vasodilation, and increase the heart's glucose utilisation (Gupta, 2013; Lee & Kim, 2017; Y. Li & Rosenblit, 2018). Dipeptidyl peptidase 4 (DPP-4) inhibitors catalyse endogenous GLP-1 and prolong their effects. Sitagliptin use leads to glucose uptake in non-ischemic cardiomyopathy patients. In obese and insulin-resistant mouse models, DPP-4 inhibitors have been shown to prevent fibrosis and oxidative stress, thus preventing myocardial diastolic dysfunction and cardiac hypertrophy (Godinho et al., 2015; Gupta & Kalra, 2011). However, the role of these inhibitors in DCM is not fully understood.

Metformin is a first-line anti-diabetic drug that improves glucose uptake via the insulin-independent AMPK signalling pathway. Metformin increases cardiac autophagy and ameliorates the effects of DCM in animal models (Inzucchi, 2005; Lee & Kim, 2017). Metformin was also shown to reduce mortality while improving the clinical outcomes in overweight patients with HF and T2DM, regardless of the increased risk of lactic acidosis (Ingelsson et al., 2010). However, the effectiveness of Metformin in protecting diabetic myocardium declines over time. In contrast to the latter, Whittington et al., 2013 demonstrated that chronic exposure to metformin could be cardioprotective through the AMP-activated protein kinase (AMPK)/ peroxisome proliferator-activated receptor gamma coactivator 1-alpha (PGC-1α)/ mitofusin 2 (Mfn-2) pathway (Whittington et al., 2013). In rat hearts, administration of metformin caused increased AMPK activity, which is thought to be behind the metformin's cardioprotective effects, led to the reduction of infarct size (Solskov et al., 2008). A study conducted on leptin receptor deficient db/db mice showed that administering metformin in low doses at the time of reperfusion, increases chances of survival and protects the heart against ischemia-induced HF by ameliorating mitochondrial function through the AMPK pathway in conjunction with endothelial nitric oxide synthase (eNOS) and PGC-1α (Gundewar et al., 2009).

1.6.2 Lifestyle changes

Patients with type 2 diabetes suffer from uncontrolled cardiovascular and metabolic functions such as dysglycaemia, dyslipidaemia, arterial hypertension, obesity and reduced cardiorespiratory fitness (CRF) (Kemps et al., 2019). There is crosstalk between these functions, which are further influenced by the patient's lifestyle, genetic and epigenetic background. An inactive lifestyle encourages adipose tissue lipid storage, where chronic excess calorie intake exceeds energy expenditure through exercise (Figure 1.5) (Vettor & Conci, 2017). Due to this, plasma free fatty acid levels increase, causing cellular stress such as peripheral insulin insensitivity, elevated inflammatory activation in diverse tissues, vasculature dysfunction and skeletal muscle metabolism. Therefore, regular physical activity and a balanced diet can ameliorate DCM (Pappachan et al., 2013).

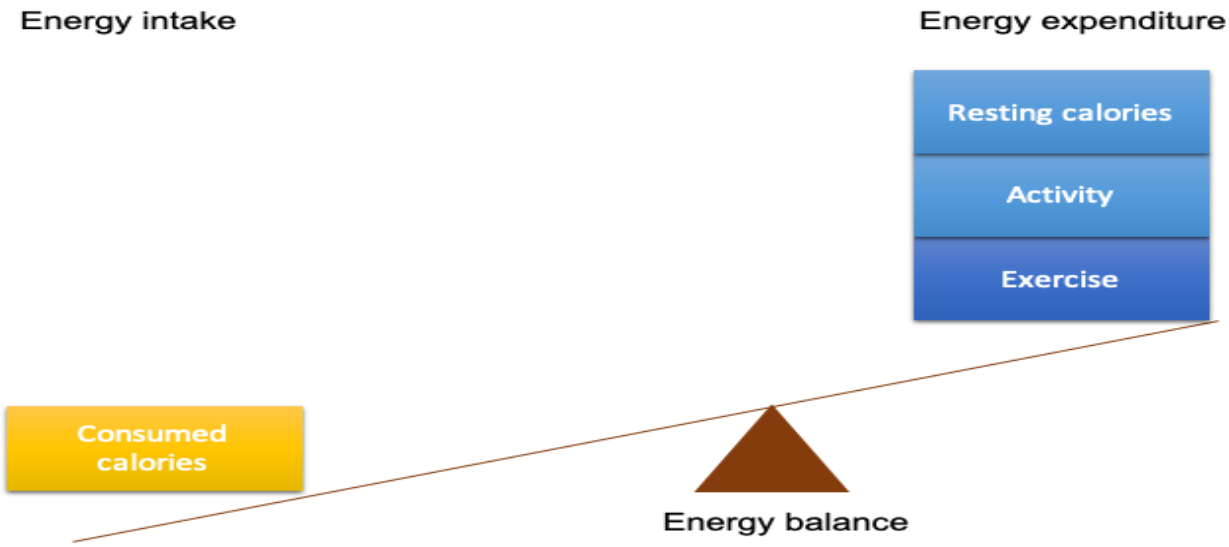

Figure 1.6: Energy imbalance in T2DM patients resulting from the accumulation of calories due to energy not being expended in exercise, activities and increased resting calories

1.6.5 Lipid-lowering medications

Statins are blood lipid-lowering medications used in diabetics because of their high likelihood of developing atheroma. Low-density lipoprotein cholesterol (LDL-C) particle size is reduced in diabetic individuals and is a risk factor for atherogenic events with almost normal plasma levels. Statins reduce cardiovascular mortality and events in diabetic patients, including vascular risk factors in many clinical trials (Chogtu, 2015; Karlsson et al., 2018). A study by Al-Rasheed and co-authors (2017) on diabetic rat hearts showed simvastatin stopped hyperglycaemia/hyperlipidaemia-induced oxidative stress and increased antioxidant defences (Al-Rasheed et al., 2017). Chronic use of fluvastatin treatment has been shown to reduce cardiac dysfunction in rats with streptozotocin-induced DM, which was thought to be attributed to reduced oxidative stress (Shida et al., 2014). Additionally, statins are helpful as a first-line medication to prevent the establishment of cardiovascular disease. Atorvastatin decreases myocardial fibrosis, intra-myocardial inflammation and ameliorates LV function in rat models of DCM without its LDL-C lowering effect (Akahori et al., 2014; Antonopoulos et al., 2012). Simvastatin and fluvastatin have been shown to have a cardioprotective effect on DCM (Al-Rasheed et al., 2017; Shida et al., 2014).

1.6.6 Sodium-glucose cotransporter 2 (SGLT2) inhibitors

There is increasing evidence that SGLT2 inhibitors possess both reno- and cardioprotective effects. Trials using SGLT2 inhibitors have shown approximately 30% reduced risk of hospitalisation due to HF and reduced risk of CV related mortality. This was more pronounced in patients with systolic dysfunction before treatment (Packer, 2020). Sodium-glucose cotransporter inhibitors achieve reno- and cardioprotection by stimulating a transcriptional response mimicking cellular starvation, inducing

sirtuin 1 (SIRT1)/AMPK and inhibiting protein kinase B (Akt)/ mammalian target of rapamycin (mTOR) signalling, promoting autophagy without glucose or insulin and activate low energy sensors without affecting SGLT2 proteins. Furthermore, they trigger SIRT1/AMPK and inhibit Akt/mTOR signalling, causing a decrease in oxidative stress, ameliorating mitochondrial structure and function while repressing inflammation, restricting coronary microvascular injury, and increasing activity contractile performance and halting the development of cardiomyopathy. Also, the AMPK/SIRT1 induction and autophagic flux are associated with the downregulation of ion exchangers involved in the pathogenesis of diabetic renal and cardiac diseases (Packer, 2020).

Additionally, other findings have linked SGLT2 inhibitors to myocardial ion homeostasis in T2DM, also protecting the heart against myocardial remodelling (Kaplan et al., 2018). It was recently demonstrated that SGLT2 inhibitor empagliflozin inhibits the sodium hydrogen exchanger in cardiomyocytes, resulting in decreased cytoplasmic Na^{+} and Ca^{2+} levels while synergistically causing an increase in mitochondrial Ca^{2+} levels. However, since the heart lacks SGLT2 receptors, the mechanism by which sodium hydrogen exchanger functions in cardiomyocytes is still unknown (Verma & McMurray, 2018). Results from the Empagliflozin Cardiovascular Outcome Trial in Type 2 Diabetes Mellitus Patients (EMPA-REG OUTCOME) showed reduced primary composite myocardial outcome and death versus placebo use, with genital infections being the primary side effect (Striepe et al., 2017). Dapagliflozin was shown to confer cardioprotection in angiotensin II stressed diabetic mice. This resulted in decreased ROS and regulated Ca^{2+} transport through its membrane channels. Additionally, there was reduced fibrosis and inflammation due to the cardioprotection while systolic function was ameliorated (Arow et al., 2020). Another side effect associated with SGLT2 inhibitors is diabetic ketoacidosis (DKA), although it has been observed in 2 in 1000 patients (Fralick et al., 2021). Taken together, even though there are treatment strategies that are available for T2DM individuals that could aid early corrective treatment of these individuals, early detection at the asymptomatic stage is currently a hurdle that has to be overcome. One of the ways in which this would be made possible is by discovering biomarkers that would be sensitive and specific for the detection of DCM at its asymptomatic stage.

1.6.7 Angiotensin receptor neprilysin inhibitor (ARNI)

Angiotensin receptor neprilysin inhibitor (ARNI) constitutes of neprilysin inhibition and angiotensin type 1 receptor blockade (A. H. Kim et al., 2022). All biological active natriuretic peptides including atrial natriuretic peptide (ANP), B-type natriuretic peptic and C-type natriuretic peptide) are inhibited by the neprilysin inhibitor while the angiotensin type 1 receptor blockade inhibits the renin angiotensin system (Wachter et al., 2020). ARNI has been shown to have therapeutic effects in patients with Heart failure with reduced ejection fraction (HFrEF) as validated by the Prospective Comparison of Angiotensin Receptor–Neprilysin Inhibitor with Angiotensin-Converting–Enzyme Inhibitor to

Determine Impact on Global Mortality and Morbidity in Heart Failure (PARADIGM-HF) trial, which showed at 20% reduction in CVD mortality or hospitalization with ARNI administration (Y. Wang et al., 2019). However, the PARAGON-HF study showed no significant differences in both the rate of hospitalization and CVD mortality in patients with HFPEF (Solomon et al., 2019).

1.6.8 Angiotensin-converting enzyme inhibitor (ACEi) and angioten receptor blockers (ARBs)

Angiotensin II (ANG II) is a vasoconstrictor that also stimulates the production of the proteins causing cardiomyocyte hypertrophy and the formation of collagen in the fibroblasts culminating in myocardial fibrosis. ACE inhibitors inhibit the conversion of angiotensin ANG I to ANG II, thus reducing it levels in the circulatory system and tissue concentration (Bell & Goncalves, 2019). Additionally, ACE inhibitors increase the production of bradykinin and prostacyclin level which leads to nitric oxide (NO) release causing the reduction of both cardiomyocyte hypertrophy and myocardial fibrosis.

ARBs also reduce the impact of ANG II on the cardiovascular system and inhibit the interaction of ANG II with its angiotensin II type 1 receptor (AT 1) (Kanwar et al., 2016). ABRs are commonly prescribed to patients with no tolerance for ACE inhibitors or ARNI due to adverse effects that these have. However, no study has shown decreased in all-cause mortality following the use of ARBs (Yusuf et al., 2003)

1.6.9 Beta blockers

Both beta blockers and ACE inhibitors have been shown to reduce mortality and hospitalizations in patients with diabetes mellitus. In contrast to non-selective beta-blockers which have adverse effects on glycaemic control and increased probability of future diabetes, selective beta blockers (bisoprolol, carvedilol and nebivolol) have reduces occurrences of these (Rosano et al., 2017). However, the use of beta blockers has been linked to hypoglycaemia and increased probability of cardiovascular events in diabetic patients (Tsujimoto et al., 2017). In HF patients with an EF of 50% or more, β-blocker usage was linked to elevated risk of hospitalizations (Silverman et al., 2019).

1.7 Current diagnostic methods

Recent data suggest that non-invasive imaging techniques, for DCM diagnosis, are available in clinical practice (Korosoglou & Humpert, 2007). They provide structural and functional information related to tissue and organ physiology. They provide information on early detection concerning disease pathology, progression and interventions (Maya & Villarreal, 2010). In clinical settings, echocardiography is regarded as a diagnostic method for detecting early changes of myocardial structure and function and is especially relevant in DCM (Korosoglou & Humpert, 2007). A recent publication in Cardiovascular Diabetology by Lorenzo-Almorós and co-workers gave a brief discussion on the primary imaging systems used to detect DCM, as well as the drawbacks associated with each technique (Lorenzo-Almorós et al., 2017). This section summarises these modalities and additional information relevant to their use in a clinical setting.

1.7.1 Echocardiography

Echocardiography is a non-invasive diagnostic tool for detecting structural cardiac alterations and is the current gold standard for detecting DCM. Using this technique, early functional changes in diastolic filling and ventricular hypertrophy can be observed (Nishimura & Tajik, 1997). Conventional Doppler uses 2-dimensional (2D) imaging which allows calculation of the E/A ratio. Its reduction is essential for detecting increased LV mass and diastolic dysfunction, a prominent phenotype of DCM (Lorenzo-Almorós et al., 2017). While Tissue Doppler Imaging (TDI) detects early LVDD, Speckle tracking echocardiography (STE), on the other hand, is a qualitative and quantitative analysis of tissue degeneration and motion. Speckle tracking echocardiography is used to measure the speckle in relation to interference patterns and acoustic reflection in 2D and 3D echo images (R. Li et al., 2014), where LV dysfunction is observed through longitudinal and circumferential strains.

In the late and middle stages of DCM, diastolic and systolic dysfunction are observed respectively using strain-to-strain rate. Both TDI and STE have been used in both animal and human studies. Although previously identified at 12 and 18 weeks in rats, echocardiography assessment has shown that LV systolic dysfunction coupled with reduced velocity of circumferential fibre shortening may develop 30 days after induction of T2DM using streptozotocin (Wichi et al., 2007). In human studies, a cohort of 1030 type 2 diabetic patients, echocardiographic abnormalities were recorded in 49.8% of patients, LV hypertrophy (21%), left atrial enlargement (19.6%), and mainly associated with a high prevalence of diastolic dysfunction (19.4%) (Jørgensen, Jensen, Mogelvang, et al., 2016). Using STE, Loncarevic and colleagues demonstrated that in comparison with nondiabetic subjects, diabetic patients without hypertension or coronary disease displayed increased LV mass, impaired LV relaxation and lower LV

ejection fraction (Loncarevic et al., 2016). However, echocardiography has been shown to have limitations overcome by other diagnostic imaging methods such as MRI.

1.7.2 Magnetic resonance imaging

Magnetic resonance imaging has a broader range of spatial and temporal resolution for evaluating LV ejection fraction and myocardial mass distribution, which echocardiography lacks. For example, the gradient-echo-MRI and phase-contrast-MRI produce a display of the cardiac cycles by radiofrequency pulses and electrocardiogram. This includes visualization of moving fluids and heart valve velocities (Ferreira et al., 2013). Diastolic dysfunction and LV mass are observed using phase MRI in the early, middle and late stages of disease progression, respectively (Table 1.2). Another example is tagged-MRI, which detects cardiac abnormalities through radiofrequency pulses along cycles using strain rates and torsion recoveries (Moore et al., 2000). Increased LV mass and volume is observed in the middle stage and diastolic dysfunction in the late stage (Widya et al., 2013). Nevertheless, a few drawbacks associated with MRI have been identified, including its tendency to cause claustrophobia, its limited use on pacemaker patients, and its underestimation of diastolic dysfunction as reviewed by Lorenzo-Almorós (Lorenzo-Almorós et al., 2017).

Magnetic resonance imaging studies performed four weeks after the induction of T2DM in mice have shown significant myocardial morphology and functionality deficits. These defects include increased LV end-systolic diameter and volume, reduced LV ejection fraction and cardiac output, decreased LV circumferential shortening as well as diminished LV peak ejection and filling rates (Shah et al., 2014). Despite slight recording of LV volumes, mass and ejection fraction and echocardiographic indices of diastolic function when using echocardiography, MRI has detected impaired LV dysfunction and reduced peak systolic circumferential strain in these patients. Furthermore, these findings were consistent with impaired myocardial energy metabolism and steatosis in these patients. These results suggest that MRI can be a powerful technique to assess LV remodelling and information relevant to fibrosis, intramyocardial motion, triglyceride content, and myocardial energetics (Lorenzo-Almorós et al., 2017; Shah et al., 2014). However, as with echocardiography, the precise time of development of these complications in diabetic subjects is inconsistent.

1.7.3 Multi-slice computed tomography and nuclear imaging techniques

Multi-slice computed tomography (multi-slice CT) and nuclear imaging are increasingly being studied as imaging modalities for detecting DCM. Multi-slice CT calculates ventricular function parameters by assessing changes in cardiac volume. This is accomplished by using reconstructed X-ray images for cross-sectional tomography. Multi-slice computed tomography can detect end-stage DCM by measuring calcification and systolic dysfunction (Barsanti et al., 2015; Bax et al., 2007). Although

radiation exposure and the use of contrast media may influence multi-slice CT to diagnose DCM, it has emerged as one of the most exciting technological revolutions in cardiac imaging as it can successfully detect ischemic heart disease. It has also been suggested that the X-ray tomography technique can be more suitable in pre-clinical studies in which animals are terminated post-experiments to avoid the probability of cancer due to radiation exposure (Kalisz & Rajiah, 2017). Therefore, the rapid developments in multi-slice CT scanners have made it possible for them to be potentially used in patients with suspected DCM cases over the last few years.

Some nuclear imaging techniques used to measure cardiac autonomic dysfunction include gated-single photon emission computed tomography (G-SPECT) and positron emission tomography (PET). G-SPECT uses γ- emitting radioisotopes and the electrocardiogram to acquire heart contractions over the interval from one early ventricular depolarization (R wave) to the next, while PET extricates γ-rays emitted indirectly by a positron-emitting radionuclide and formulates 3D images by computer tomography analysis (Barsanti et al., 2015). Both G-SPECT and PET detect early metabolic changes and perfusion changes in the late stage. As with multi-slice CT, limited research has been reported on the potential use of nuclear imaging to detect early-stage cardiac complications associated with DCM. However, these imaging techniques are also not freely available to prediabetic and T2DM patients to assess the possible occurrence of DCM. This is due to high costs and a lack of trained personal, especially in resource developing countries.

Table 1.1 Summary of imaging techniques, their advantages and disadvantages

Imaging technique	Advantages	Disadvantages
Echocardiography	Observe changes in diastolic filling and ventricular hypertrophy. Conventional Doppler has parameters to calculate the E/A ratio used to detect LV mass and diastolic dysfunction. STE measures speckle resulting from interference patterns and acoustic reflection in 2D and 3D images. STE conducts a qualitative and quantitative analysis of tissue degeneration and motion. Longitudinal and circumferential strains show the degree of LV dysfunction. Stain to strain rate measures diastolic and systolic dysfunction in the middle and late stages of DCM. TDI and STE can be used in early DCM detection.	No spatial and temporal resolution
Magnetic resonance imaging	Contains spatial and temporal resolution to evaluate LV ejection fraction and myocardial mass distribution. Gradient-echo-MRI and phase-contrast-MRI use radiofrequency pulses and electrocardiogram to show cardiac cycles, myocardial valve velocity and moving fluids. Phase MRI gives a clear indication of diastolic dysfunction and LV mass in all phases of disease progression.	May cause claustrophobia. Pacemaker patients cannot use it. Underestimates diastolic dysfunction. Multi-slice computed tomography detects end-stage DCM.

	Tagged MIR uses radiofrequency pulses, strain rates and torsion recoveries to detect cardiac abnormalities. Early metabolic changes and late perfusion alteration can be detected using G-PECT and PET	
Multi-slice computed tomography and nuclear imaging	Calculates ventricular function through cardiac volume changes by making x-ray images	Radiation exposure

1.8 Potential biomarkers for DCM

1.8.1 Biomarkers and their significance

Biomarkers are defined as measurable features of an organism that represents a particular physiological state. In medical research, biomarkers are often molecules released within bodily fluids, such as serum, urine or blood, used for disease identification. Biomarkers have several functions. They enable early and timely detection of the condition, act as an indicator of disease prognosis and monitor response to interventions (Strimbu & Tavel, 2010). While conventional diagnostic methods like echocardiography may be specific and sensitive, this non-invasive diagnostic point of care tool is not always routinely used due to the healthcare-related cost. Ongoing research has been conducted in many fields for biomarker discovery, including Alzheimer's disease (Hampel et al., 2018), periodontal disease (Tsuchida et al., 2018) and cancer (Bratulic et al., 2019) in search for biomarkers that would detect these diseases at their inception stages. An example of this is the breast cancer type 1 susceptibility protein (BRCA1/BRCA2), which has been used to detect breast cancer development (Przybytkowski et al., 2020; Walsh et al., 2016). Similarly, in DCM, a few biomarkers have been associated with detecting this disease and are reviewed below.

1.8.2 Metabolic biomarkers

1.8.2.1 Insulin-like growth factor binding protein 7 (IGFBP-7)

Insulin-like growth factor-binding protein 7 (IGFBP-7) is a protein that modulates the structure of insulin-like growth factor 1 (IGF-1). This adaptive response is associated with increased expression of IGFB-7 and IGF-1 and blocks downstream PI3K/AKT signalling, which is important for insulin signalling. Compared to IGFBP, IGFBP-7 has a lower binding affinity to IGF-1 (Evdokimova et al., 2012; Verhagen et al., 2014). Serum IGFBP-7 levels were found to be increased in patients with heart failure with reduced ejection fraction (HFrEF) and heart failure with preserved ejection fraction (HFpEF) (Hage et al., 2018). Therefore, IGFBP-7 is an interesting biomarker, especially for individuals with HFpEF (Barroso et al., 2016). Furthermore, IGFBP-7 has been correlated with diastolic dysfunction, one of the important traits of HFpEF, to insulin resistance and risk of metabolic syndrome, which was linked with chronic low-grade inflammation (Piek et al., 2018).

1.8.3 Cardiac biomarkers of contractility in DCM

1.8.3.1 Cardiac troponins

Troponin is a complex of three proteins secreted in the blood in response to cardiac muscle injury. These proteins include Troponin I (TnI), C (TnC) and T (TnT) in striated muscles. Troponins modulate Ca^{2+} mediated contact between actin and myosin. TnC is the Ca^{2+} binding subunit in the complex, and its interaction with TnI and TnT is essential for myocardial contraction (Johnston et al., 2017). TnT regulates the interaction of the different troponin complexes with the thin filaments, while TnI

inhibits ATP-ase activity of actomyosin. TnI and TnT myocardial specific isoforms are sensitive necrosis markers and are routinely used in clinical practice. Furthermore, in human myocardial biopsies, TnI and TnT are known to be phosphorylated, causing reduced myofilament function and Ca^{2+} sensitivity (Varughese et al., 2010; Vikhorev & Vikhoreva, 2018). Apart from the troponins, Activin A has also been shown to regulate heart contractility.

1.8.3.2 Activin A

Autocrine and paracrine molecules may be released by epicardial adipose tissue (EAT). Interestingly, isolation of these secreted factors in patients with T2DM induced contractile dysfunction and insulin resistance in primary rat cardiomyocytes (Wu et al., 2012). Protein kinase B/Akt is a key regulator of myocardial glucose uptake and activates an insulin-mediated phosphorylation by activin A and angiopoietin-2. Activin A, which belongs to the TGFβ family, is released by T2DM patients from cultivated EAT biopsies that inhibited insulin action through Akt pathway blockage (Lin et al., 2016). In T2DM patients, plasma activin A levels were indirectly proportional to myocardial glucose metabolism and proportional to LV mass, reflecting this molecule‘s unfavourable role in early human DCM (Fitzpatrick et al., 2009).

Table 1.2 Summary of biomarkers associated with DCM

Biomarker type	Examples	Preclinical detection
Metabolic biomarkers	IGFBP-7	Yes
Biomarkers of contractility	TnI, TnC and TnT	No
	Activin A	Yes
Biomarkers of hypertrophy	NT-proBNP, ANP	No
	CT-1	Yes
	ST2L and sST2	No
Pro-steatosis myocardial biomarker	H-FABP	Yes
Fibrosis associated biomarkers	Gal-3	Yes
	HE4	No
	MMPs	No
	GDF-15	No
	CHI3L1 or YKL-40	No

1.8.4 Biomarkers of hypertrophy

1.8.4.1 Natriuretic peptides

Diabetic-induced hypertrophy is a condition within the myocardium that increases protein synthesis and reactivation of foetal genes. This adaptive response is associated with increased expression of atrial natriuretic peptide (ANP) and β-myosin heavy chain (Table 1.3). However, the perpetual expression of these responses leads to myocardial dysfunction. Therefore, early detection of pro-hypertrophic inducers could aid in the prognosis of subclinical DCM. As such, the natriuretic peptide family, brain natriuretic peptide (BNP) and N-terminal proBNP (NT-proBNP) have been linked to increased HF incidence (Nakagawa et al., 2018; Nishikimi et al., 2006). However, the half-life of BNP is about 20 minutes and is higher than that of ANP, while NT-proBNP remains in the system longer than 120 minutes (Raizada et al., 2007). Since ANP clears faster in the system, BNP and NT-proBNP are thus used as biomarkers. Elevated NT-proBNP levels have been associated with 96% of cases of T1DM patients, while increased ANP levels have been shown after early diastolic dysfunction. Nonetheless, both peptides could only detect diastolic dysfunction in symptomatic diabetic patients with restrictive filling or pseudonormal mitral flow and not in asymptomatic patients (Dahlström, 2004; Nakagawa et al., 2018).

1.8.4.2 Cardiotrophin-1 (CT-1)

Another biomarker that has been investigated extensively is cardiotrophin-1 (CT-1), which belongs to the gp130 cytokine family. CT-1 is produced primarily from cardiomyocytes after oxidative and mechanical stress or renin-angiotensin-aldosterone (RAA) system and is currently being explored as an alternative biomarker. Cardiotrophin-1 can control myocardial hypertrophy, fibrosis, contractility and ischemia by lowering cell proliferation, apoptosis, oxidative stress, and inflammation because of janus kinase/signal transducer and activator of transcription (JAK/STAT) and mitogen-activated protein kinase (MAPK) pathways. In addition, Cardiotrophin-1 has been reported to stimulate cardiovascular remodelling and HF (Abdul-Ghani et al., 2017; Hishinuma et al., 1999). CT-1 is also a key regulator of myocardial glucose metabolism by elevating insulin-stimulated glucose uptake. In T2DM patients, elevated CT-1 levels are proportional to basal glycaemia and left ventricular hypertrophy. Additionally, increased CT-1 levels have also been shown in patients showing impaired glucose tolerance or those newly diagnosed with diabetes (Abdul-Ghani et al., 2017; Watanabe et al., 2018). Conversely, low concentrations were shown in non-diabetic obese and overweight individuals. CT-1 expression is not limited to DCM, and increased expression has been demonstrated in other cardiomyopathies such as in ischemia (Brar et al., 2001).

1.8.4.3 Suppression of Tumorigenicity 2 (ST2)

ST2 is a member of the interleukin-1 receptor family, which is expressed in the fibroblasts, ventricular endothelial cells and cardiomyocytes. There are two forms: a membrane-bound (ST2L) and a soluble circulating form (sST2) (Aimo et al., 2017; Gül et al., 2017). Interleukin-33 (IL) 33 is a ligand for ST2 that is a mediator of inflammation in several diseases like asthma, rheumatoid arthritis, pulmonary fibrosis and collagen disease (Gül et al., 2017). The IL-33/ST2 system has also recently been shown to play a role in CVD pathogenesis. The ST2L is an interleukin-33 that reduces fibrosis and hypertrophy in response to cardiac stress. In *in vivo* and *in vitro* models have shown that ST2L transduces the effects of interleukin-33, while surplus soluble sST2 is associated with cardiac fibrosis and ventricular dysfunction (Aimo et al., 2017). Both ST2L and sST2 are upregulated in fibroblasts and cardiomyocytes after myocardial infarction.

1.8.4.4 Human epididymis protein 4 (HE4)

The human epididymis protein 4 (HE4), also known as the wap four-disulphide core domain 2 (WFDC2 or WAP-4C), is a novel biomarker showing prognostic value in acute heart failure (Piek et al., 2017, 2018). The primary function of HE4 has yet to be elucidated but is currently associated with increased fibrosis (Zhang et al., 2018). In acute and chronic HF patients, the amount of HE4 expressed has been correlated to its severity. At the same time, the expression of HE4 s and Gal-3 were associated with organ fibrosis. However, increased HE4 serum levels have also been associated with tissue and organ injury other than from HF, such as ovarian cancer and chronic kidney disease (Piek et al., 2017; Zhang et al., 2018). This marker is not specific to heart failure as increased HE4 plasma levels were linked with several cancer types, including ovarian cancer and chronic kidney disease (CKD) (Innao et al., 2016; Nagy et al., 2012).

1.8.4.5 Matrix metalloproteinases (MMPs)

The matrix metalloproteinases (MMPs) are a family of extracellular proteins regulated by inflammatory signals to mediate changes in the extracellular matrix. MMPs are important in vascular remodelling and play a key role in advancing atherosclerotic plaque rupture and the development of cardiomyopathy.

As such, there are different groups of MMPs, namely interstitial collagenases (MMP-1, -8, -13, and -14), stromelysins (MMP-3, -7, -10, and -11) and macrophage elastase (MMP-12). MMP-2, MMP-8, and MMP-9 have been identified as proteases that form part of the atherosclerotic plaque rupture and clinical events by degrading structural components of the plaque matrix (Naito et al., 2009). However, tissue inhibitor of MMP (TIMPS) antagonists prohibits their activity and TIMP-1 and MMP-9 are linked with CVD death, HF or both (Papazafiropoulou & Tentolouris, 2009). MMP-9 is elevated in myocardial fibrosis and HF. In mice, pharmacological and genetic inhibition of MMPs improves cardiac remodelling (Yamamoto & Takai, 2009). MMP-2 also increases post-myocardial infarction and is an independent predictor of all-cause mortality in post-acute coronary syndrome (DeLeon-Pennell et al.,

2017). Increased MMP-2 levels are concomitant to ischemic cerebrovascular events (H. Y. Kim & Han, 2006). Contrary to MMP-2, elevated MMP-8 levels are linked to unstable plaque phenotype. MMP-7 and MMP-12 plasma levels are increased in T2DM and are associated with severe atherosclerosis and elevated CAD events (Olejarz et al., 2020).

1.8.4.6 Growth differentiation factor-15 (GDF-15)

The growth differentiation factor-15 (GDF-15), also known as macrophage inhibitory factor-1, is a divergent member of the transforming growth factor-β cytokine superfamily, known for reflecting vascular endothelium damage resulting from oxidative stress and inflammation (Kumric et al., 2021). GDF-15 has been shown to predict mortality and CVD events in community-dwelling elderly individuals and patients who undergo cardiac surgery (L. Daniels et al., 2011; Doerstling et al., 2018). However, little research has been done on GDF-15 in diabetes. GDF-15 levels have been reported to increase T1DM and have been independently linked with CVD hospitalization or mortality (Adela & Banerjee, 2015). In the Relaxin for the Treatment of Acute Heart Failure (RELAX-AHF) study, patients with acute HF showed elevated GDF-15 levels, correlated with increased adverse outcomes (Cotter et al., 2015).

1.8.4.7 Chitinase-3-like protein 1 (CHI3L1 or YKL-40)

Chitinase-3-like protein 1 (CHI3L1 or YKL-40) is a glycoprotein whose plasma levels are increased in diabetic or obese patients, including those with myocardial infarction. Plasma levels are proportional to the insulin resistance of and fatty acids and triglycerides in T2DM patients. YKL-40 plays a role in the proliferation and differentiation of cells and can protect the heart by stopping inflammation, apoptosis, tissue remodelling and fibrosis. YKL-40 is a p38 and JNK MAPK inhibitor that inhibits TNF-α-and IL-1-induced inflammatory responses, reducing MMP expression. YKL-40 production is controlled by NF-kB and the protein specificity 1 (Sp1). SP 1, PPARα and nuclear receptor subfamily 2 group F member 2 (NR2F2) are involved in reducing FA usage in the hypertrophied heart. Therefore, YKL-40 is a prospective DCM biomarker, which could be used to prevent or treat the established condition.

However, although there are several biomarkers linked to DCM, they have not been used commercially or as drug targets for improving diabetic cardiomyopathy. Most biomarkers can detect DCM, but there is still an avenue of DCM that requires extensive study, which is its asymptomatic stage because most DCM biomarkers are either sensitive or specific and seldom fulfil both criteria. Early identification of DCM at the asymptomatic stage would enable corrective treatment for these patients, thus preventing the progression of the disease to the HF stage in which nothing can be done to remedy both functional and structural changes in the heart. From the biomarkers reviewed above, the following biomarkers show promise in forming part of the biomarker panel: IGFBP-7, Activin A, CT-1, H-FABP, and Gal-3

has been associated with the early stage of DCM, sST2 an indicator of diastolic dysfunction, and HE4 is a fibrosis marker, although not specific to DCM or CVDs.

1.8.5 Pro-steatosis myocardial biomarkers for DCM

1.8.5.1 Heart-type fatty acid-binding protein (H-FABP)

Fat deposition in the myocardium might be a protective response to provide fuel storage for oxidation and prevent exposure to harmful lipid metabolites like ceramides. In DCM, an imbalance between lipid storage and lipid oxidation can cause mechanical dysfunction. Lipid droplet quantification in cardiomyocytes using MRI has been linked to cardiac steatosis. However, it could not be correlated to diastolic dysfunction (Lorenzo-Almorós et al., 2017). For this reason, pro-steatosis factors released from the myocardium could aid in early DCM identification. Heart-type fatty acid-binding protein (H-FABP) is a 15 kDa cytoplasmic protein that balances long-chain fatty acid in myocardial tissues. H-FABP is mainly expressed in the skeletal muscle, liver, kidney and myocardial tissue.

Compared to cardiac troponin, which has a shorter half-life, H-FABP is observed in the bloodstream for approximately 12-14 hours (Suresh et al., 2018). H-FABP shuttles fatty acids to the mitochondria for catabolism and ATP production. After lipid transport, H-FABP is upregulated and found in the sarcolemma but cannot be detected in the serum of healthy individuals. Following myocardial injuries like myocardial infarction, systolic dysfunction or HF, H-FABP is released into the plasma. Remarkably, H-FABP's presence leads to early myocardial injury in T2DM patients (Ho et al., 2018; Lorenzo-Almorós et al., 2017). However, although sensitive to DCM, this biomarker lacks specificity for this disease state.

1.8.6 Fibrosis associated biomarkers

1.8.6.1 Galectin-3 (Gal-3)

During DCM development, extracellular matrix (ECM) protein deposition impairs contractility and ultimately leads to cardiac stiffness and advancement towards HF. Therefore, ECM proteins could be useful biomarkers for early identification, diagnosis, and prevention of fibrosis in DCM. The galectin-3 (Gal-3) is a member of the lectin family proteins, and its expression is increased in multiple organs, including the heart and is involved in the development of fibrosis. Elevated plasma Gal-3 levels have been observed in HF and DCM and are linked to cardiac dysfunction and reduced LV filling pressures (De Boer et al., 2011). Animal studies confirmed the involvement of Gal-3 in cardiac remodelling with both knockdown and pharmacological restriction of Gal-3, culminating in decreased myocardial remodelling and fibrosis. Since HF affects multiple organs, these organs could indirectly increase Gal-3 plasma levels in HF patients. Gal-3 is expressed in multiple organs and various cell types such as macrophages, eosinophils, neutrophils, and mast cells (De Boer et al., 2010, 2011). Several animal

studies have shown that Gal-3 is involved in renal fibrosis, chronic obstructive pulmonary disease (COPD), and many cancer types (Feng et al., 2017).

Thus, plasma Gal-3 levels correlate with increased cardiac Gal-3 production as well as concomitant multi-organ and tissues and comorbidities like obesity (Suthahar et al., 2018). Regrettably, both clinical and animal studies linking Gal-3 to HF have given conflicting outcomes. Some clinical studies have shown that Gal-3 levels were not proportional to echocardiography parameters. In patients with dilated and inflammatory cardiomyopathy, biopsy results did not correlate to plasma levels. Gal-3 is not cardiac, and it is unknown which organs and/or tissues lead to elevated plasma levels and how much HF contributes (Filipe et al., 2015; Meijers et al., 2016). However, de Boer and co-workers reported that Gal-3 had a strong predictive value for heart failure with preserved ejection fraction independent of NT-proBNP (De Boer et al., 2011).1.9

1.9 Rodent models of T2DM

Rodents, particularly mice and rats have been widely used to study the pathophysiological mechanisms underlying the development of DCM (Lee & Kim, 2021). This is owing to their genomes which are possess a 99% sequence homology to that of humans and both having about 30, 000 protein coding genes. Additionally, mice are the preferred model because of their short breeding cycle and the ability to alter their genetic code either to gain or lose function (Lee & Kim, 2021; Tate et al., 2019). Although there are numerous animal models that are covered with respect to T2DM, in the present study we review the ones that could potential surrogates to study of DCM.

1.9.1 C57BLKS/J db/db mice

C57BLKS/J db/db mice have a mutation on chromosome 4 restricting the expression of the leptin receptor and are used to study metabolic abnormalities like obesity, dylipidemia and T2DM. Because of the vast differences in pathophysiology of T2DM the results obtained are comparable but cannot be fully translated to humans (Faita et al., 2018). However, these mice are characterized by overweight, insulin resistance, high plasma cholesterol and triglycerides, and hyperglycaemia by six weeks after birth, resulting from impaired peripheral insulin action and a steady β-cell failure. Furthermore, they develop hepatic steatosis that could become non-alcoholic steatohepatitis (NASH) (Takahashi et al., 2012). Apart from this, low grade

inflammation can lead to cardiovascular damage in the form of atherosclerosis or altered cardiac structure and function (Eguchi & Manabe, 2014).

A relevant role in the complex pathophysiology of cardiovascular damage during the course of obesity and type 2 diabetes is certainly played by low-grade inflammation, strong promoter of atherosclerosis but also able to drive abnormalities in cardiac function and structure (Faita et al., 2018).

1.9.2 Leptin-deficient *Lep^{ob}/Lep^{ob} (ob/ob)* mouse

The Lep$^{ob/ob}$ mouse model is derived from a spontaneous mutation in 1949 by the Jackson Laboratory which exhibits adverse obesity. It was only in 1994 that the mutated protein was identified as leptin (King, 2012). An increase in weight is observed from 2 weeks and simultaneously develop hyperinsulinemia. Around 4 weeks the mice become hyperglycaemic with a steady increase in hyperglycaemia until it reaches its peak between 3-5 months, where a rapid decrease is observed as the mice age. Additionally, these mice experience hyperlipidaemia, are unable to regulate temperature and are prone to a sedentary lifestyle. The ob/ob mouse have also been classified as infertile (Kleinert et al., 2018). Since these mice are leptin deficient, once leptin is administered, many of their diabetic manifestations including hyperglycaemia and hyperinsulinemia are corrected before the obesity, suggesting obesity plays a secondary role in their pathogenesis. Contrary to this, human obesity is due to lifestyle and manifold genetic inheritance, while T2DM patients usually have aberrated leptin levels, these are probably secondary T2DM development (B. Wang et al., 2014)

1.9.3 Cardiomyocyte-selective insulin receptor knockout (CIRKO)

The insulin receptors in CIRKO mice are ablated shortly after birth (Hu et al., 2003) and are often used to observe the effect of reduced insulin signalling without systemic metabolic alterations (Riehle & Bauersachs, 2019). Numerous studies have observed a decrease in heart size when substrate usage had been altered (Belke et al., 2002; Lopez-Izquierdo et al., 2014; Sena et al., 2007). Also, these mice display metabolic features like increased glycolysis and reduced FA oxidation, which is characteristic of DCM, and foetal patterns of myosin genes (Lopez-Izquierdo et al., 2014).

1.10 Conclusion

Cardiovascular death associated with diabetes is a major cause of the global disease burden, with diabetics having a two to four-fold increased risk of HF than non-diabetics. Coronary artery disease is the leading cause of cardiovascular disease in Western countries. However, the disease dynamics differ in SSA with cardiomyopathy, contributing to approximately 30% of all cases. In addition, diabetic patients who develop cardiomyopathy have a worse survival prognosis than non-diabetic patients. Early screening for DCM can prevent or delay the progression of HF. However, there are currently no biomarkers that can detect the early onset of DCM. TDI- and Speckle Tract Imaging (STI) echocardiograph analysis are the only imaging technologies available to detect asymptomatic DCM. However, in South Africa (SA), TDI is performed only in tertiary health care institutions.

Thus, early detection of diabetic HF is undocumented, unnoticed, and only recognized at an advanced stage, leading to increased HF mortality. In line with the pathogenesis, since the current imaging techniques are not accessible, especially in resource-poor countries, several studies have been conducted in search of biomarkers that would detect diabetic cardiomyopathy at its asymptomatic stage. Understanding both the mechanisms and pathogenesis of DCM paved the way for discovering biomarkers to identify this disease at the asymptomatic stage to enable corrective treatment and lengthen life span. Although this search progresses, many of these biomarkers are either not available, not specific to the heart, or not associated with the asymptomatic stage. Therefore, the search for biomarkers with the criteria mentioned above continues, and perhaps a panel of biomarkers could be a prospective solution in detecting DCM at this critical stage.

10. Background to the current study

A key challenge in the management of DCM is early diagnosis and timeous treatment of the disease. This will prevent the early onset of cardiomyopathy and prolong death due to HF in the diabetic population. SA is a resource-poor country, with limited access to diagnostic equipment and trained research physicians, especially in rural areas. In the absence of sufficient resources, an effective approach to perform large-scale diagnosis and risk profiling of patients are required. Implementing a "point-of-care" diagnostic test/biomarker throughout SSA could be an alternative when echocardiography facilities are unavailable or inaccessible.

Therefore, this study **hypothesises** that Biomarkers identified in this study will aid in identifying DCM at its preclinical stage. The general **aim** of this study was to identify a prognostics profile that can detect the sub-clinical onset of diabetic induced cardiomyopathy.

To achieve our aim, the following objectives were performed:

1. To perform a meta-analysis of the publicly available type 2 diabetes mellitus and diabetic cardiomyopathy transcriptomic data and to generate a priority list of candidate genes that can detect diabetic cardiomyopathy.
2. To validate these potential biomarkers in serum and heart tissue obtained from 6-16-weeks diabetic db/db mice and compare the results to the current diagnostic N-terminal pro B-type natriuretic peptide.
3. To validate these potential biomarkers using an *in vitro* H9c2 cell line cultured in conditions mimicking a diabetic environment.
4. To perform sensitivity and specificity of the identified biomarkers.

The present study was therefore conducted into the following phases:

Phase 1

In this phase, a bioinformatics approach was used to identify candidate genes belonging to either T2DM or CVD using the ArrayExpress database. Subsequently, a pipeline was formulated to source common identifiers among these to form part of a DCM candidate gene list, which contained 228 candidate genes. The top 5 candidate genes with a $p < 6x10^{-6}$ were used for further downstream analysis.

Phase 2

In this phase, an *in vivo* db/db mouse model was used to conduct gene validation experiments, whilst cardiac function was assessed using the echocardiography technique.

Phase 3

In this phase, functional analysis was performed in an H9c2 cardiomyocyte cell line was used to validate the biomarkers *in vitro*. First, the genes were knocked down, and a diabetic environment was mimicked using high glucose and palmitic acid. After this, the expression levels of these genes and their effectors were analysed using Real-Time quantitative reverse transcription polymerase chain reaction (qRT PCR) and Western blot analysis, respectively.

Phase 4

The sensitivity and specificity of these genes were tested using receiver-operating characteristic curve (ROC) analysis.

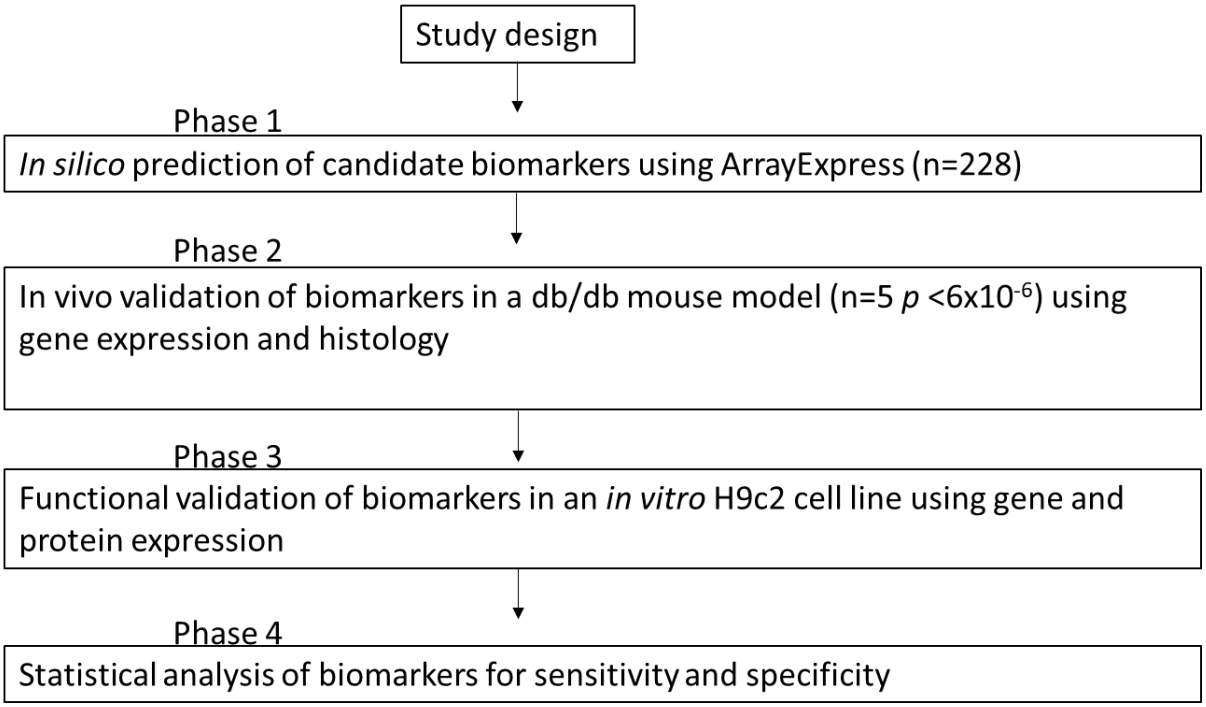

Figure 1.6: Experimental design of the current study. The study was divided into four phases which included an *in silico* prediction method, *in vivo,* and functional validation in a mouse model and H9c2 cells, respectively and finally, statistical analysis of biomarkers was conducted

CHAPTER 2

MATERIALS AND METHODS

2.1 Phase 1: *In silico* prediction of biomarkers of diabetic cardiomyopathy2.1.1 Data acquisition

To identify candidate genes that are differentially expressed in DCM, the ArrayExpress database was screened for studies with publicly available microarray datasets belonging to Homo sapiens over 35 years of age (http://www.ebi.ac.uk/arrayexpress). These studies included healthy controls and patients diagnosed with either T2DM or CVD. Studies involving ischemia, coronary artery disease, and hypertension were excluded, and studies with left ventricular dysfunction (LVD), left ventricular ejection fraction (LVEF) were included. Several search terms were used in the screening process for both subgroups (Table A7), with no restriction on the tissue or cell type, ethnic group, or gender investigated.

2.1.2 Data processing

For studies using the Affymetrix platform, raw datasets were obtained from Gene Expression Omnibus using R scripting and the R package, GEOquery (Rustici et al., 2013)(Rainer et al., 2006). Samples within these datasets fulfilling the specified criteria were then normalised for the Robust-Multi array Average (RMA) using the R package, Simpleaffy. In instances where the studies' data was generated on the Agilent platform, normalised datasets were attained in the same manner as previously described for the Affymetrix platform. Studies using a custom spotted oligonucleotide array were also included. These raw datasets were imported into R using the ArrayExpress package, while the Limma package was used for normalisation. The microarray probe identifiers (IDs) in all the processed datasets were then converted to Ensemble IDs, using a custom Python script accessing both the Ensembl My Structured Query Language (MySQL) and the Biological Database Network (bioDBnet) database (Mudunuri et al., 2009) (Rigden & Fernández, 2018). Probe sets, mapping multiple Ensembl IDs and technical replicates, were averaged to resolve probe redundancy using R and Ruby scripting (Figure 2.1).

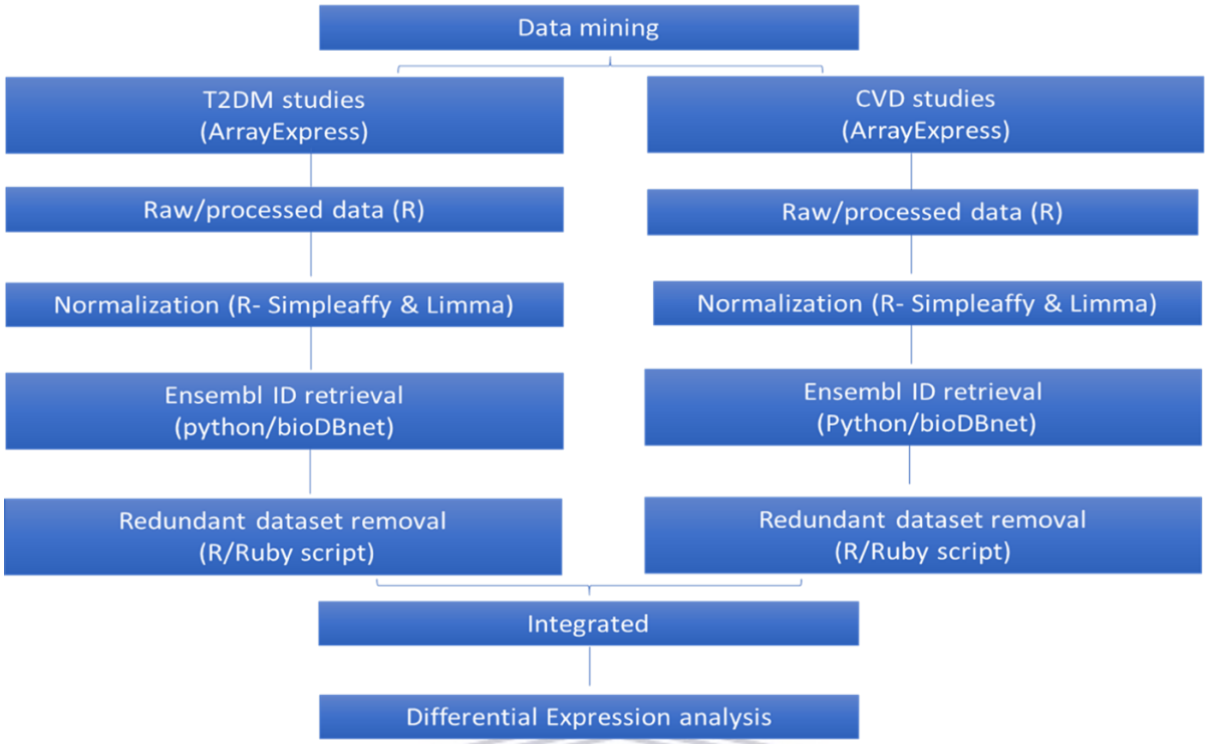

Figure 2.1 *In silico* pipeline used to obtain candidate genes. Data mining of type 2 diabetes mellitus (T2DM) and cardiovascular diseases (CVDs) datasets was conducted using Array Express. These datasets were processed using R and normalized using the Simpleaffy, and Limma packages within R. Ensemble gene IDs were retrieved through Python and bioDBnet. Redundant datasets were subsequently removed using R and Ruby scripting. The T2DM and CVD datasets were combined, and common gene IDs formed the integrated dataset. Subsequently, differential expression analysis was conducted for all datasets.

2. 1.3 Data analysis

Differential expression analysis was performed in three stages, namely to obtain differentially expressed genes (DEGs) from the T2DM datasets only, to obtain DEGs from the CVD datasets only, and to obtain DEGs for integrated datasets from both T2DM and CVD. To this end, common Ensembl IDs were combined using a data binning approach referred to as quantile discretization (QD), which integrates different microarray data at the gene expression level. This study used a QD range of 128 to combine datasets in the T2DM and CVD only subgroups for statistical differential expression analysis. For T2DM only datasets, 15 485 common Ensemble IDs were used, while the CVD only dataset analysis was performed with 16 450 common Ensembl IDs. A QD range of 1028 and a total of 7095 common Ensemble IDs was used to perform differential expression analysis for the integration subgroup (i.e. T2DM and CVD datasets). Genes with a *p*-value of <0.05 were regarded as significantly different using the Wilcoxon Rank Sum Test with Bonferroni and Benjamin-Hochberg correction for multiple testing. Furthermore, a *p*-value of $<6x10^{-6}$ was used as a predictive cut off value for further downstream

analysis. This cut off was based on a preliminary test of the first twenty genes which was conducted using enzyme-linked immunosorbent (ELISA) which showed the first five genes (data not included) could be prospective candidates for early DCM detection. Additionally, the amount of serum used per assay was depended on the dilution factor obtained for each assay and the integrity of the work could not be compromised thus due to this constraint the study was limited to these genes

Summary of findings: After the p<value of $<6x10^{-6}$ was used as a cut off value for the top five genes, which included USP34, ZKSCAN4, LOXL2, IGF1, and ETFβ were used for validation experiments using the serum and heart tissue of an in vivo db/db mouse model.

2.4 Phase 2: Validation of genes as biomarkers of DCM in an *in vivo* model

2.4.1 Ethical approval

The South African Medical Research Council (SAMRC) Ethics Committee of Research on Animals (ECRA) (REF 05/15) and the Ethics Committee of the University of the Western Cape (ECUWC) (REF A16/2/1) granted ethical approval for this study. The study was performed in accordance with the principles and guidelines of the SAMRC as outlined in Guidelines on Ethics for Medical Research: Use of Animals in Research and Training, 2004 (http://www.mrc.ac.za/ethics/ethicsbook3.pdf).

2.4.2 Animal sample size and randomization

Eighty C57BLKS/J leptin receptor-deficient homozygous db/db mice ($Lepr^{db/db}$) (*n*=40) and their heterozygous control littermate ($Lepr^{db/+}$) (*n*=40) were housed at the South African Medical Research Council (SAMRC) Primate Unit and Delft Animal Centre (PUDAC). The mice received standard laboratory chow pellets (Afresh Vention, Cape Town, South Africa) *ad libitum* with free access to drinking water. They were kept in a controlled environment with a 12-hour light/dark cycle. Following a week of acclimatization (at 5-weeks of age), each group was further subdivided into five groups with *n*=6-8 animals per group (Figure 3.2). These groups represent the number of animals to be terminated at different time points for tissue sample collection.

2.4.3 Body weight and fasting plasma glucose

The tail prick method (OneTouch Select®, LifeScan Inc., Milipitas, CA, USA) was used to determine body weights and 4-hour fasting blood glucose concentrations. These were recorded once a week (Philis-Tsimikas et al., 2011).

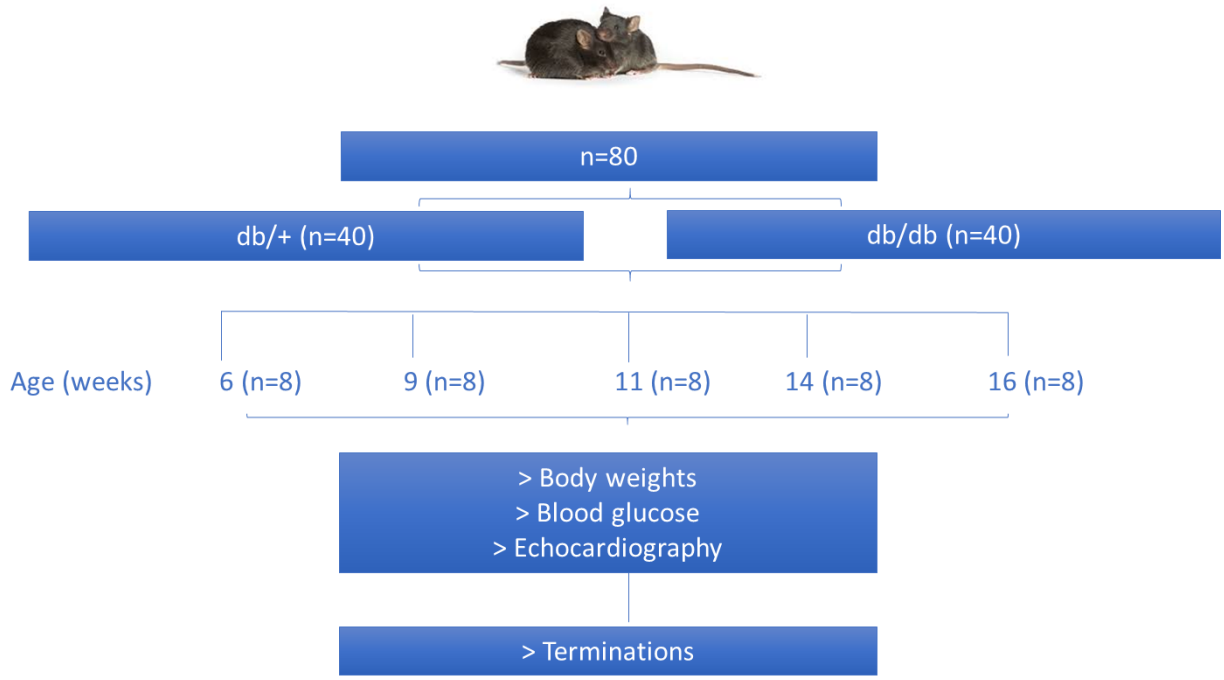

Figure 2.2: Timeline of the animal trial. C57BLKS/J leptin receptor-deficient heterozygous littermate control db/+ and homozygous db/db mice db/db mice with *n*=40 per group were subdivided into five groups which were grouped by age (6-16 weeks) with n=8/group. Body weights, blood glucose, echocardiography and terminations were conducted weekly

2.4.4 Echocardiography

Mice were placed in a holding chamber and anaesthetized with 1.0-2.5% isoflurane to maintain light sedation throughout the procedure. After that, they were placed on an immobilized heating platform in the supine position to keep the body temperature at 37 °C. Echocardiogram (ECG) electrodes were used to monitor the heart rate (HR) and respiratory physiology. Their chests were shaved and warmed ultrasound gel was applied to the area of interest. Doppler echocardiography was conducted using a VEVO 2100 ultrasound system (Fujifilm, Visualsonics, Ontario, Canada) with a 30 MHz linear transducer. The following were then measured in systole and diastole: the left ventricular internal diameter, interventricular septum thickness, posterior wall thickness. The EF was measured to determine systolic dysfunction. The following measurements were conducted to assess left ventricular dysfunction: mitral E and A wave flow velocity, E: A ratio, deceleration time of mitral E wave velocity, and isovolumic relaxation time (IVRT). All measurements were then conducted offline using the mean of at least three consecutive cardiac cycles.

2.4.5 Tissue collection

At weeks 6, 9, 11, 14, and 16, mice (n=8/group) were anaesthetised using sodium pentobarbital and then euthanized by exsanguination, followed by serum, heart and liver collections. The heart and liver samples were stored in RNAlater at -20 °Cfor RNA extraction or -80 °C for without RNAlater for protein extraction. The serum was collected in SST II tubes and stored at -80 °C after processing and later used to conduct lipograms, liver enzyme profiles and (ELISA assays).

2.4.6 Lipid profile and liver enzyme analysis

Serum samples were sent to PathCare Medical Diagnostic Laboratories (Cape Town, South Africa) to screen for total cholesterol, triglycerides, low-density lipoproteins (LDL), high-density lipoprotein (HDL), Alanine Transaminase (ALT) and Aspartate Transaminase (AST) to evaluate differences in lipograms and liver enzyme profiles.

2.4.7 Myocardial tissue RNA extraction

Approximately 30 mg of heart tissue was placed into a new 2 mL tube containing 1 mL of Qiazol® (Qiagen, Hilden, Germany) and a stainless-steel bead. Samples were then homogenized using the Qiagen Tissue lyser (Qiagen, Hilden, Germany) at 25Hz for 2 minutes, and this was repeated twice. The homogenate was centrifuged at 13 000 x g for 10 minutes at 4 °C, and the supernatant was transferred to a 1.5 mL tube, and 0.2 mL of chloroform (Sigma-Aldrich, Missouri, USA) was added to each tube. The tube was inverted three times and incubated for 1 minute on ice after inverting. After that, it was centrifuged at 13 000 x g for 10 minutes. Subsequently, the upper aqueous phase was transferred to a clean 1.5mL Eppendorf tube (Eppendorf, Hamburg, Germany) without disturbing the white organic phase. 0.5 mL isopropanol (Sigma-Aldrich, Missouri, USA) was used to precipitate RNA, and the tubes were inverted several times before samples were incubated overnight at -20 °C. The following day, the tubes were centrifuged at 13 000 x g for 30 minutes at 4 ºC to pellet the RNA. The supernatant was discarded, and the pellet was washed 2x with 1mL of 70 % ethanol and centrifuged at 13 000 x g for 15 minutes at 4 °C. The wash step was repeated twice, and after the final wash, the supernatant was discarded, and the pellet was air-dried for 30 minutes in a PCR hood. The pellet was re-suspended in 50 µL RNase free water (Ambion, Texas, USA) and incubated for 10 minutes at 55 °C stored at -80 °C.

2.4.8 Ribonucleic acid (RNA) quantification and purity

RNA was quantified using the NanoDrop® 1000 spectrophotometer (Thermo Fisher Scientific, Massachusetts, USA) according to the manufacturer's instructions. Briefly, 2 µL of distilled water was pipetted onto the pedestal of the NanoDrop® (Thermo Fisher Scientific, Massachusetts, USA) to blank the machine, followed by which 2 µL of each sample was pipetted for RNA quantification. A 260 to

280 nm ratio was used to assess the RNA purity, and 260 to 230 nm was used to evaluate DNA contamination. A ratio of 1.8 indicates DNA purity, while a ratio of 2 indicates RNA purity. However, if the ratio is significantly lower in either case, it could indicate the presence of protein, phenol or other contaminants that absorb strongly at or close to 280 nm.

2.4.9 DNase treatment

RNA samples were DNase treated to remove genomic DNA using a Turbo DNase kit (Ambion, Texas, USA, according to the manufacturer's recommendations. Briefly, 5 µL of 10x DNase buffer and 1.5 µL of DNase and RNase-free water (Ambion, Texas, USA) was added to 20 µg of RNA in a total reaction volume of 50 µL. Samples were mixed and incubated at 37 °C for 30 minutes, after which another 1.5 µL of DNase was added and incubated at 37 °C for an additional 30 minutes. The reaction was stopped by adding 10 µL DNase inactivation reagent, and the suspension was mixed by placing tubes on an orbital shaker for 2 minutes. After that, the tubes were centrifuged at 10 000 x g for 1.5 minutes, and the supernatant was transferred to a new tube. RNA concentrations were determined using a NanoDrop® 1000 spectrophotometer (Thermo Fisher Scientific, Massachusetts, USA).

2.4.10 RNA integrity

The Agilent 2100 Bioanalyzer (Agilent Technologies, Santa Clara, California, USA) was used to determine RNA integrity according to the manufacturer's recommendations. Briefly, 350 µL of RNaseZAP (Thermo Fisher Scientific, Massachusetts, USA) was used to decontaminate the bioanalyzer for 1 minute, followed by 350 µL RNase-free water for 10 seconds. The bioanalyzer lid was left open for 10 seconds to dry the electrodes upon decontamination. The DNase treated RNA samples were prepared by transferring 20 µL of sample and 0.5 µL RNA ladder into tubes placed in a 70 °C heating block for 2 minutes. The samples and ladder were loaded on an RNA chip priming station once denatured, and 9 µL of gel-dye mix was added into the well-marked **G**. The chip priming station was positioned at the 1 mL marker, pressed until held by the chip and the plunger was released at 30 seconds. After that, 9 µL of gel-dye mix was added into two wells marked G (light), and 5 µL of RNA 600 Nano marker was added in all 12 sample wells, including the ladder well. This was followed by adding 1 µL of RNA ladder into the ladder well, 1 µL RNA sample into each of the 12 sample wells and 1 µL sample ladder into each unused well. The chip was vortexed at 543 x g for 30 seconds, placed in the chamber of the Agilent bioanalyzer and run within 5 minutes. When the run was complete, the chip was removed, and the electrodes were washed by placing a chip filled with 350 µL of RNase-free waster into the chamber for 10 seconds. RNA integrity was determined using 2100 Expert Software (Agilent Technologies, Santa Clara, California, USA).

2.4.11 Complimentary DNA (cDNA) synthesis

According to the manufacturer's instructions, the High-Capacity cDNA kit (Applied Biosystems, CA, USA) was used to transcribe total RNA to cDNA (Thermo Fisher Scientific, Massachusetts, USA). A 1 µg DNase treated RNA solution was transferred into a 0.2 mL tube (Axygen, California, USA) with RNase-free water to a final volume of 10 µL. The master mixes were prepared in 2 separate tubes labelled reverse transcriptase-Plus (RT-Plus) and reverse transcriptase-Minus (RT-Minus) (Table 2.3), and deoxynucleotide triphosphates (dNTPs), reaction buffer, random primers, RNase inhibitor, RNase-free water and reverse transcriptase were used to prepare the master mixes. RT-Minus master mix tube was used as a negative control and contained similar constituents to the RT-Plus tube, with the reverse transcriptase enzyme replaced with water. The cDNA synthesis reaction was prepared by adding 10 µL of RT-Plus or RT-Minus master mix into a 0.2 mL tube with 1 µg of RNA, and RNase-free water to a final volume of 20 µL. The tubes were briefly vortexed, spun down and placed in the Applied Biosystem Instrument (ABI) 2720 thermal cycler (Applied Biosystems, California, USA). The thermal cycler was programmed to incubate at 25 °C for 10 minutes, 37 °C for 120 minutes and 85 °C for 5 seconds to deactivate the reverse transcriptase enzyme. Upon completion, the cDNA samples were stored at -80 °C until further use.

Table 2.1: Reaction mixture used to reverse transcribe the DNase treated RNA

Reaction mixture	R-Plus Volume/Reaction (µL)	R-Minus Volume/Reaction (µL)
RNA	10	10
10× RT buffer	2	2
25× dNTP mix	0.8	0.8
10× Random primers	2	2
RNase inhibitor	1	1
Reverse transcriptase	1	-
Nuclease-free water	3.2	4.2
Total volume	20	20

*1µg of DNase treated RNA made up to a final volume of 10 µL in RNase-free water

2.4.12 cDNA testing for genomic DNA contamination

Genomic DNA contamination was determined with the use of Actin-β (Actβ) exon spanning primers, using the cDNA previously generated from the RT-Plus and RT-Minus reverse transcriptase reaction (Table 2.4). To prepare a master mix, 1 µL of each primer pair (Actβ, 10 µM), 12.5µL SYBR® Green PCR master mix (Applied Biosystems, California, USA) and RNase-free water to a final volume of 24µL, were used (Table 2.4). To 1 µL of RT-Plus or RT-Minus cDNA, 24 µL of SYBR® green master mix was added in a MicroAmp® Optical 96-well Reaction Plate (Applied Biosystems, California, USA). The plate was sealed with MicorAmp® Optical Adhesive Film (Thermo Fisher Scientific, Massachusetts, USA), vortexed on a plate shaker for 10 minutes, briefly centrifuged for 2 minutes at 3 000 x g and placed in the ABI 7500 Sequence Detection System (Applied Biosystems, California, USA) for quantitative PCR analysis. Complimentary DNA amplification was conducted using the cycling conditions as indicated in Table 2.5. The threshold cycle (Ct) and baseline acquired during the exponential phase were used to determine the cDNA quantity for each reaction. If the difference in Ct values were equal to or greater than 10 between the corresponding RT-Minus and RT-Plus strand, the presence of contamination was deemed as negligible.

Table 2.2: A master mix used in the detection of contaminated genomic DNA

Components	Volume/Reaction (µL)	Final Concentration
SYBR Green PCR Mix	12.5	1x
Actβ Forward primer (10 µM) 5'GGGCCCGGACTCATCGTACT-3'	1	400 nM
Actβ Reverse primer (10 µM) 5'-GCCTCACTGTCCACCTTCCA-3'	1	400 nM
RNase-free water	9.5	
Cdna	1	-
Total	**25**	

Table 2.3 Universal cycling conditions used for testing of cDNA

Step	Temperature °C	Time	Cycles
Activation and Denaturation	50	2 minutes	1
Fluorescence data collection	95	15 seconds	40
Dissociation Curve	95	15 seconds	1

2.4.13 Quantitative Real-time PCR analysis (qRT-PCR)

Taqman® gene expression assays from Applied Biosystems were used to quantify genes identified from the candidate gene list (Table A7; Table 3.4). For qRT-PCR, the reaction mixture consisted of 5 µL of pre-designed Taqman® primers (Applied Biosystems, California, USA) and water to a final volume of 9 µL (Table 2.7). After that, the plate was sealed, placed onto a shaker for 10 minutes, briefly centrifuged at 3 000 x g for 2 minutes and then placed in an ABI 7500 Sequence Detection System (Applied Biosystems, California, USA) to conduct the qRT-PCR with the cycling conditions described in Table 2.3. The Total Rat Heart RNA (Applied Biosystems, California, USA) and the non-template control were used. Actβ and hypoxanthine phosphoribosyl transferase 1 (Hprt1) were used as endogenous housekeeping genes.

Table 2.4 List of Taqman probes used in *in vitro* QRT-PCR analysis

Gene ID	Assay ID	Ensembl ID	Catalog Number
USP34	Rn01231137_m1	ENSG00000115464	4351372
ZKSCAN4	Rn01525205_m1	ENSG00000187626	4351372
LOXL2	Rn01466080_m1	ENSG00000134013	4331182
IGF1	Rn00710306_m1	ENSG00000017427	4331182
ETFβ	Rn01454706_m1	ENSG00000105379	4331182

Table 2.5 PCR-reaction mix used to conduct the QRT-PCR reaction

PCR Reaction	Per Reaction (µL)
Taq polymerase master mix	5
Probe assay	0.5
Nuclease-free water	3.5
Cdna	1
Total	**9**

Table 2.6 List of Taqman probes assays used in *in vivo* QRT-PCR analysis

Gene ID	Assay ID	Ensembl ID	Catalog Number
USP34	Mm01231150_m1	NM_001190401.2	4331182
ZKSCAN4	Mm01165490_mH	NM_001039115.2	4351372
LOXL2	Mm00804740_m1	NM_033325.2	4331182
IGF1	Mm00439560_m1	NM_001111276.1	4331182
ETFβ	Mm00503341_m1	NM_026695.3	4331182

2.4.14 Enzyme-linked immunosorbent (ELISA) assays for the identification of serum biomarkers

Mouse serum was used to assess USP34, ZKSCAN4, IGF1, SLC16A1, LOXL2, ETFβ and pro-BNP protein expression using ELISA kits (MyBioSource Inc, San Diego, CA, USA) according to the manufacturer's instructions. Briefly, 100 µL of standards, blank control and samples were added to the appropriate wells, followed by which 50 µL of the conjugate was added to the standard and sample wells. The plate was covered, gently mixed and incubated for an hour at 37 °C. After that, the mixture was decanted, and each well was emptied. Thereafter, each well was washed five times with 1x wash solution and the contents discarded. After washing, the plate was inverted and blot dried onto paper towels until no moisture remained. Fifty microliters of substrate A and B were added to each well, covered with foil and incubated for 10-15 minutes at 37 °C. The reaction was completed by adding 50

µL stop solution and absorbance measured using ELx800™ Absorbance microplate reader (Bio-Tek Instruments, Inc., Winooski, VT, USA). Concentrations were determined using the Gen5 software. The readings were normalised to the standard protein concentration and expressed as mg/mL.

2.4.15 Histopathology2.4.15.1 Tissue fixation and embedding

Heart and liver tissues were weighed and fixed in 4 % formalin for a minimum of 16 hours before they were processed using a Leica TP 1020 automated processor (Leica Biosystems, Buffalo Grove, IL, USA) and embedded in paraffin wax. Paraffin-embedded tissues were cut into 4 µm sections.

2.4.15.2 Haematoxylin and Eosin (H&E) staining

To assess whether DCM pathology had established, heart and liver tissue were submerged in Mayer's Haematoxylin stain (KImix Chemicals, Cape Town, South Africa) for 12 minutes, rinsed in 10 dips of water and subsequently washed in tap water to neutralise the acid, thus staining the nuclei. The slides were then counterstained with eosin for 2 minutes to stain the cytoplasm and acidophilic structures, then dipped 20 times in water and dehydrated by dipping them 20 times in 95 % ethanol and 100 % ethanol, respectively. This was followed by the clearing of the tissues in 2 changes of xylene. Permanent mounting media (Richard-Allan Scientific, Kalamazoo, USA) was used to mount the slides.

2.4.15.3 Masson's Trachoma stain

To discriminate between collagen fibres and smooth muscle tissues, tissue slides were stained with Masson's' Trichrome (Biocom Africa, Pretoria, SA). The slides were re-fixed in pre-heated (56-64 $^{\circ}$C) Bouin's fluid for 60 minutes, cooled for 10 minutes and then washed in tap water as well as distilled water. The slides were then stained with the Wiegert's Iron Haematoxylin (equal parts of Wiegert's A and B) working solution for 5 minutes and then rinsed in running tap water for 2 minutes. After that, the Biebrich Scarler/Acid Fuchsin solution was applied to the slides for 15 minutes and then rinsed with distilled water. The slides were differentiated in Phosphomolybdic/Phosphotungstic Acid Solution for 10-15 minutes. The Aniline Blue Solution was applied to the slides for 10-15 minutes, rinsed in distilled water and then placed in 1 % Acetic Acid solution for 3-5 minutes. The slides were dehydrated using 95 % ethanol, followed by 100 % ethanol, cleared in xylene and mounted as described in the previous section.

2.4.15.4 LOXL2 and ETFβ immunohistochemistry

To further assess any changes in collagen crosslinking and energy metabolism, respectively, the anti-LOXL2 (Biocom Africa, Pretoria, SA) and anti-ETFβ (Biocom Africa, Pretoria, SA) stains were used. Briefly, heart tissue sections were blocked in 3 % hydrogen peroxide (H_2O_2) (Thermo Fisher Scientific, Massachusetts, USA) for 5 minutes and rinsed in distilled water for 5 minutes. Sections were placed in 0.01 M citrate buffer (pH6.0) and treated in a Dako Pascal pressure chamber (Diagnostech,

Johannesburg, SA) at 125 ℃ for 30 seconds and 90 ℃ for 10 seconds. The slides were cooled for 20 minutes, rinsed in distilled water for 5 minutes, and 0.05 M Tris-buffered saline (TBS) (pH 7.2) for 5 minutes. Normal goat serum (1:20) (Sigma-Aldrich, Missouri, USA) was added to all slides in a moisture chamber for 20 minutes at room temperature (18 ˚C to 20 ˚C). Excess serum was blotted off, and 100 µL of anti-LOXL2/anti-ETFB (1:200), added to each section in a moisture chamber, and incubated at 4°C overnight. The slides were then jet washed and rinsed in a staining jar containing 0.05 M TBS (pH7.2) for 5 minutes. The slides were dried around the sections, and (1:200) biotinylated anti-rabbit IgG (Sigma-Aldrich, Missouri, USA) was added to all slides in the moisture chamber for 30 minutes at room temperature. The slides were then jet washed and rinsed in a staining jar with 0.05 M TBS (pH7.2) for 5 minutes. The slides were dried around the sections, and Vectastain (Vector Laboratories, INC, Burlingame, CA) was added to each slide in a moisture chamber and incubated for 60 minutes at room temperature. The slides were jet washed and rinsed in a staining jar with 0.05M TBS (pH7.2) for 5 minutes. Slides were dried around sections, and Liquid DAB + substrate solution (Merck KGA, Darmstadt, Germany) was added to the slides over the sink for 5 minutes. The slides were washed in distilled water for 5 minutes, counterstained with haematoxylin for 2-4 minutes and rinsed well in tap water. They were subsequently left in tap water to neutralise the acid ("blueing") for 30 minutes and dried completely. Permanent media (Richard-Allan Scientific, Kalamazoo, USA) was used to mount the slides.

2.4.15.5 Image Acquisition and analysis

Stained micrographs for heart and liver tissues were captured in non-overlapping fields of 1mm^2 under 40x magnification using the NIS Elements imaging software (Tokyo, Japan). Five independent frames were used to assess the degree of pathology (micro-and macro- vesicles, inflammation) using the ImageJ 1.51v software for liver histology. Similarly, five independent frames were used to assess the degree of pathology in heart slides.

Summary of findings: Data obtained from serum validation experiments showed that the genes LOXL2 and ETFB were differentially expressed. Thus functional validation of these genes was conducted in an *in vitro* H9c2 rat heart derived model using siRNAs.

2.5 Phase 3: *In vitro* functional validation of markers

2.5.1 *In vitro* cell line

Embryonic rat heart derived H9c2 cardiomyoblasts obtained from the European Collection of Cell Cultures (ECACC No. 8809294) were used to conduct all the *in vitro* experiments. Cryopreserved H9c2 cardiomyoblasts, stored in a 1 mL cryotube containing 80 % foetal bovine serum (FBS) (Lonza, Walkersville, MD, USA) 10 % each of Dulbecco's Modified Eagle's Medium (DMEM) (Lonza,

Walkersville, MD, USA) and dimethyl sulfoxide (DMSO) (Sigma-Aldrich, Missouri, USA), were thawed in a 37 °C water bath. The contents were transferred into a 50 mL tube with 10 mL DMEM (containing 10 % FBS and 1 % penicillin/streptomycin (pen/strep) when thawed and centrifuged at 1500 x g for five minutes to remove excess DMSO. After that, the cardiomyoblasts were resuspended in 18 mL DMEM, transferred into a T75 flask and incubated under standard tissue culture (TC) conditions (37 °C, 5 % CO_2 and water-saturated atmosphere) until 70-80 % confluent.

2.5.2 Sub-culturing

Cells were split and/or sub-cultured (1:9 ratio) in a pre-warmed complete growth DMEM [supplemented with 10 % FBS and 1 % penicillin/streptomycin (pen/strep)] at 70-80 % confluence, after which cells were incubated under standard TC conditions. The H9c2 cardiomyoblasts were washed with pre-warmed Dulbecco's phosphate-buffered saline (DPBS) (Lonza, Walkersville, MD, USA) and incubated in 4 mL trypsin (Lonza, Walkersville, MD, USA) at 37 °C until the cells were dislodged, or for a maximum of 4 minutes in CO_2 under TC conditions. The media was refreshed every third day, and the sub-culturing of H9c2 cardiomyoblasts was not allowed to *ex*ceed 20 passages. Cardiomyoblasts were viewed under a NIKON Eclipse Ti inverted microscope (Nikon Tokyo, Japan) to ensure cells were dislodged. After that, 8 mL of DMEM media was pipetted into the T75 flask to halt the reaction, and the cells were thoroughly re-suspended. The cell suspension was then transferred into a 50 mL centrifuge tube and centrifuged at 1500 rpm x g for 5 minutes. The supernatant was removed, and the cells were re-suspended in 10 mL warmed DMEM media Lonza, Walkersville, MD, USA). Determination of cell viability and cell density was conducted as discussed in section 2.5.3 before seeding cells in suitable multi-well plates section 2.5.4 for subsequent assays.

2.5.3 Determination of cell viability

Using the Automated Cell Counter Countess TM (Invitrogen, Carlsbad, CA, USA), a trypan blue dye (Invitrogen, Carlsbad, CA, USA) exclusion test was used to determine the number of viable cells according to the manufacturer's specifications. Briefly, following trypsinisation, 1:1 cell suspension was prepared by diluting 10 µL of cells with 10 µL of 0.4 % (w/v) trypan blue dye solution. Ten microliters of the resultant mixture were then placed onto the Countess™ (Invitrogen, Carlsbad, CA, USA) cell counting chamber slide port. The slide was placed onto the instrument slide inlet to measure the total number of viable and non-viable cells. Cell viability above 70 % was considered seed worthy.

2.5.4 Seeding of cells in multi-well plates, differentiation and hyperglycemia and/or hyperlipidemia induction

H9c2 cardiomyoblasts were seeded at the relevant seeding density (Table 2.1) in the required TC plate in complete growth DMEM (Lonza, Walkersville, MD, USA) under standard TC conditions (37 °C, 95 % humidified air and 5 % CO_2).

Table 2.5: Seeding densities of H9c2 cardiomyoblasts in Multi-well plates

	Multi-well plate	Growth area (cm^2)	Seeding density (cells/well)	Volume (µL)
H9c2	6	10	2×10^5	3 000
	24	2.0	5×10^4	1 000
	96	0.3	2×10^4	200

Confluent H9c2 cardiomyoblasts (after 2-3 days), seeded either in 6-well, 24-well or 96-well plates, were differentiated into adult cardiomyocytes by substituting growth media with differentiation media consisting of DMEM [supplemented with 10 mM all-trans-retinoic acid (RA)] and 1 % horse serum for six days.

2.5.6 Functional knockdown of LOXL2 and ETFB

Small interfering RNA (siRNA) against LOXL2 (RSS306495) and ETFB (RSS354369) were purchased from (Invitrogen, Carlsbad, CA, USA). The OPTI-MEM was used to dilute the siRNAs to a final concentration of 100 nM. A 7.5µl volume of Lipofectamine® RNAiMAX (Invitrogen, Carlsbad, CA, USA) was used to transfect the cells/per well in a six-well plate for 6 h. After this, the cells were refreshed with normal OPTI-MEM media. Then, cells were stimulated with the conditions below for 48 h.

A. 5.5 mM glucose normal glucose (NG)
B. Group 2: 10 mm Intermediate glucose (IG) + 50 µM palmitic acid (PA)
C. Group 3: 33 mM high glucose (HG) + 100 µM PA
D. Group 4: IG + 50 µM PA + 10 nM Insulin (INS)
E. Group 5: HG + 100 µM PA + 100 nM INS

2.5.7 Protein expression

2.5.7.1 Total protein concentration

Following the differentiation and stress induction, 100µL of ice-cold lysis buffer (Invitrogen, Carlsbad, CA, USA) was added per 6-well plate. Cells were scraped using a rubber cell scraper (Invitrogen, Carlsbad, CA, USA), and after that, cells of 3 wells were pooled and transferred to a 2 mL tube with

stainless-steel beads. The cell suspension containing the bead was placed in a pre-cooled TissueLyser block (Qiagen, Hilden, Germany) and homogenised at 25Hz for 1 minute using a Qiagen TissueLyser (Qiagen, Hilden, Germany). This step was repeated three times, with cells placed for 1 minute on ice between homogenisation. After that, lysed cells were centrifuged at 4℃ for 15 minutes at 15 000 x g. The supernatant containing whole cell lysates were then transferred to 1.5mL tubes and stored at -20℃ until use.

2.5.7.2 Protein concentration determination and gel electrophoresis

The protein concentrations of treated cardiomyocytes were determined using the RC DC™ protein assay kit (Bio-Rad, Hercules, CA, USA) according to the manufacturer's specifications. Five microliters of BSA standards (0.125, 0.25, 0.5, 0.75, 1, 1.5 and 2.0 mg/mL) and cell lysates were pipetted into a 96-well plate. A 25 µl volume of reagent A (containing 20 µL RC Reagent C and 1mL of RC reagent A) and 200 µL of reagent B were pipetted into standard and sample wells. The plate contents were mixed on a microplate shaker for 10 seconds, incubated at room temperature (RT) for 10 minutes, and the absorbance read at 695 nm using a BioTek® ELX800 plate reader (BioTek Instruments Inc., Winooski, VT, USA) using Gen 5® software (Molecular Devices, California, USA). The concentration of each sample was calculated using the standard curve with linear equation (y=mx+c), which was generated using absorbance values from the BSA standards based on its mean absorbance value.

Sample buffer was prepared using 50 µL ß-mecaptoethanol (Fluka, Bucharest, Romania) to 950 µL 2x Laemmli Sample buffer (SB) (Bio-Rad, Hercules, CA, USA). A 30 µg protein lysate was mixed with equal volumes of sample buffer and denatured at 95 ºC for 5 minutes. Next, the protein/SB mixture, as well as 12 µL of a Precision Plus Protein Western C (Bio-Rad, Hercules, CA, USA) standard, were loaded onto a Mini-Protean® TGX™ (Bio-Rad, Hercules, CA, USA) gel and placed in a Bio-Rad Mini Protein® Tetra Cell tank filled with 1x Tris/Glycine/SDS running buffer. The tetra cell tank was connected to the PowerPac™ Basic power supply, and SDS-PAGE gel electrophoresis was conducted at 150 V for 60 minutes.

2.5.7.4 Protein expression by Western blot analysis

2.5.7.4.1 Transfer of gel to PVDF membrane

Polyvinylidene fluoride (PVDF) membrane(s) were incubated and were activated by immersion in i00% ethanol for 1 minute. The PVDF membranes were then incubated in cold 1x transfer buffer (1x transfer buffer, ethanol and dH_2O) with 6x 7cm x 9 cm pieces of filter paper and equilibrated for 2-3 minutes on an orbital shaker. Three pieces of filter paper were placed on the electrode cassette of the Trans-Blot® Turbo™ Transfer System (Bio-Rad, Hercules, CA, USA).to make a gel-membrane sandwich. The PVDF membrane was placed on top of the filter paper, the 1-SDS-PAGE gels were placed on the

membrane and the remaining 3 layers of filter paper were placed on top of the gel. Bubbles were eliminated by rolling the sandwich with a 2 cm stripette (Bio-Rad, Hercules, CA, USA). The cassette was closed, placed into a Trans-Blot® Turbo™ Transfer System (Bio-Rad, Hercules, CA, USA) and run for 8 minutes to transfer proteins from the gel onto the PVDF membranes. The membranes were either Ponceau S stained (2.5.7.4.2) or labelled with antibodies (2.5.7.4.3).

2.5.7.4.2 Ponceau S stain

To ensure the successful transfer of proteins onto the membrane, 50 mL Ponceau S Staining Solution (Sigma-Aldrich, St Louis, MO USA) was used to stain the membrane. It was incubated at RT for 10 minutes in a shaker. The membrane was washed for 1 minute with 1x Tris-buffered saline containing Tween-20 (TBST-20) to reverse the stain.

2.5.7.4.3 Antibody labelling

The PVDF membranes containing protein samples were blocked in 5% (w/v) skim milk (prepared in 1x TBST-20) at RT for 60-120 minutes on a shaker. Subsequently, the membranes were probed with specific primary antibodies (Table 2.6) in 5 mL 1x TBST-20 at 4ºC overnight with shaking. Next, StrepTactin horseradish peroxidase (HRP) conjugated secondary antibody in 2.5% (w/v) skim milk for 60 minutes (prepared in 1x TBST-20) was used for detection. The membrane was washed and incubated with the substrate for 5 minutes. The protein was detected using a Chemidoc-XRS imager (Bio-Rad, Hercules, CA, USA) and then normalised to β-actin.

Table 2.6: List of antibodies and the dilution used for Western blot analysis

Antibody	Dilution	Company
	Primary antibody	
LOXL2	1: 500	Biocom Africa
ETFβ	1:500	Biocom Africa
β-Actin	1: 1 000	Santa Cruz
ProBNP	1: 500	Biocom Africa
Smad2	1: 500	Biocom Africa
TGFβ	1: 500	Biocom Africa
Cpt2	1: 500	Biocom Africa
Acadm	1: 500	Biocom Africa
	Secondary antibody	
Donkey anti-mouse IgG-HRP	1: 4 000	Santa Cruz
Donkey anti-rabbit IgG-HRP	1: 4 000	Santa Cruz

2.6 Phase 4: Statistical analysis of biomarkers for Sensitivity and specificity

Principal component analysis (PCA) and receiver operating characteristic curve (ROC) were used to conduct sensitivity and specificity analysis. The generalised linear model was initially used to statistically test for significant differences between lean and obese mice at each week for each biomarker. The results were regarded as significant with a $p<0.001$. The PCA was conducted by combining the data of pro-BNP, LOXL2 and ETFβ. At the same time, the logistic regression model was used to perform receiver operating characteristic curves to test the diagnostic ability of the biomarkers, with $p<0.05$ giving the test significance.

2.7 Statistical analysis

For the *in vivo* study, results were expressed as the mean ± SEM, $n=8$, while for *in vitro* experiments, each assay was conducted three times to ensure reproducibility. Statistical analysis was conducted using GraphPad Prism software version 5.0 (GraphPad Software, Inc., La Jolla, USA). Comparisons between groups were performed using two-way ANOVA. A p-value of ≤ 0.05 was deemed as statistically significant.

CHAPTER 3

RESULTS

3.1 Phase 1: Computational prediction for early-onset DCM biomarkers

3.1.1 Curation and acquisition of T2DM and CVD datasets using an *in silico* approach.

A meta-analysis of publicly available T2DM and CVD transcriptomic datasets was performed using ArrayExpress. Briefly, using the previously described pipeline in section 3.1, eleven and seven GSE datasets (Table 4.1) were acquired as possible prognostic candidates for T2DM and CVD, respectively. These data sets were further integrated to identify differentially expressed genes (DEGs) associated with DCM (Figure 3.1). Search terms used to extract these datasets are listed in Table 3.1. Integration of the two datasets resulted in identifying 228 genes linked to DCM (Figure 3.1, Table A7). Of these, the first five genes were selected according to the Wilcoxon score, and a *p*-value of $<6 \times 10^{-6}$ considered a predictive cut off value for further downstream analysis (Table 3.2). As previously stated, to prevent bias, the top 5 USP34, ZKSCAN4, LOXL2, IGF1and ETFβ genes were selected according to their Wilcoxon score. An extensive literature search was conducted to associate these genes with DCM pathology (Table 3.2) to gain further biological insight into the function of identified genes. Functional annotation associates the identified genes were linked to major biological pathways associated with energy metabolism, fibrosis and apoptosis. The USP34, IGF1 and ETFβ were associated with energy metabolism, while LOXL2 and ZKSCAN4 genes are associated with fibrosis, which is one of the hallmarks of DCM disease progression (Table 3.2).

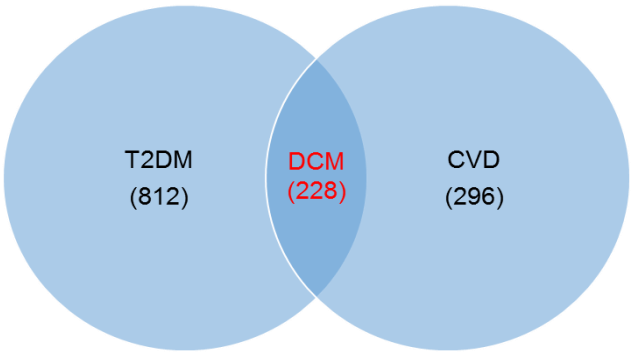

Figure 3.1: Venn diagram of differentially expressed genes (DEGs). Within the type 2 diabetes mellitus (T2DM) with 812 genes and cardiovascular disease (CVD) datasets, 812 and 296 candidate genes were identified, respectively. Integration of the T2DM and CVD datasets, a diabetic cardiomyopathy (DCM) dataset consisting of 228 was generated, in which possible candidate genes were identified.

Table 3.1: Platforms and search terms used within ArrayExpress to identify datasets related to T2DM and CVD

	T2DM	CVD
Search terms used	"diabetic cardiomyopathy", "diabetic heart", "left ventricular hypertrophy", "diabetes mellitus", and "type 2 diabetes mellitus"	"heart", "heart failure", "heart left ventricle", "diastolic dysfunction", "left ventricular dysfunction"
Datasets	GSE23561, GSE40234, GSE29231, GSE13760, GSE38642, GSE29221, GSE21340, E-CBIL-28, E-MEXP1270, E-MEXP2559, E-MTAB2854	GSE 26887, GSE1869, GSE5406, GSE43435, GSE21125, GSE9128, E-TABM-480
Platforms	Affymetrix: E-CBIL-28, E-MEXP1270, E-MEXP2559, E-MTAB2854 Agilent: GSE23561, GSE40234, GSE29231, GSE13760, GSE38642, GSE29221, GSE21340	Affymetrix: E-TABM-480 Agilent: GSE 26887, GSE1869, GSE5406, GSE43435, GSE21125, GSE9128

Table 3.2: Functional association of the top five genes using literature

Gene ID	p-value	Function related to DCM pathology	Findings to date	Tissue type	References
USP34	4.22E-07	Metabolism, signal transduction, apoptosis	Congenital heart disease Brain metastasis	Heart Brain	(Hwang et al., 2016; Oh et al., 2017; Sy et al., 2013; Szot et al., 2018; S. Zhao et al., 2015)
ZKSCAN4	1.30E-06	hypertrophy, fibrosis, and cardiac dysfunction	Cardiac hypertrophy	Heart	(Ecker et al., 2009; Y. Kim et al., 2014; Ota et al., 2004; C. J. Yu et al., 2017)

LOXL2	3.26E-06	Fibrosis	Fibrosis	Heart	(Cosgrove et al., 2018; Erasmus et al., 2020; Kober et al., 2018; Neumann et al., 2018; Steppan et al., 2019; Yang et al., 2016; Zhan et al., 2017)
IGF1	5.08E-06	Cellular growth and repair, metabolism, hypertrophy	Cardiac hypertrophy	Heart	(Andreassen et al., 2009; Chisalita et al., 2011; Ingelsson et al., 2010)
ETFβ	5.65E-06	Metabolism and ATP production	glutaric aciduria type II, cancer	Heart	(Johnson et al., 2020; Lloyd et al., 2017; Ruiz-Pinto et al., 2018; Sudo et al., 2015; Xu et al., n.d.; Q. Zhao et al., 2016)

3.1.2 Summary

After integrating microarray data from publicly available repositories, 228 possible novel drug candidates for therapeutic interventions and/or biomarkers for early detection of DCM were identified. However, to prevent bias in selecting the potential DCM biomarkers, only the top 5 genes (USP34, ETFβ, LOXL2, ZKSCAN4 and IGF1) were selected based on the Wilcoxon score and $p<6x10^{-6}$ for subsequent characterization and *in vivo* validation experiments.

3.2.3 Liver pathology and serum analysis of liver enzymes (AST and ALT) as risk predictors of DCM

The liver is an essential organ for glucose and fatty acid metabolism and homeostasis after meals and fasting. Patients presenting with non-alcoholic fatty liver disease (NAFLD) are more likely to develop CVD than their non-NAFLD counterparts. Furthermore, it has been reported that CVD is the leading cause of death among NAFLD patients (Stepanova & Younossi, 2012; Targher et al., 2007). The liver enzymes alanine aminotransferase (ALT) and aspartate aminotransferase (AST) are used to monitor liver function and the degree of liver injury. At the same time, hepatotoxicity is characterised by increased fat deposition in hepatocytes, which have been linked to hepatic insulin resistance and T2DM. In the present study, significantly elevated expression of the liver enzymes ALT was observed at 6 ($p\leq 0.05$), 14 ($p\leq 0.01$) and 16 ($p\leq 0.01$) weeks, respectively. While for AST at six weeks, a significant decrease is observed followed by a significant increase at 14 ($p\leq 0.01$) and week 16 ($p\leq 0.01$) in the db/db mice when compared to their db/+ counterparts (Figure 3.4). Liver tissues were subjected to histological analysis (Figure 3.6) to ascertain whether the changes in serum liver enzyme levels coincided with changes in tissue. Haematoxylin and eosin-stained liver sections showed vesicular formation from week six and macro-vesicles formed from week 9, which both indicate lipid accumulation in the liver.

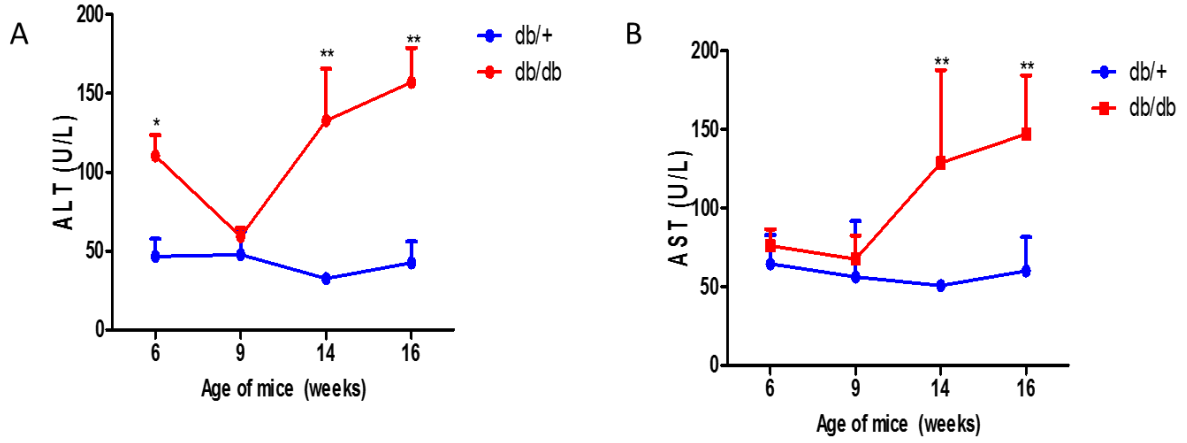

Figure 3.9: Liver enzyme profile of Leptin receptor-deficient db/db mice at 6-16 weeks. ALT A) and AST B) of homozygous Leptin receptor-deficient diabetic mice db/db mice and their heterozygous Leptin receptor-deficient db/+. Results are expressed as mean ± SEM of 8 animals per group. *p<0.05 and **p<0.01 versus nondiabetic age-matched control (db/+).

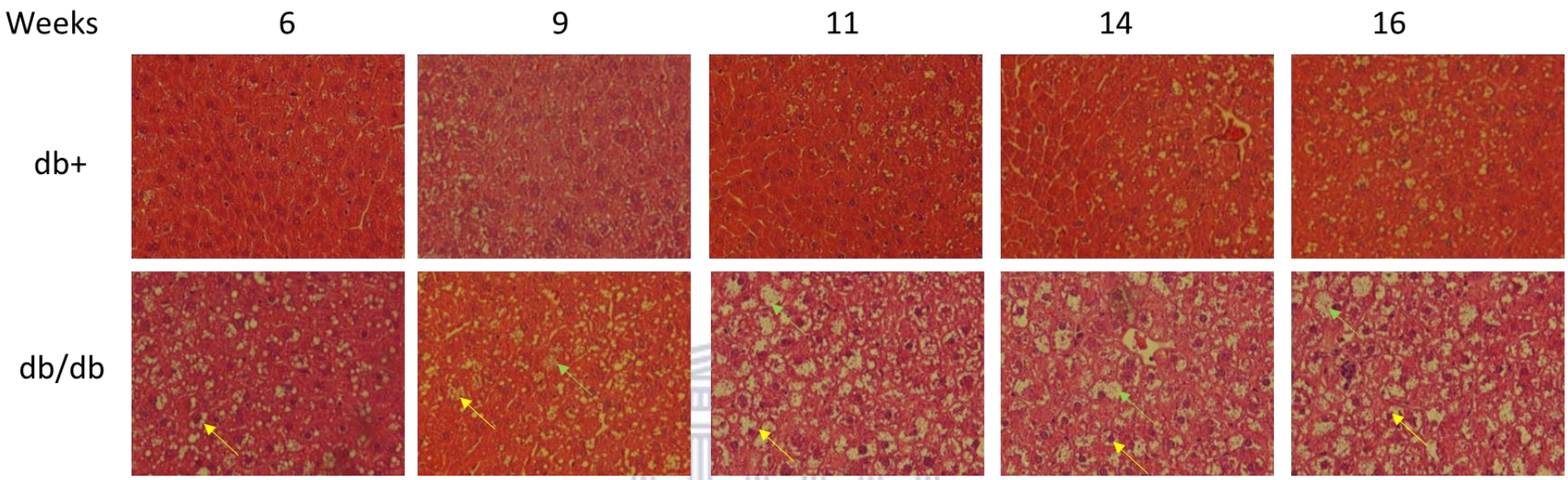

Figure 3.10: Hepatocellular pathological changes. Representative image of liver cross-sections from Leptin receptor-deficient db/db mice and their homozygous control db/+ control group. Histological observation of haematoxylin-eosin (H&E) sections. Microvesicular steatosis was (yellow arrows) observed in the livers of db/db mice from as early as 6-11 weeks, and at 14 weeks, macrovascular (green arrows) changes were apparent. Homozygous control db/+ at 6-16 weeks and leptin receptor-deficient db/db at 6-16 weeks. (Magnification x400)

3.2 PHASE 2: Validation of candidate genes *in vivo*

3.2.1 Morphometric risk factors of diabetic cardiomyopathy

Type 2 diabetes mellitus is a known risk factor for DCM. Individuals with T2DM present with increased body weight which is associated with chronic hyperglycaemia. Db/db mice are a model used for T2DM research and have similar traits such as spontaneous weight gain and increased fasting plasma glucose concentrations.

Morphometric observations: Six to sixteen-week-db/db and their lean db/+ controls were fed a standard chow diet for 11 weeks. Weekly, body weights and fasting blood glucose were conducted. The body weights of the db/db mice were significantly ($p<0.0001$) increased as early as six weeks (Figure 3.2 A). A significant increase in blood glucose was observed from week 9 to 16 in the db/db mice ($p<0.0001$) (Figure 3.3D). In contrast, there were no significant changes observed in the heart weights of db/db mice compared to their db/+counterpart. However, heart weight to tibia length showed a significant decrease at weeks 9 ($p<0.01$) and 11 ($p <0.05$ (Figure 3.2 B and C). In figure 3.2, a divergence in body weight, heart weight: tibia length and liver weights are observed from weeks six to fourteen, which can be explained by the weight gain observed during this weeks, while the convergence at week sixteen can be associated to a decline/plateau in weight during this week.

Triglycerides, LDL-cholesterol, total cholesterol, and increased blood glucose are known risk factors associated with T2DM, contributing to decreased cardiac contractility. This study demonstrated significantly increased LDL and triglyceride levels at weeks 6 and 16 ($p<0.01$) in the db/db mice. Additionally, the total cholesterol was significantly increased in db/db mice from week 6 to week 16 ($p<0.0001$) (Figure 3.3A-C).

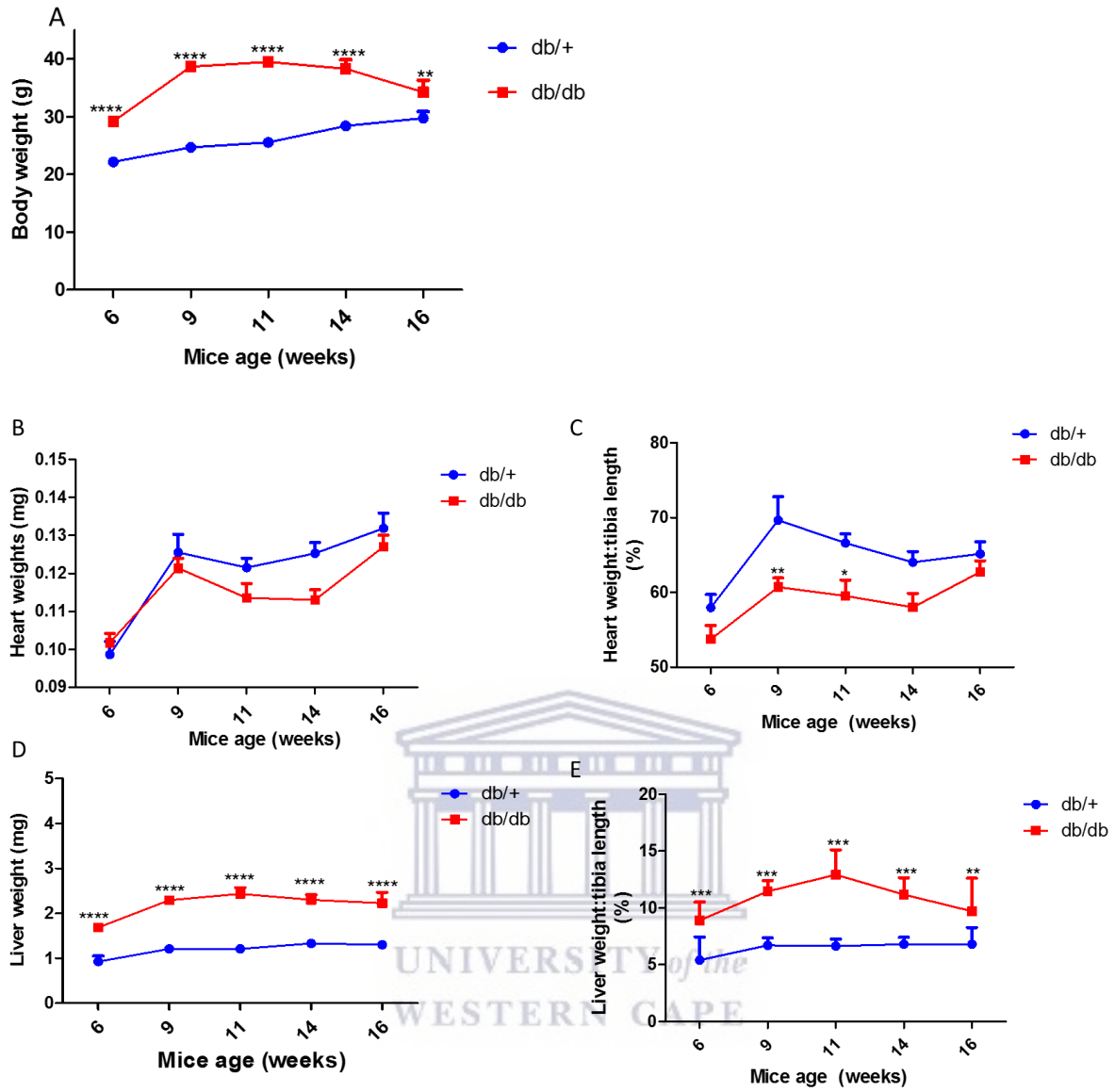

Figure 3.2: Morphometric analysis of 6-16-week-old Leptin receptor-deficient db/db mice.

Body weight (A), heart weight (B) Heart weight: tibia length (C) Liver weight D), and Liver weight: tibia length E) of homozygous Leptin receptor-deficient diabetic mice db/db mice and their heterozygous Leptin receptor-deficient db+. Results are expressed as the mean ± SEM of n=8 animals per group. * p <0.05, **p<0.01, ***p<0.001 and ****p<0.0001 versus nondiabetic age-matched control (db/+).

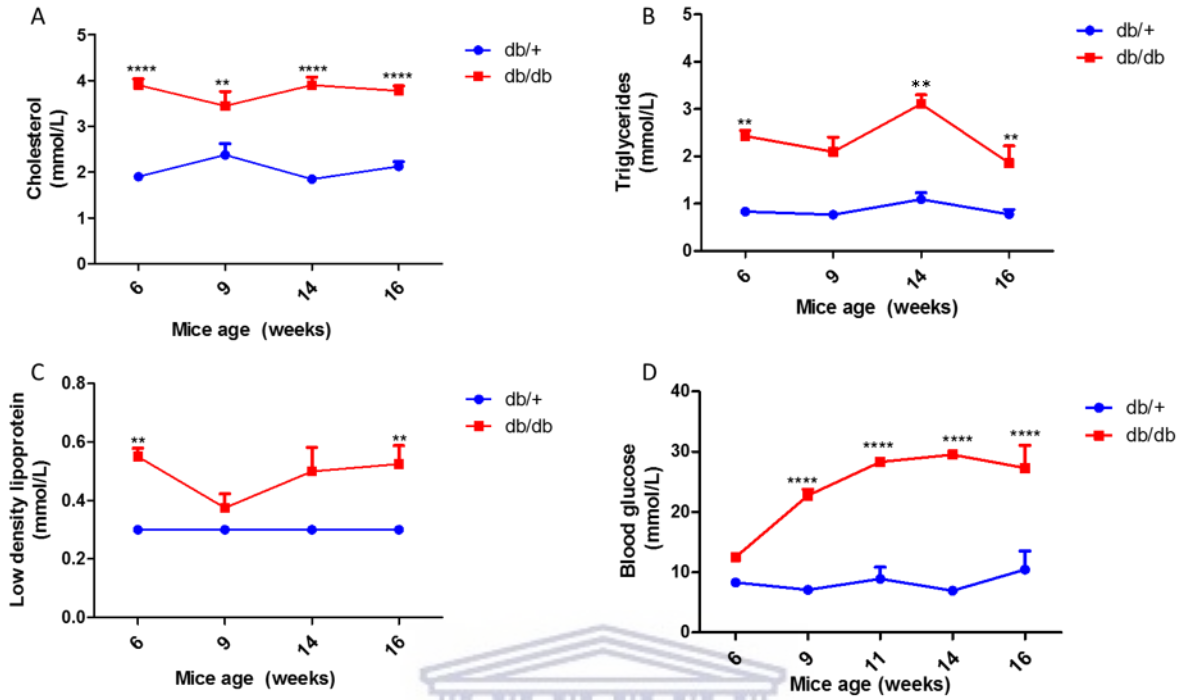

Figure 3.3: Lipid profile and blood glucose of Leptin receptor-deficient db/db mice at 6-16 weeks. Cholesterol (A), Triglyceride (B), Low-density lipoproteins (LDL) (C) and blood glucose (D) of db/db mice and their heterozygous Leptin receptor-deficient db/+. Results are expressed as mean ± SEM of n=8 animals per group. **p<0.01 and ****p<0.0001 versus nondiabetic age-matched control (db/+)

3.2.2 Confirmation of known predictors for cardiovascular risk using echocardiography

Type 2 diabetes is associated with cardiovascular changes that lead to the thickening of the myocardium that manifest mainly as diastolic dysfunction and later systolic dysfunction. Additionally, mice will present with reduced ejection fraction and left ventricular hypertrophy (Boudina et al., 2007; Dludla et al., 2017). Tissue Doppler Imaging is a non-invasive imaging technique that is the current gold standard for detecting DCM at its early asymptomatic stage (Lorenzo-Almorós et al., 2017). In this study, echocardiography analysis parameters are summarized in Table 3.3. There were no significant differences in the heart rate (HR) throughout the study. To measure changes in the LV, the following parameters were tested without significant differences observed: interventricular septum (IVS): d: diastole; s: systole; left ventricle internal diameter (LVID); left ventricle posterior wall (LVPW) and left ventricle mass (LV mass). Furthermore, the following parameters were measured to assess diastolic function: E wave; A wave; isovolumic relaxation time (IVRT) and E wave deceleration (E_{DT}). The E wave showed a significant decrease at weeks 11 ($p<0.05$), 14 ($p<0.05$) and 16 ($p<0.001$), while there were no significant differences observed with the A wave. For the IVRT and $E_{DT,}$ significant changes only occurred at weeks 14 ($p<0.001$) and 16 ($p<0.001$). Additionally, ejection fraction (Figure 3.4) was

significantly decreased at 14 ($p<0.05$) and 16 weeks ($p<0.05$). At week 16, the E: A ratio was significantly reduced ($p<0.001$) when the obese mice were compared to their db/+ counterparts (Figure 3.4) while reduced ventricular wall thickness was significant at week 16 ($p<0.05$).

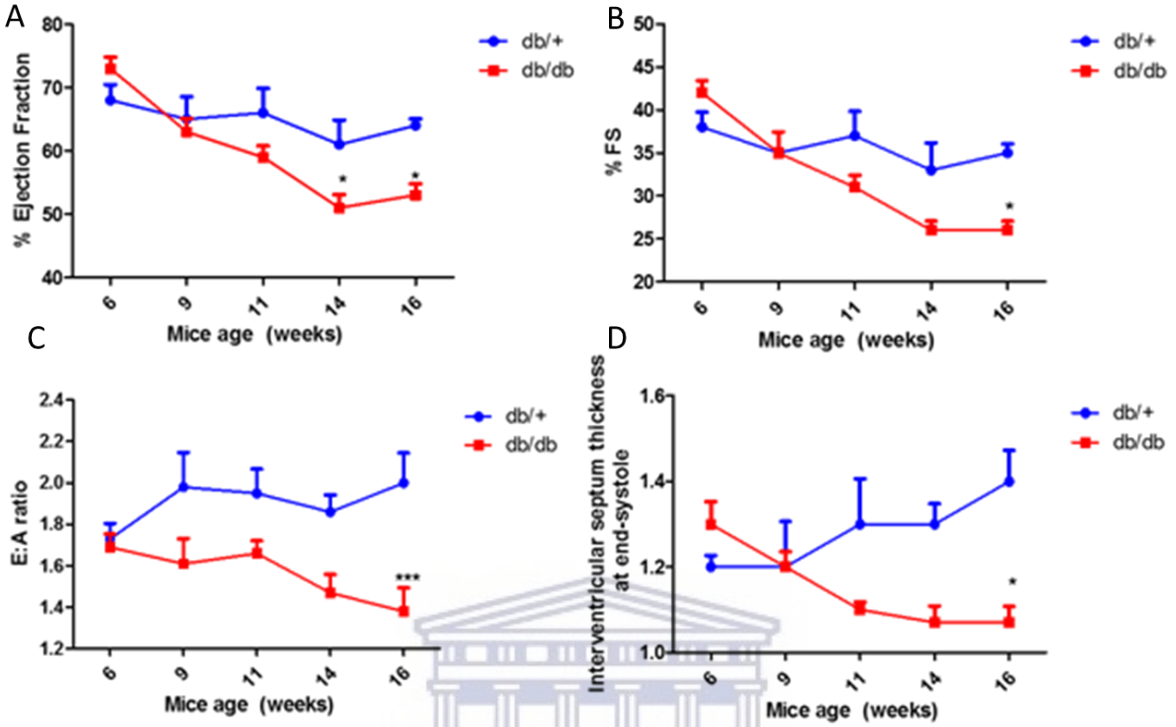

Figure 3.4: Determination of cardiovascular dysfunction using echocardiography of Leptin receptor-deficient db/db mice at 6-16 weeks. Ejection fraction (A) Fractional shortening (B) E: A ratio and (C) interventricular septum thickness (D). Results are expressed as mean ± SEM of 8 animals per group. *p<0.05 and ***p<0.001 versus nondiabetic age-matched control (db/+).

Table 3.3 Echocardiography characteristics of the lean and obese mice from week 6 to 16.

	6 weeks		9 weeks		11 weeks		14 weeks		16 weeks	
	Lean (db/+) (n=8)	**Obese** (db/db) (n=8)	**Lean** (db/+) (n=7)	**Obese** (db/db) (n=8)	**Lean** (db/+) (n=8)	**Obese** (db/db) (n=8)	**Lean** (db/+) (n=6)	**Obese** (db/db) (n=6)	**Lean** (db/+) (n=8)	**Obese** (db/db) (n=8)
Heart Rate	408±52	397±17	408±43	372±26	380±35	388±36	383±34	353±20	410±35	398±28
Left ventricle										
IVS, d (mm)	0.71±0.06	0.72±0.06	0.78±0.11	0.75±0.07	0.81±0.14	0.79±0.07	0.83±0.07	0.75±0.07	0.82±0.08	0.77±0.09
IVS, s (mm)	1.15±0.07	1.22±0.15	1.23±0.32	1.17±0.10	1.28±0.32	1.15±0.05	1.27±0.13	1.07±0.11	1.36±0.20	1.08±0.11
LVID, d (mm)	3.68±0.29	3.79±0.24	3.81±0.32	3.75±0.18	4.04±0.25	3.91±0.32	3.99±0.26	4.05±0.27	4.16±0.22	3.95±0.42
LVID, s (mm)	2.29±0.30	2.23±0.24	2.47±0.47	2.49±0.22	2.56±0.46	2.71±0.25	2.96±0.37	3.07±0.22	2.67±0.26	2.92±0.29
LVPW, d (mm)	0.68±0.07	0.77±0.17	0.73±0.05	0.70±0.13	0.78±0.13	0.81±0.05	0.78±0.09	0.80±0.07	0.73±0.09	0.79±1.06
LVPW, s (mm)	1.06±0.15	1.12±0.18	1.08±0,17	1.05±0.19	1.16±0.24	1.12±0.11	1.14±0.12	1.01±0.07	1.14±0.15	1.06±0.16
LV mass (mg)	78±11	90±6	99±10	94±21	119±17	113±11	120±15	115±11	121±21	113±30
Diastolic function										
E wave (mm/s)	808±116	734±61	822±108	652±85	792±106	694±61*	710±82	582±101*	775±66	606±154**
A wave (mm/s)	477±110	437±48	437±133	415±78	421±124	421±41	388±68	397±59	398±76	441±92
IVRT (ms)	13±3	13±7	11±1	15±5	13±3	17±3	17±3	27±6**	15±2	21±6**
E_{DT} (ms)	22±9	27±6	22±7	26±6	21±10	24±8	25±3	36±7*	21±6	32±4**

IVS: interventricular septum; d: diastole; s: systole; LVID: left ventricle internal diameter; LVPW: left ventricle posterior wall; LV mass: left ventricle mass; IVRT: isovolumetric relaxation time; E_{DT}: E wave deceleration time. Data are expressed as mean±SD. $^{*}p<0.05$, $^{**}p<0.01$ compared to age-matched wild type control using Mann-Whitney test.

3.2.4 Markers of fibrosis, hypertrophy, and apoptosis were measured as predictors of cardiac dysfunction

The markers of fibrosis, hypertrophy and apoptosis were measured in this section to confirm the establishment of DCM. Natriuretic peptide A (NPPA) is released in response to mechanical stretch of the atrial wall and elevated systemic blood pressure. In this study, NPPA levels showed increased expression at 6, 9, 14 and 16 weeks, with significance at ages 6 ($p \leq 0.05$) and 14 weeks ($p \leq 0.05$) in db/db mice when compared to the db/+ control (Figure 3.6 A). Connective tissue growth factor (CTGF) is a matricellular protein expressed in the vascular wall, regulating various macro-and microvascular pathologies. As such, dysregulation of CTFG has been strongly linked to the development of fibrosis. In this study, CTGF expression was significantly increased ($p \leq 0.05$) at week 14 only in db/db mice when compared to their db/+ counterpart ($p \leq 0.05$). Week 9 and 11 showed a decreased trend, whereas weeks 6 and 16 were similar to the control (mean±). The gene expression levels of the proapoptotic protein and the Bcl-2Associated X-protein (BAX) antiapoptotic protein B-cell lymphoma-2 (BCL-2) were also assessed. In this study, BAX and BCL-2 showed significant changes at 11 ($p \leq 0.05$) and 14 ($p \leq 0.05$) weeks compared to db/+ control. The observations made in this study with respect to gene expression changes which occurred only at certain weeks are consistent with other studies which have shown age-dependent alterations both at genetic and phenotype levels (Dalbøge et al., 2013; Dludla et al., 2017).

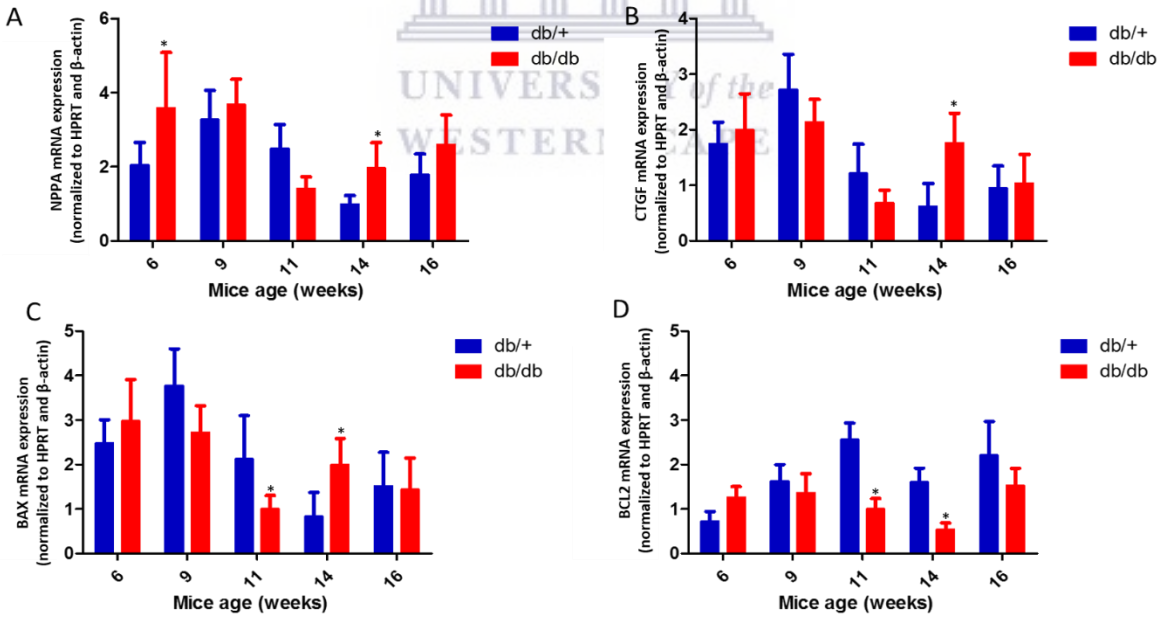

Figure 3.6: Hypertrophic, fibrosis and apoptosis markers in 6-16-week-old Leptin receptor-deficient db/db mice. Natriuretic Peptide A (NPPA) (A), connective tissue growth factor (CTGF) (B), B-cell lymphoma 2 (BCL-2) (C) and Bcl-2-associated X protein (BAX) (D). Genes were assessed at weeks 6-16 of spontaneous development of diabetes. Blue and red lines represent db/+ and db/db mice, respectively. Results are expressed as the mean ± SEM of n=8 animals per group

3.2.5 mRNA expression analysis of potential DCM biomarkers in heart tissue of 6-16 week old db/db mice

Cardiac tissue from db/db mice and their db/+ control counterparts was used to investigate the differential expressed pattern of the top 5 proposed DCM biomarkers (ZKSCAN4, IGF1, USP34, ETFβ and LOXL2) as obtained from the ArrayExpress database. Results obtained showed that ZKSCAN4, a transcriptional repressor of p53, was increased at 6- and 16-weeks, with significant changes observed at week 16 ($p<0.05$, 1-fold change) (Figure 3.7 A). Gene expression analysis for IGF-1 showed a significant increase at week 6 ($p < 0.05$, 1.5-fold change), then expression was down-regulated in the diabetic rat from 9 weeks onwards (Figure 3.7A). A 4-fold decrease ($p<0.0001$) of USP34 expression was observed at 9 weeks in the db/db mice compared to their db/+ controls. No other differential expression was observed for USP34. In addition, our study using qRT-PCR analysis revealed that cardiac mRNA expression of the ETFβ gene was significantly increased at 11 weeks, where after no changes could be observed in ETFβ expression when the db/db were compared to their age-matched db/+ control. At week 11, LOXL2 showed a ($p<0.001$, 2.2-fold) differential increase, a further increased mRNA expression was observed at weeks 14 ($p<0.05$, 0.8-fold change) and 16 ($p<0.05$, 0.5-fold change) in expression of db/db mice when compared to db/+ control (Figure 3.7D).

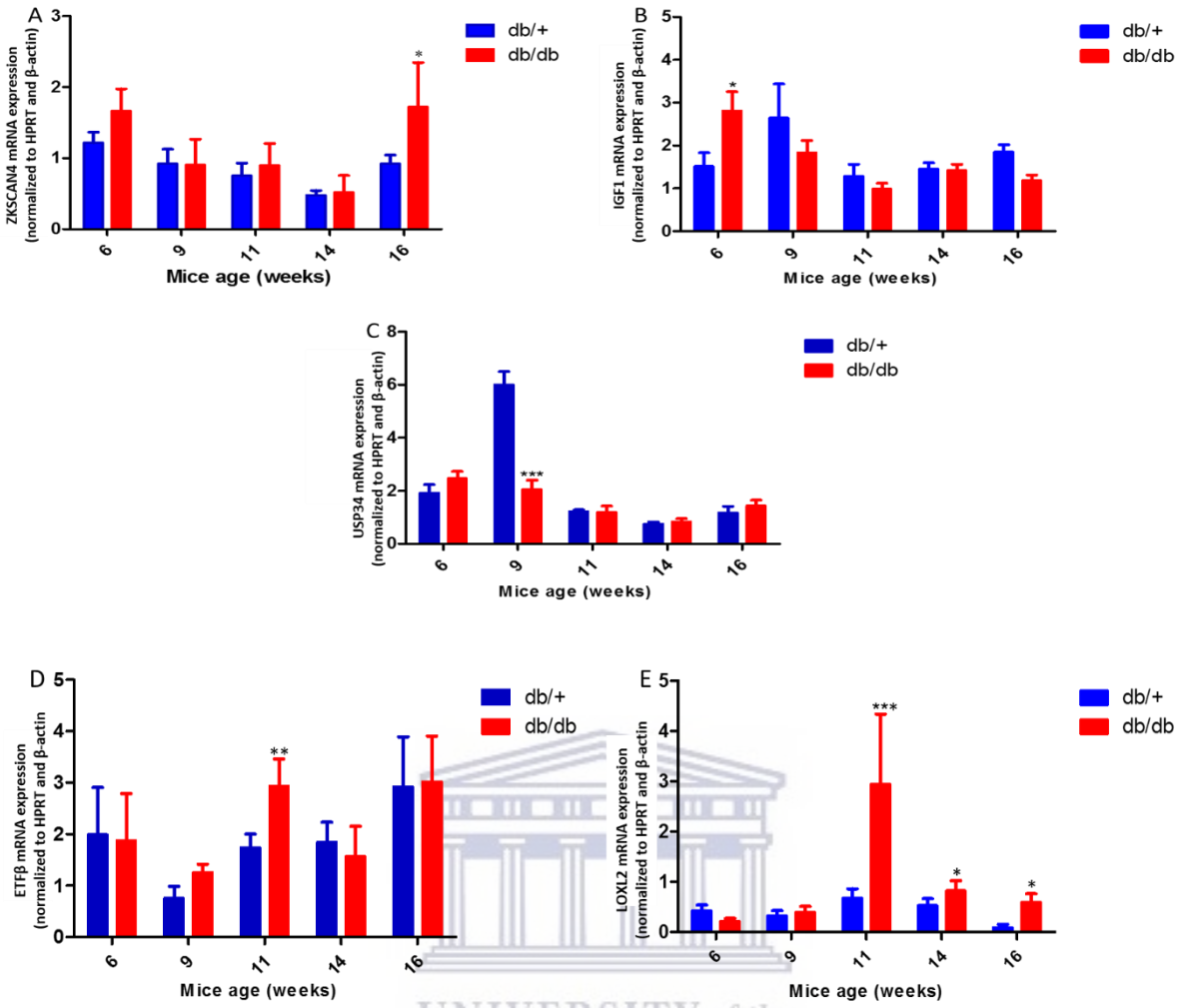

Figure 3.7: mRNA expression of candidate genes in myocardial tissue in 6-16-week-old Lepton receptor-deficient db/db mice. Differential expression of Zinc Finger with KRAB and SCAN Domains 4 (ZKSCAN4) (A), Insulin-like growth factor 1 (IGF1) (B) Ubiquitin carboxyl-terminal hydrolase 34 (USP34) (C), Electron transfer flavoprotein subunit beta (ETFβ) (D) and Lysyl Oxidase Like 2 (LOXL2) (E) in heart tissue of leptin receptor-deficient mice db/db compares to age-matched lean control db/+. Results are expressed as mean ± SEM of n=8 animals per group. *p<0.05, **p<0.01, ***p<0.001 and ****p<0.0001 versus nondiabetic age-matched control (db/+)

3.2.5 UPS34, ZKSCAN4, IGF1, ETFβ, LOXL2 and NT-pro-BNP protein expression in serum of obese mice

In order to explore the use of the proposed candidate genes as possible serum prognostic/diagnostic markers, we tested if the identified proteins are released from the cardiac interstitial space into the circulation during a disease state. This study showed no difference in serum protein expression of UPS34, ZKSCAN4 and IGF1 (Figure 3.8 A-C), respectively. Conversely, serum protein levels of LOXL2 were elevated from weeks 6 to 16. However, statistically, significant differences were only observed at weeks 9 ($p<0.01$) and 11 ($p<0.01$) when compared to their db/+ counterparts (Figure 3.8 D). Conversely, serum expression of ETFβ was significantly reduced at 11, 14 and 16 ($p<0.001$, $p<0.001$ and $p<0.05$) when compared to their none diabetic controls (Figure 3.8 E). The discrepancy between the mRNA and protein expression levels of ETFβ, can be explained by the 40% variation protein and mRNA levels ascribed to regulation between DNA transcription, translation and posttranslational modification of protein products (Koussounadis et al., 2015; Perl et al., 2017).

Measurements of serum NT-proB-type Natriuretic Peptide (NT-pro-BNP) were performed and it is released in response to increased cardiac pressure. These changes are often associated with HF and other myocardial changes. NT-pro-BNP levels are increased in response to cardiac changes/HF and are reduced under physiological conditions or when managed through treatment. In the current study, increased levels of NT-pro-BNP were observed only at week 14 ($p<0.01$) (Figure. 3.8 F).

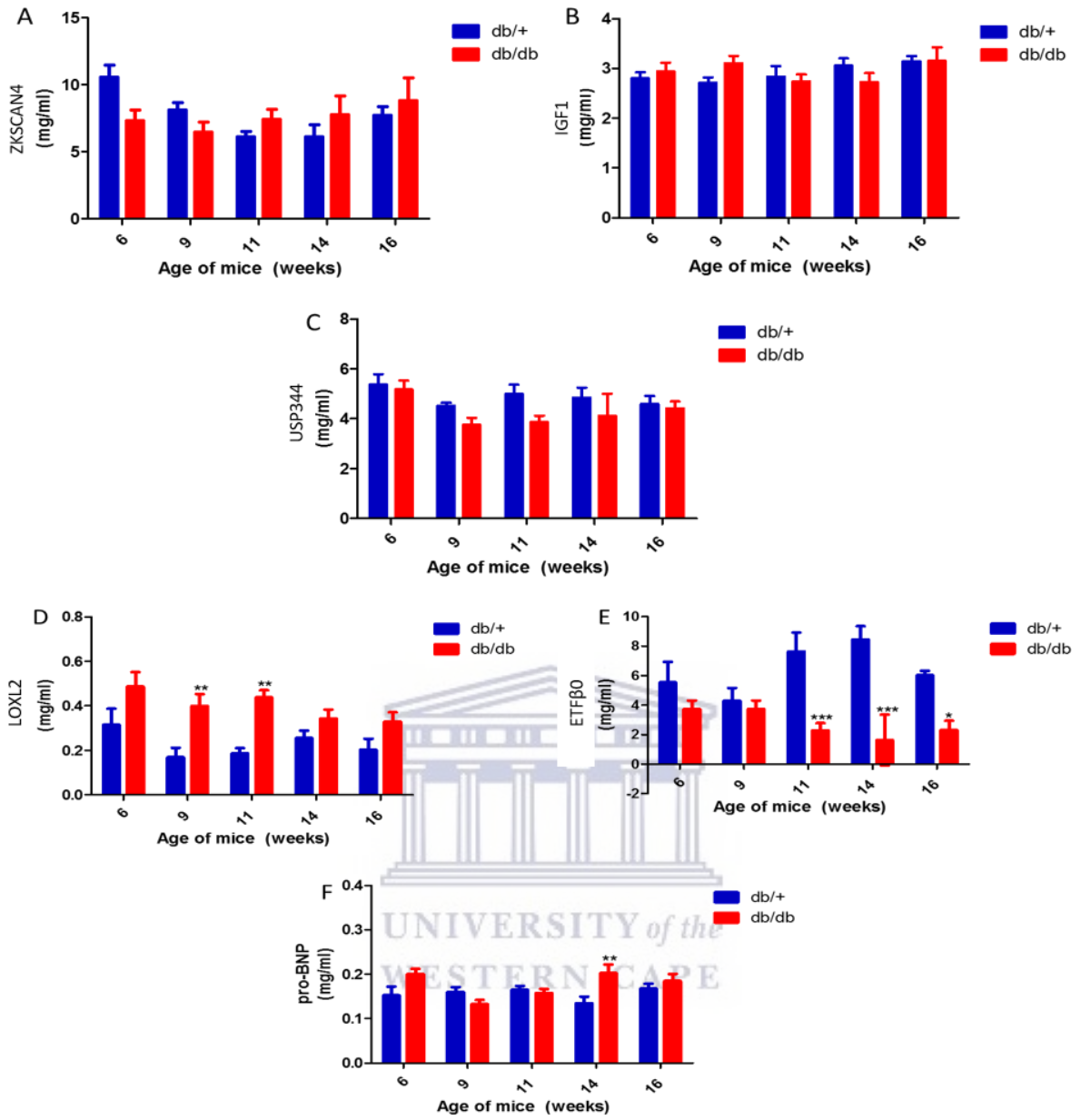

Figure 3.8: Expression of serum biomarkers in 6-16-week-old Lepton receptor-deficient db/db mice. Zinc Finger with KRAB and SCAN Domains 4 (ZKSCAN4) (A), Insulin-like growth factor 1 (IGF1) (B) Ubiquitin carboxyl-terminal hydrolase 34 (USP34) (C), Electron transfer flavoprotein subunit beta (ETFβ) (D) and Lysyl Oxidase Like 2 (LOXL2) (E) N-terminal prohormone of brain natriuretic peptide NT-pro-BNP (F) of leptin receptor-deficient mice db/db compared to aged-matched lean control db/+. Results are expressed as mean ± SEM of n=8 animals per group. *p <0.05, **p <0.01 and ***p<0.0001 versus nondiabetic age-matched control (db/+).

3.2.6 ETFβ, LOXL2 and NT-pro BNP correlation analysis with mitral E: A ratio

In clinical practice, the E: A ratio indicates the degree of HF, guiding the implementation of interventions. As such, this study examined the correlation between serum markers that were significantly expressed (ETFB and LOXL2) as well as NT-proBNP and the mitral E: A ratio. Pearson correlation efficiency was used to determine the linear relationship between the proposed biomarkers. According to Pearson correlation analysis, an r of 1 shows a perfect positive correlation, an r of -1 depicts a negative correlation, whilst an r of 0 indicates no relationship. A significant positive correlation was observed when ETFβ was correlated to the E: A ratio (Pearson correlation, r = 0.675, $p<0.05$). A negative correlation was observed when serum LOXL2 levels were correlated to the E: A ratio (Pearson correlation, r = - 0.66, p = 0.05). Similarly, a negative correlation was observed when NT-proBNP was correlated with the E: A ratio (Pearson correlation, r = -0.09, p =ns). (Figure 3.9 A-C).

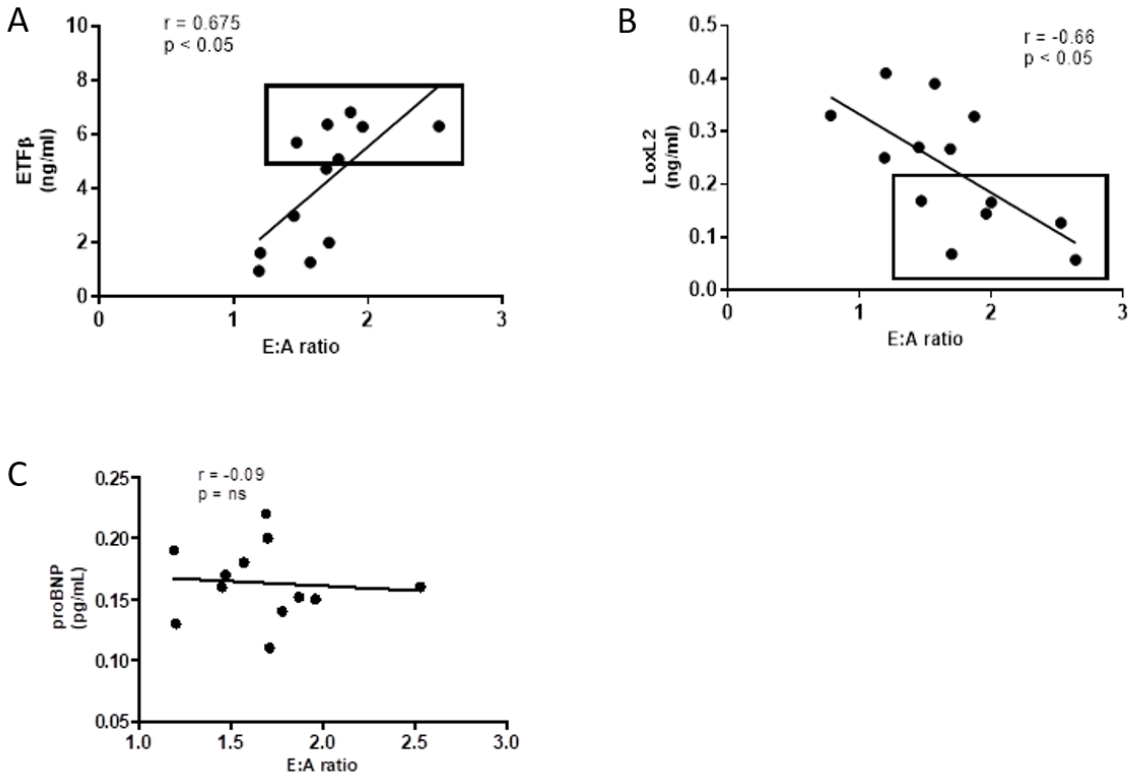

Figure 3.9 Serum correlation of biomarkers (ETFβ, LOXL2 and proBNP) to E: A ratio of Leptin receptor-deficient db/db mice at 6-16 weeks. Correlation between ETFβ and NT-pro-BNP (A), correlation between ETFβ and E: A ratio (B), correlation between LOXL2 and E: A ratio (C), correlation between proBNP and E: A ratio

3.2.7 Haematoxylin and eosin stain (H&E) and Masson's trichrome staining of db/+ vs db/db mice hearts did not show pathology

Haematoxylin and eosin (H&E) staining is one of the prominent stains in tissue histology, with pathologists using it to assess tissue biopsies in medical diagnosis. Staining with H&E showed no significant changes between db/+ and db/db mice. The histological sections were sent to the IDEXX laboratories for pathological examination to confirm this. The pathologist confirmed that there were no DCM associated lesions such as interstitial fibrosis or collagen deposition (Figure 3.10). Interestingly, though the myocardial fibres showed increased diameter when correlated with echocardiography data, the results showed no significant increase in LV wall thickness (Table 2, Figure 3.10). Subsequently, the tissues were stained with Masson's Trichrome, which discriminates between collagen and smooth muscle by using three dyes that selectively stain for muscle, collagen fibres, fibrin and erythrocytes. Similarly, no significant collagen deposition from weeks 6 to 16 could be observed (Figure 3.11).

3.2.8 Both ETFβ and LOXL2 are increased in cardiac histology sections of db/db mice

Immunostaining of cardiac tissue sections showed increased levels of ETFβ and LOXL2 proteins in the interstitial space of db/db mice compared with their lean db/+ controls from weeks 9 and 11, respectively. Staining of myocardial tissue with anti-ETFβ showed a trend towards increased protein expression when db/db was compared to age-matched db/+ control (Figure 3.12). Myocardial tissue staining with anti-LOXL2 showed a significantly increased immunostaining from weeks 11 to 16 ($p<0.001$). Our findings suggested that LOXL2 and ETFβ could be potential markers for identifying DCM early compared to traditional stains, such as H&E.

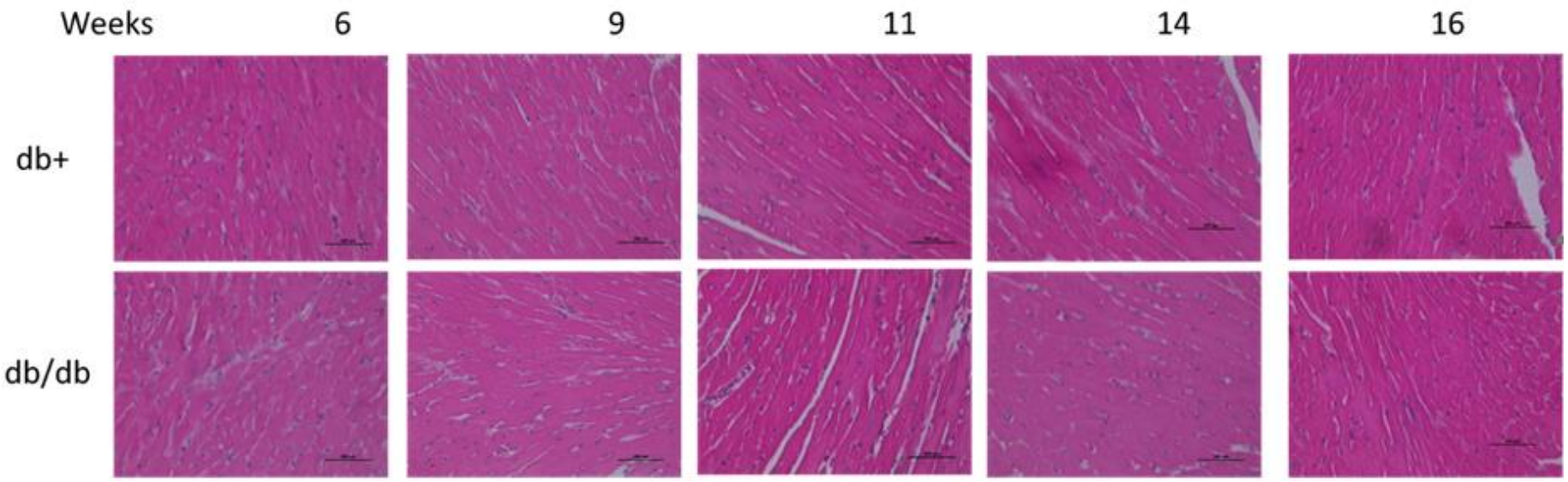

Figure 3.10 No pathology observed in Hematoxylin and eosin-stained db/db cardiac section. Representative images of heart cross-sections from Leptin receptor-deficient db/db mice and their homozygous control db/+ control group. Db/+ at 6-16 weeks (A) and db/db at 6-16 weeks (B), showing no cardiac remodelling in both db/+ and db/db mice. (Magnification x400)

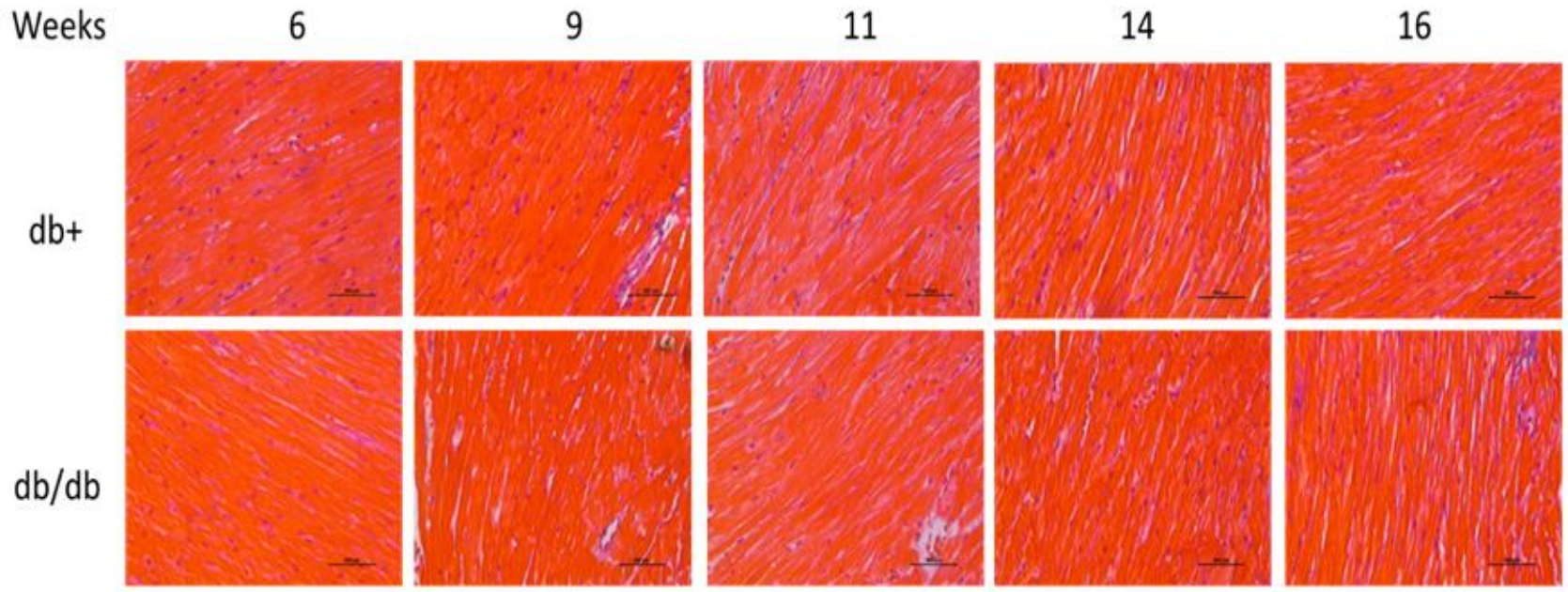

Figure 3.11 Masson's Trichrome stained cardiac sections with no increased collagen in db/db mice. Representative images of heart cross-sections from Leptin receptor-deficient db/db mice and their homozygous control db/+ control group. Db/+ at 6-16 weeks (A)and db/db at 6-16 weeks (B). (Magnification x400)

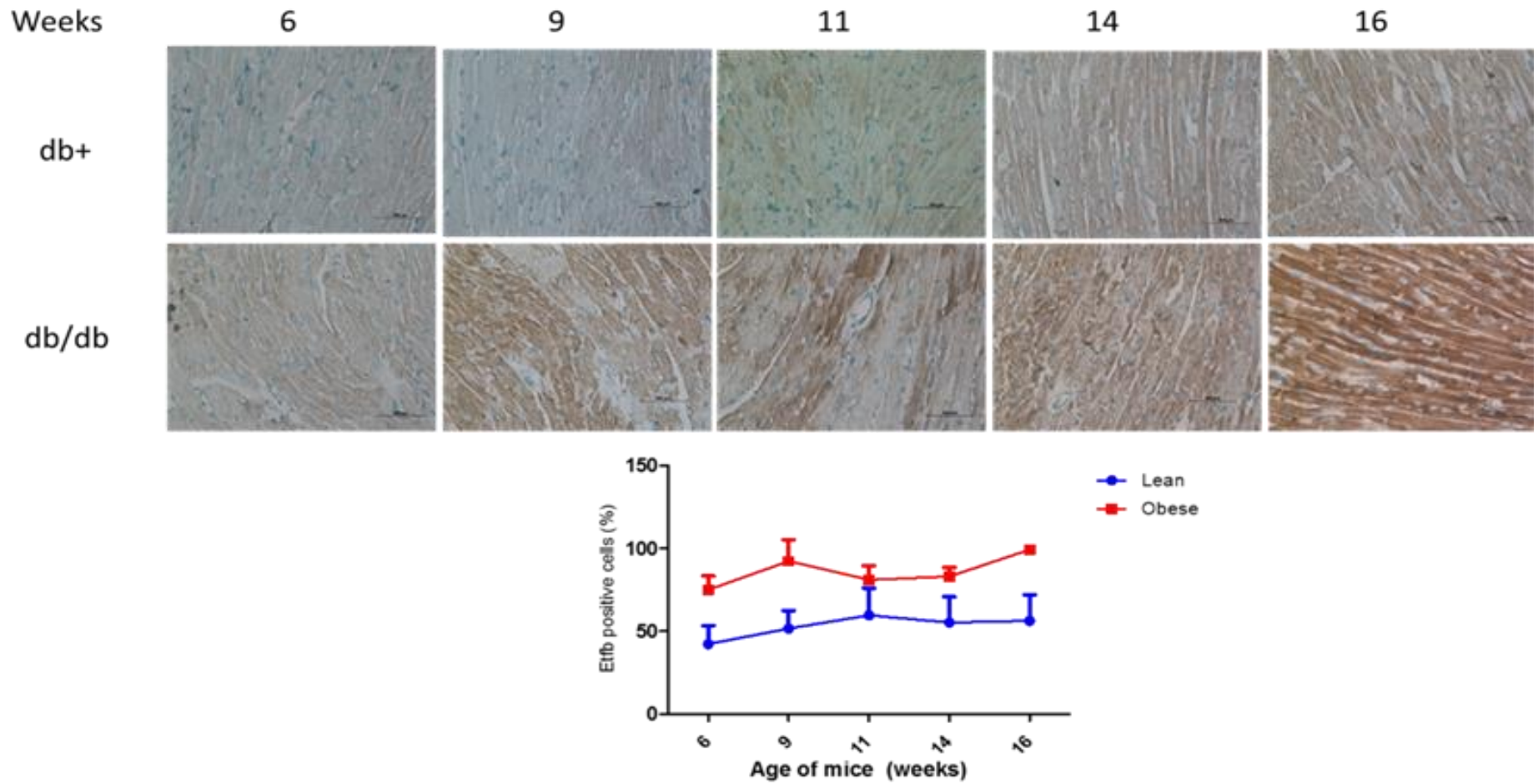

Figure 3.12 Age-dependent increased expression of anti-ETFβ in cardiac sections of db/db mice. Representative images of heart cross-sections from Leptin receptor-deficient db/db mice and their homozygous control db/+ control group. Db/+ at 6-16 weeks (A) and db/db at 6-16 weeks (B). (Magnification x400)

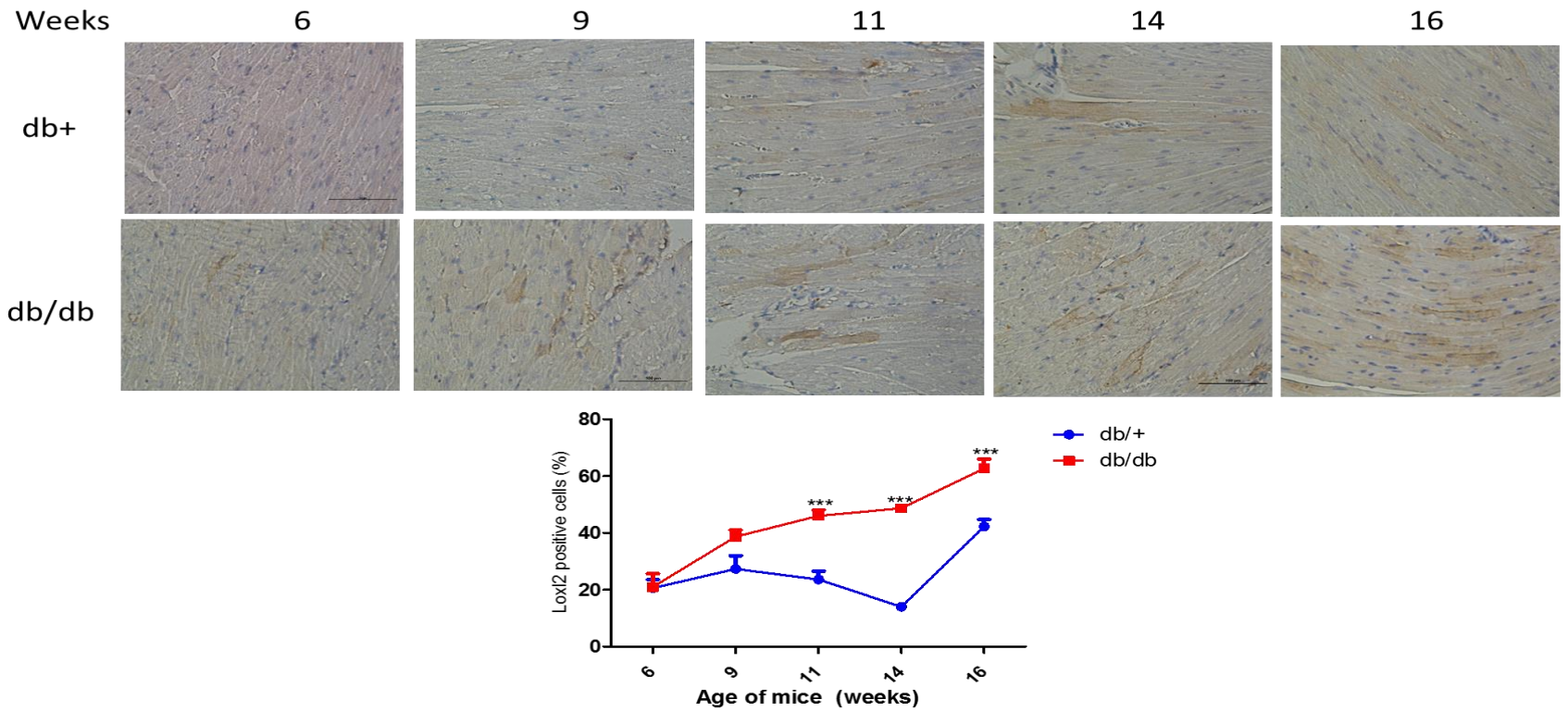

Figure 3.13 Increased expression of anti-LOXL2 in db/db mice cardiac sections. Representative images of heart cross-sections from Leptin receptor-deficient db/db mice and their homozygous control db/+ control group. Db/+ at 6-16 weeks (A) and db/db at 6-16 weeks (B). (Magnification x400)

3.2.9 Summary

The establishment of T2DM, a risk factor for DCM, was observed using morphometric measurements, lipid profiles and liver enzymes. Morphological measurements showed a significant increase in body weight, liver weight, and the ratio of liver to tibial length. However, heart weights were reduced in db/db mice compared to their db/+ littermate controls. Similar results were observed with the heart to tibia length ratios. In this study, db/db mice showed a significant increase in triglyceride, cholesterol and LDL from 6 weeks of age, while blood glucose was significantly increased from week 9. The obese db/db mice presented with increased liver enzyme AST levels from week 14, while ALT showed significant increases as early as week 6.

Additionally, changes in liver histology, showing both micro-and macro vesicles, were also established by week 6 and 9 respectively in db/db mice compared to their db/+ controls. Myocardial mRNA expression of LOXL2 and IGF1 was significantly different between db/db and age-matched db/+ control. Serum analysis successfully discriminated between the identified biomarkers, with the serum expression of LOXL2 and ETFβ being significantly different and could detect it earlier than NT-pro-BNP. Of the five candidate biomarkers tested, LOXL2 was the only marker that remained significantly different in both heart and serum of db/db compared to db/+ control. Interestingly, serum analysis of ETFβ was found to be significantly reduced, while serum LOXL2 levels were significantly increased, and both occurred earlier than the changes observed in NT-pro-BNP. Based on the above findings and the aim of the current study to identify biomarkers that detect DCM at an early stage, only LOXL2 and ETFβ were explored as possible candidate biomarkers from here onwards. Results obtained showed that reduced interventricular septum was observed at week 16.

Similarly, the ejection fraction ($p<0.05$, weeks 14 and 16) and E: A ratio ($p<0.001$, week 16) were reduced. The serum levels of ETFβ were positively correlated to ejection fraction and E: A ratio ($p=0.003$, $p<0.001$). Whereas LOXL2 serum expression was negatively associated with ejection fraction and E: A ratio. The traditional histological stains such as H&E and Masson's Trichrome stain were used to confirm DCM pathology; however, no significant differences were observed. Nevertheless, when the histology sections were stained with anti-ETFβ and anti-LOXL2, the difference in fibrotic tissue could be observed. Thus, we observed concordant results between mRNA expression and serum protein abundance of LOXL2 in the context of biomarker target discovery.

3.3 Phase 3: Effect of silencing LOXL2 and EFTβ on their up-and downstream effectors

Although clinical research and *in vivo* studies using animal models like ob/ob or db/db mice are widely used to study DCM disease pathology, the respective models are also used to gain further molecular insights into the underlying mechanisms that drive the observed DCM pathology. In this study, H9c2 rat heart derived cardiomyocytes were used for this purpose. The genes LOXL2 and EFTβ were transiently silenced by introducing small interfering RNA (siRNA) or scramble RNA (scrRNA) as control integrated into H9c2 cells for 24 and 48 hours, respectively. After this, a DCM like environment was simulated by exposing the cells to high glucose (HG) and palmitic acid (PAL). The functional role of LOXL2 and ETFβ, as well as its downstream effectors, were assessed.

3.3.1 siLOXL2

Following transfection with the siLOXL2 and scrambled (scr) LOXL2 for 24 hours and further exposure to HG and PAL, mRNA levels of scr LOXL2 were significantly increased when compared to the control and siLOXL2 ($p<0.001$), while cells treated with siLOXL2 was significantly decreased (Figure 3.14A). Similarly, siLOXL2 protein expression was significantly decreased when compared to the control-treated with PAL and HG ($p<0.001$) (Figure 3.14A and B). Transforming growth factor beta (TGFβ) has been shown to promote the production of extracellular matrix (ECM) and collagen production. Therefore, in this study, the expression of the downstream effectors of LOXL2, TGFβ and collagen 1a (Col1A), collagens typically provide scaffolding for cells, were assessed post LOXL2 silencing. Results obtained showed that H9c2 cells transfection with the siLOXL2 and post-treated with HG and PAL resulted in a significant increased TGFβ mRNA ($p<0.001$) expression, while Col1A mRNA expression was significantly decreased ($p<0.01$) when compared to the scr LOXL2 control (Figure 3.14 C and D). Finally, the protein expression of the following genes BCL-2 (involved in apoptosis), CPT2 (involved in beta-oxidation), NT-proBNP (known marker of CVD) and TGF were also assessed. Results obtained showed no significant differences when the scr LOXL2 was compared to the siLOXL2. Finally, no significant differences were observed in the protein expression of BCL-2, carnitine palmitoyltransferase 2 (CPT2), NT-proBNP and TGFβ. However, a ($p<0.01$) significant difference was observed with phosphor anti-Smad (Smads are upstream regulators of TGFβ).

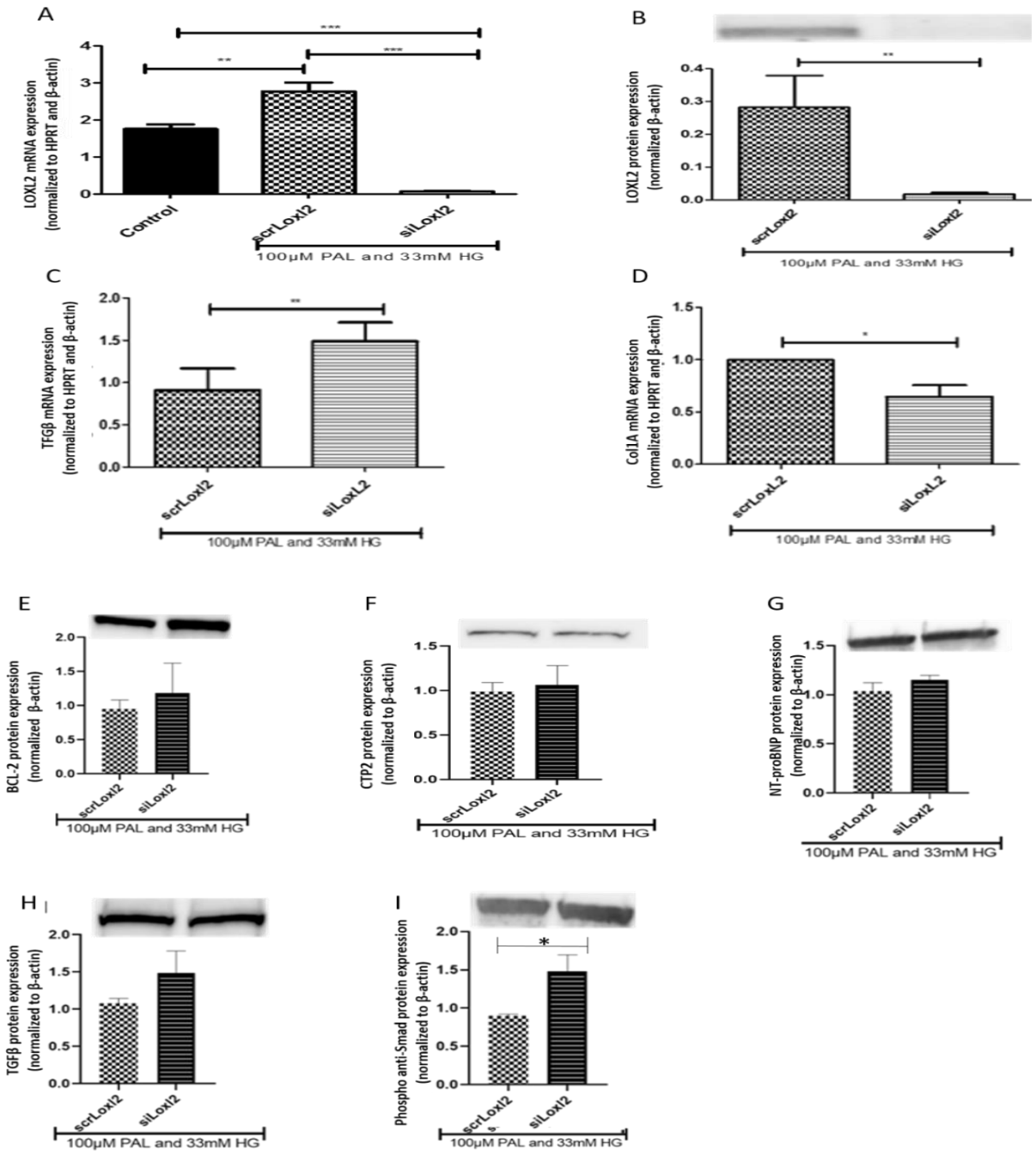

Figure 3.14 Effect of LOXL2 knockdown on transcription growth factor beta (TGFβ), B-cell lymphoma 2 (BCL-2), Carnitine palmitoyltransferase II (*CPT2*), N-terminal prohormone of brain natriuretic peptide (NT-proBNP), phosphor anti-mothers against decapentaplegic (Smad) and collagen 1A (Col1A) expression. LOXL2 siRNA or scramble control transfected H9c2 cells exposed to 100µM PAL and 33mM HG. The expression levels were normalized relative to the control. LoxL2 mRNA expression A) LoxL2 protein expression B) TGF mRNA expression C) and Col1A expression D) BCL-2 protein expression E) CPT2 protein expression F) NT-pro-BNP G) TGF protein expression H) and phosphor anti-Smad protein expression. The statistical significance was evaluated using the Student's t-test. This graph represents the SEM of triplicate samples. $p<0.05$, $p<0.01$ and $p<0.001$ when compared to control or scrambled control.

3.3.2 siETFβ

H9c2 cells were transfected with ETFβ or scrRNA for 48 hours and exposed to HG and PAL. HG and PAL exposure significantly decreased mRNA expression of ETFβ when compared to the scrambled control ($p<0.01$). A similar effect was observed when ETFβ was compared to scr ETFβ ($p<0.01$) (Figure 3.15A). Concentrations of 100 nM or more have been shown to yield nonspecific silencing effects when compared to their lower counterparts of 30 nM or less (Semizarov et al., 2003). In the present study, a concentration of 100 nM was found to be effective for transfecting either with siLOXL2 (Figure 3.16A) or ETFβ (Figure 3.15A) respectively. In addition, to assess whether ETFβ was required for Acyl-CoA dehydrogenase medium chain (ACADM, oxidoreductase enzyme, required for producing acetyl coA) and collagen 1A (Col1A) expression, the effect of siETFβ mRNA of ACADM and Col1a1 were assessed. H9c2 cells transfected with siRNA protein and mRNA expression of ACADM (p = ns) and Col1A ($p<0.05$) was significantly decreased compared to the scrambled control. Furthermore, the expression of carnitine palmitoyltransferase 1 (CPT1), involved in beta-oxidation, and ACADM was not significantly changed following siRNA transfection; however, the expression of NT-proBNP was significantly reduced in transfected H9c2 cells ($p<0.001$).

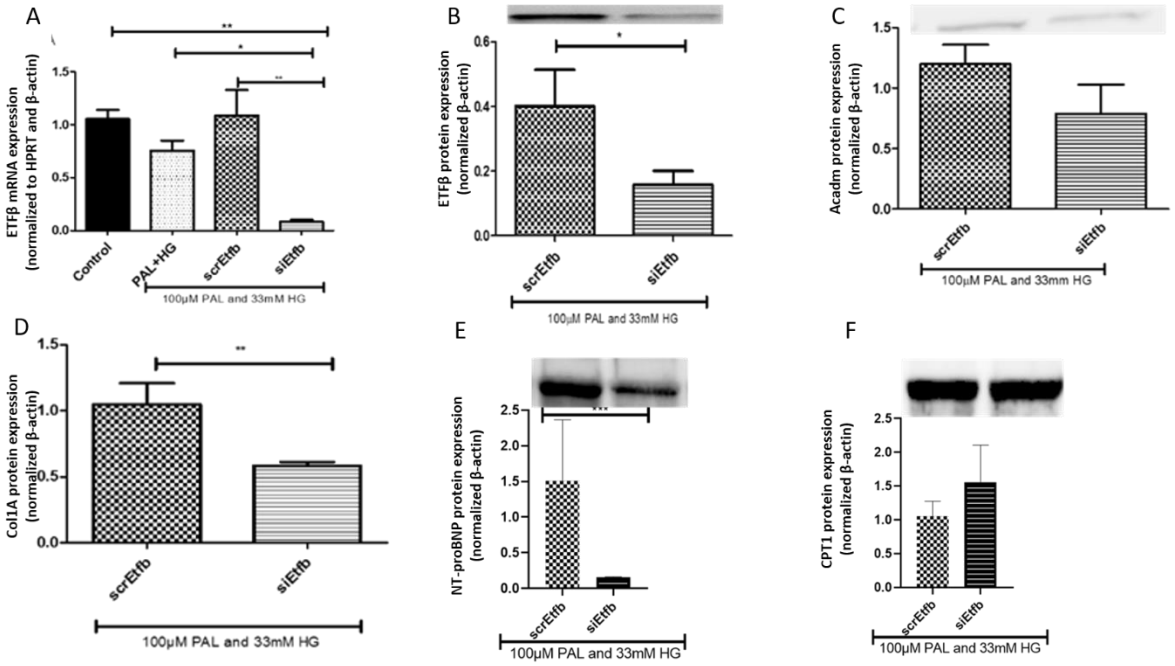

Figure 3.15: Effect of ETFβ knockdown on Acadm, CPT1, NT-proBNP and Col1a1. ETFβ siRNA or scramble control transfected H9c2 cells exposed to 100μM PAL and 33mM HG. ETFβ mRNA expression A) ETFβ protein expression B), Acadm protein expression C), Col1a1 mRNA expression D), NT-proBNP protein expression E), CPT1 protein expression F). The expression levels were normalized relative to the control. The statistical significance was evaluated using the Student's t-test. This graph represents the SEM of triplicate samples. $p<0.05$, $p<0.01$ or $p<0.001$ when compared to control or scrambled control.

3.3.3 Summary

The expression of LOXL2 was increased in H9c2 cells, both in the normal and scrambled controls. However, a marked decrease in LOXL2 expression was observed following knockdown. At the mRNA, the results showed strikingly increased levels of TGFβ while Col1a1 reduced following transfection. In contrast to these results, the protein levels of TGFβ showed no significant differences. Similarly, the protein levels of BCL-2, CPT2, and NT-proBNP and phosphor anti-Smad remained unchanged. ETFβ expression at both mRNA and protein levels was reduced in the treated cells following transfection and exposure to HG and PAL. Furthermore, Col1a1 expression was significantly reduced at the mRNA level. Interestingly, NT-proBNP protein levels were significantly increased. While mRNA levels of Acadm were not significantly changed and a similar observation was made with CPT1.

3.4 Phase 4: Sensitivity and specificity

3.4.1 Determination of sensitivity and specificity

Since the overall aim of the study was to identify a biomarker profile that would be able to detect DCM at its asymptomatic stage, it was imperative to assess the sensitivity and specificity of the identified markers. The sensitivity and specificity test conducted in this study were to ascertain whether the identified biomarkers could be used singly, in combination and whether they were comparable or superior to the current detection methods ETFβ and LOXL2 were compared to Echocardiography, which is the gold standard detection method (imaging) and the current commercial biomarker for HF, NT-pro-BNP.

Initially, a generalized linear regression model was used to test whether a relationship been the markers and NT-pro-BNP existed. Results were considered significant if the differences between db/+ and db/db mice at each week for ETFβ, LOXL2 and NT-proBNP had a $p<0.001$. The results showed no significant differences for NT-proBNP and LOXL2 for each week (Table 3.4). Conversely, ETFβ showed significant differences at weeks 11 and 14 ($p=0.001$, $t=3.91$ and 3.67 respectively) (Table 3.4). Subsequently, the results for the three biomarkers (NT-proBNP, LOXL2 and ETFβ) were combined to perform principal component analysis (PCA), which was used to determine the correlation/relationship between these markers further (Table 3.5). Results showed that the first principal component accounted for almost 89% of the variation in the data, which was the linear combination of the three biomarkers. Then, the Receiver Operating Characteristic (ROC) curve was used to conduct sensitivity and specificity analysis. The mice groups were either specified (db+ or db/db) or unspecified, and a low area under the curve was observed when the groups were not specified (Figure 3.16, 0.679) and increased when they were specified (Figure 3.17, 0.797) for ETFβ. This was regarded as a good predictive power of the model. Furthermore, the linear combination of LOXL2 and ETFβ was tested when the groups were not specified, and an AUC of 0.795 with a cutoff point is 0.789 was obtained (Figure 3.18). Similarly, for LOXL2 and ETFβ, when the groups were specified, the AUC was increased to 0.813, with a cutoff value of 0.824. This showed the good predictive power of the model, thus, indicating the biomarkers are more sensitive when used together (Figure 3.19).

Table 3.4: Statistical analysis for all biomarkers

	Mice age (Weeks)	t value	p value
NT-proBNP	6	-2.05	0.096
	9	1.33	0.23
	11	1.85	0.1
	14	-1.05	0.34
	16	-1.22	0.25
ETFβ	6	1.94	0.09
	9	0.59	0.57
	11	3.91	0.001
	14	3.67	0.001
	16	3.08	0.022
LOXL2	6	0.11	0.92
	9	-2.39	0.04
	11	-4.29	0.09
	14	0.23	0.82
	16	-1.98	0.08

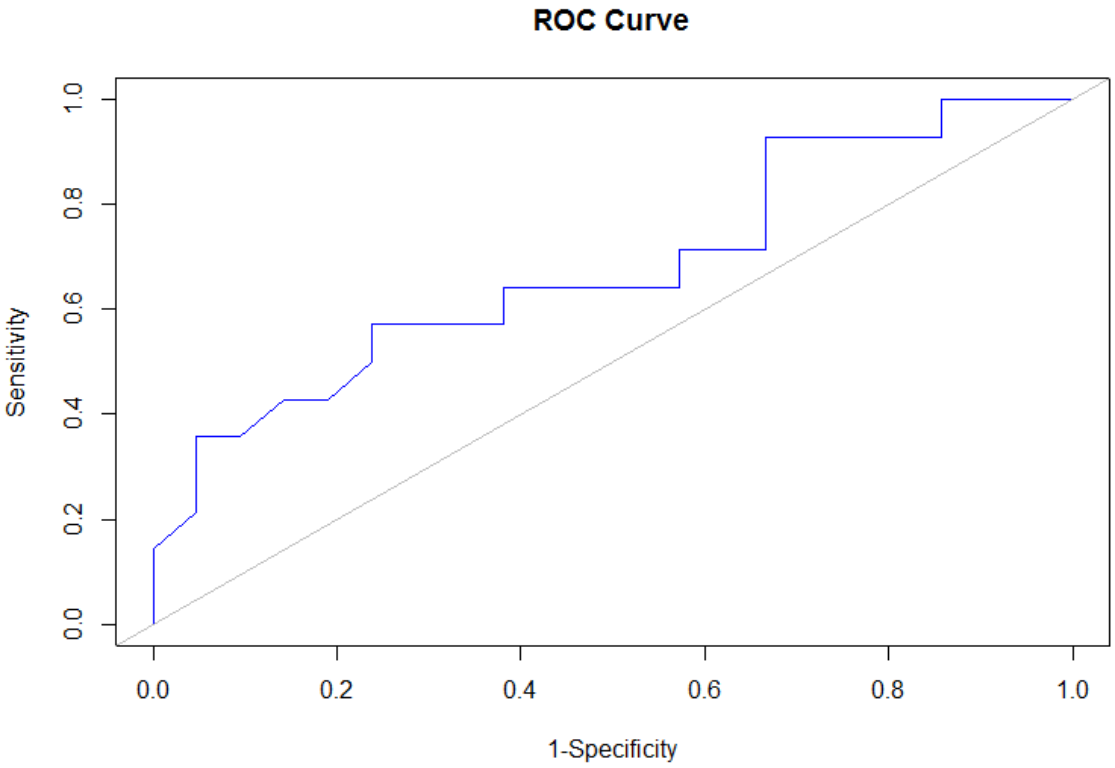

Figure 3.16: ROC curve for ETFB at different cut off points when groups are not specified.

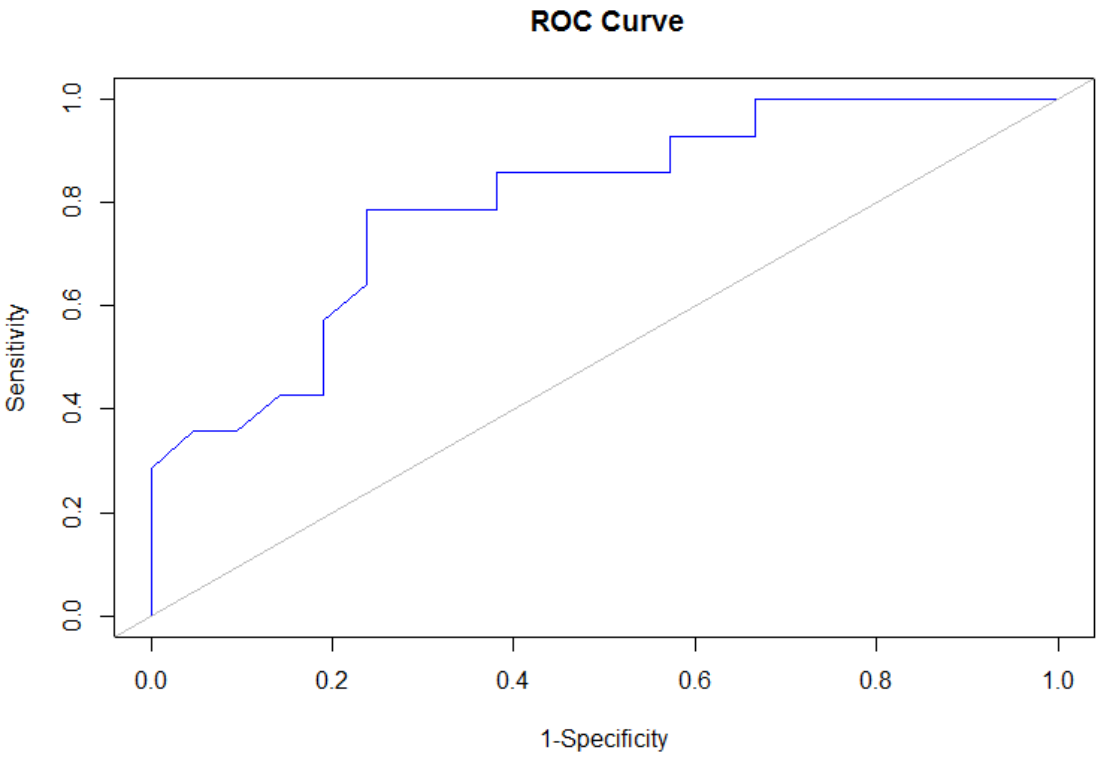

Figure 3.17: Curve of ROC at different cut off points of ETFB with groups specified.

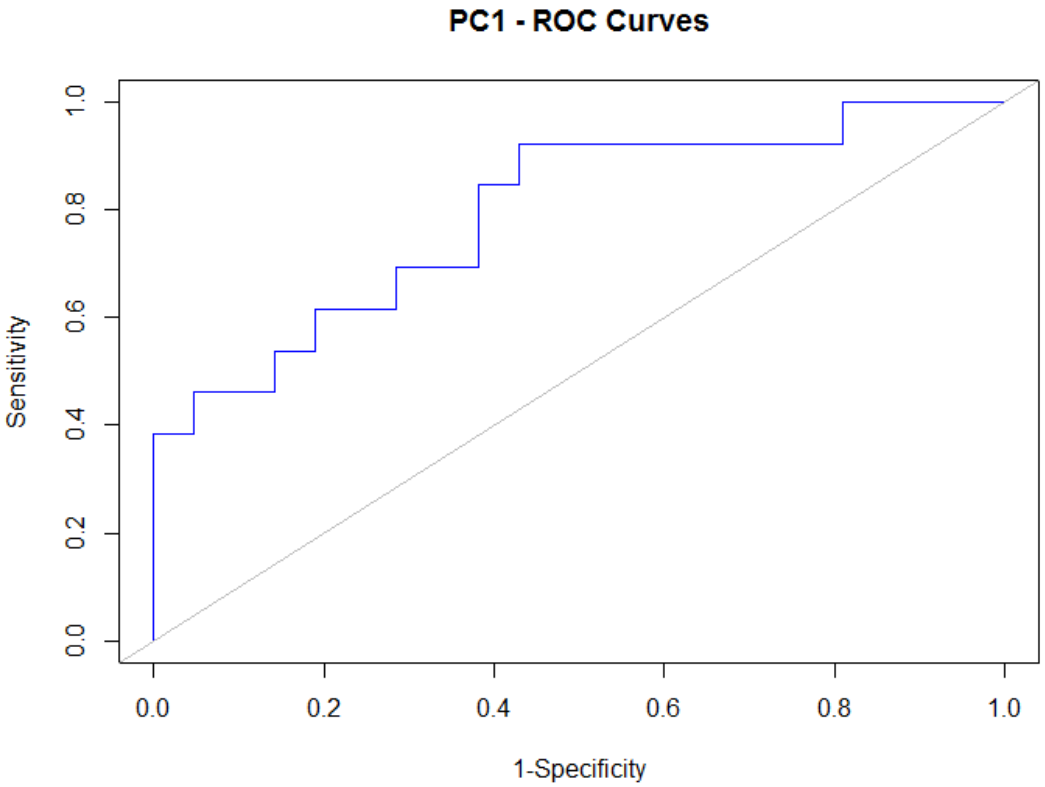

Figure 3.18: Curve of ROC at different cut off points of LOXL2 and ETFB with unspecified groups.

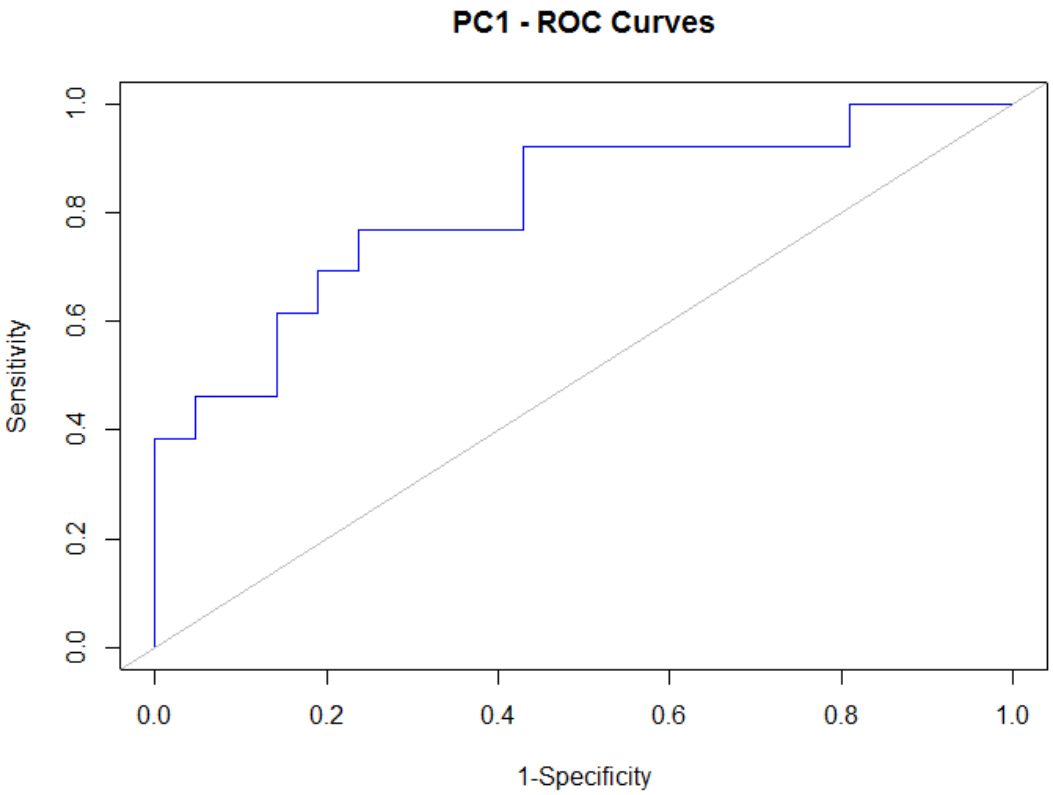

Figure 3.19: Curve of ROC at different cut off points of LOXL2 and ETFB with specified groups.

3.4.2 Summary

The data showed that the linear model did not detect any significant differences between the NT-proBNP and LOXL2. However, there were significant differences observed at weeks 11 and 14 for ETFβ. The ROC curve analysis showed ETFβ to be sensitive in determining DCM presence. Interestingly, the combined use of LOXL2 and ETFβ was shown to have a higher predictive value than when ETFβ was used on its own.

CHAPTER 4

DISCUSSION

Although much effort has been made to identify effective biomarkers for diagnosing DCM, these are elusive and are still disputed even among clinical experts (Kumric et al., 2021). As such, it would be advantageous for diabetics at risk to be screened early enough to implement corrective treatment. There are non-invasive and invasive detection methods, including TDI or MRI and endomyocardial biopsy sam
pling, respectively (Lorenzo-Almorós et al., 2017). However, individuals in resource-poor settings and those who cannot afford private health care have limited access to such facilities. Also, apart from TDI echocardiography and MRI being costly, they are not routinely performed. It requires specialised equipment and trained personnel, which is not available in all healthcare facilities. This was confirmed by various observational studies that reported a lack of highly skilled individuals to correctly interpret TDI data (Boudina & Abel, 2010; León et al., 2016; Schilling & Mann, 2012).

This leads to the argument that a rapid and cost-effective biomarker assay is required for early detection of DCM, as this may lead to corrective therapy. Hence, this study aimed to identify a prognostics profile that can detect the sub-clinical onset of diabetic induced cardiomyopathy. In this study, an *in silico* prediction of publicly available data sets was used to identify possible DCM diagnostic markers with the understanding that a cross-talk exists in disease pathology between T2DM and CVD (Liu et al., 2018; Strawbridge & van Zuydam, 2018). In this study, 15482 T2DM and 16450 CVD prognostic candidates were obtained from the ArrayExpress database. After that, the two datasets were integrated to obtain a DCM dataset in which 298 possible candidate biomarkers were generated. A Wilcoxon test score was applied to generate the top five biomarkers. Out of these biomarkers (USP34, ETFβ, LOXL2, ZKSCAN4 and IGF-1), the top two potential serum biomarkers, ETFβ, LOXL2 were further investigated. A pathway enrichment analysis and protein-protein interactions were conducted using a Kyoto Encyclopedia of Genes and Genomes (KEGG) and STRING, respectively. However, no conclusive results were obtained for these (data not included). Subsequently, a literature search was used to curate functional associations manually. Then the genes could be associated with

functions associated with DCM pathology, such as energy metabolism, fibrosis, hypertrophy and apoptosis (Chisalita et al., 2011; Szot et al., 2018; Ungvari & Csiszar, 2012).

Phase 1: Computational prediction of DCM biomarkers

Altered myocardial substrate metabolism

The required high energy levels are tightly regulated. Any alterations occurring in systemic insulin sensitivity or insulin action in the myocardium have a high impact on its metabolism and function (Abel et al., 2012). Energy from fat and carbohydrates is oxidised to supply the heart with ATP to match its mechanical power. This metabolic flexibility caters for the heart during fasting, feeding or intense exercise. However, following insulin resistance, the heart relies on fatty acid oxidation while glucose oxidation is reduced (Abel et al., 2012). This is significant in the present study because IGF-1 and ETFβ, which are important markers in energy regulation, were among the markers of interest.

IGF-1 is a small peptide hormone that controls glucose metabolism, and its expression is decreased in T2DM patients (C. Y. Wang et al., 2016). Reduced expression of IGF-1 can thus be correlated with increased FAO in DCM since substrate changes are impaired.

The ETFβ subunit is a component of the ETF heterodimer housed in the inner membrane of the mitochondria, the energy-producing centres in the cell (Ruiz-Pinto et al., 2018). The ETFα, ETFβ and ETFQO play an essential role in shuttling electrons between acyl co-enzyme A (Acyl-CoA) and ubiquinone, thus linking FAs and amino acids to the mitochondrial respiratory system in complex III. However, since increased intra-myocardial lipid is linked to impaired glucose tolerance, insulin resistance, obesity and diabetes, energy (ATP) is not produced at a high rate since the ATP-synthase becomes defective, contributing to increasing ROS production. Therefore, due to impaired energy metabolism, diastolic relaxation, an energy-requiring process, is impaired, thus affecting the functioning of the heart (Boudina et al., 2007). Ruiz-Pinto and co-authors have previously shown that downregulated ETFβ results in reduced capacity for mitochondrial dysfunction and reduced ATP production (Ruiz-Pinto et al., 2018). Thus, making ETFβ an ideal candidate.

Altered substrate preference linked to increased fibrosis and myocardial hypertrophy

Diabetes induced cardiac damage causes a detrimental increase in collagen, the main constituent of the extracellular matrix (ECM) essential for keeping the myocardial structure intact. The increased collagen thickens the ventricular wall, stiffening the myocardium and causing diastolic dysfunction (Erasmus et al., 2020), thus compromising the heart's ability to contract, reducing the amount of deoxygenated blood flowing into the heart since space is decreased by the accumulated collagen and limits the amount of oxygenated blood flowing to the rest of the body. LOXL2 is known to play a role in ECM regulation through maintaining collagen homeostasis, and its dysregulation has been associated with the pathological increase in fibrosis (Erasmus et al., 2020).

Zinc finger with KRAB and SCAN domains 4 (ZKSCAN4), formerly known as ZNF307, is part of the Zinc finger proteins (ZFPs) that are ubiquitous in the human proteome. These proteins play are role in cell growth, differentiation, development and disease. Zinc finger proteins contain a Cys2His2 (C2H2), and ZNF 307 is evolutionary conserved across species and highly expressed in the brain, lung, kidney and human heart (C. J. Yu et al., 2017). Although functional characterization of zinc finger proteins is still lagging (Sághy et al., 2020), *ZKSCAN4* has been previously expressed in the heart and shown to cause hypertrophy (C. J. Yu et al., 2017).

The use of bioinformatics analysis in gene expression profiling gives mass screening of molecular markers from patients, giving insights into diseases at the genome, transcriptome, and epigenetic levels (N. Li et al., 2018). However, the high volume of such microarray data requires validation, using empirical research and translation into useable clinical applications (N. Li et al., 2018). Thus, the identified genes were validated in a db/db mouse model.

The USP family belongs to zinc-dependent metalloproteases made up of several conserved regions (S. Zhao et al., 2015) and the primary regulators of muscle atrophy. In the heart, the E3 ligases have been associated with pathological cardiac hypertrophy, associated with defective contraction of the heart (Powell et al., 2012).

Phase 2: *In vivo* validation of candidate genes

Morphological characteristics and clinical relevance of the model

The db/db model is a well-established cardiovascular risk predictor model in which mice develop diabetes and overt signs of lipotoxicity by 8 and 9 weeks, respectively (Dludla et al., 2017). The present study confirms this, with db/db mice displaying increased body weights from week 6, while fasting blood glucose significantly increased from week nine compared with their db/+ controls. These findings were consistent with previous studies on db/db mice, showing that leptin receptor-deficient mice develop obesity and hyperglycaemia from six weeks of age, a significant change since substrate metabolism is altered to exclusive FAO reliance in diabetic hearts (Dludla et al., 2017; Kobayashi et al., 2000). Furthermore, although cardiac hypertrophy (increase in myocardial/chamber size when compared to body size) is one of the main features of DCM (Tate et al., 2019), there were no changes observed in db/db mice heart weights when compared to their db/+ counterparts. Our data support previous data shown in the studies by (Arow et al., 2020; Tate et al., 2019), where heart weights remained unchanged. In rats, heart weight/tibia length changes occur synergistically with LV hypertrophy resulting from enlarged cardiomyocyte size (Dludla et al., 2017). Unexpectedly, we observed a decrease of heart weights normalized to tibia length at weeks 11 and 14.

In contrast to our findings, Wang et al. (2017), as well as Dludla et al. (2017), showed increased heart weight to tibia length (Dludla et al., 2017; S. Wang et al., 2017). It is speculated that these weights HW: tibia lengths were increased in accordance with increased HW observed in these studies prior to normalization with tibia length, which was not observed in the present study. It is well known that increased cholesterol and triglycerides affect myocardial contractility (Jørgensen, Jensen, Biering-Sørensen, et al., 2016). The present study demonstrated increased LDL, triglycerides, and cholesterol in db/db mice compared to their db/+ counterparts, which is in line with Dludla and co-workers' observations (2017). Taken together, the metabolic changes including hyperglycaemia, alterations in LDL, high cholesterol and increased liver weight are all predictors of increased CVD. Therefore, these results show why the current model was clinically suitable to test the identified biomarkers.

Risk prediction using Echocardiography

Echocardiography is used to detect structural and functional changes in DCM. The results showed no significant differences in HR of db/db mice compared to their db/+ counterparts similar to other studies (Mori et al., 2014; Semeniuk et al., 2002). Similarly, findings by Li et al. (2014) showed no significant changes in interventricular septum (IVS) in the db/db mice when compared to the non-diabetic control (R. Li et al., 2014). Furthermore, we observed that db/db mice displayed a reduced E: A. ratio. Our findings agree with a previous study showing that 8-weeks old db/db mice had a reduced E: A ratio compared to the db/+ controls (Venardos et al., 2015). In contrast to these findings, Daniels et al. (2010) could not confirm the same findings and reported that 18 weeks old mice showed no significant E: A ratio differences. Similarly, to the findings observed by Tate and co-workers (2019), in this study, markers of diastolic function, the E_{DT} and IVRT were significantly increased from 14 weeks onwards. In contrast, EF was significantly decreased at weeks 14 and 16. Typically, transducers with a frequency higher than 10 MHz was used to conduct mouse echocardiography (Gao et al., 2011). In the study by Tate et al. (2019), a Philips iE33 ultrasound machine 12 MHz sector (Doppler and tissue Doppler) transducer, while the present study used a 30 MHz transducer on using a VEVO 2100 ultrasound system. The latter findings, though confirmed by Tate et al. (2019), were not confirmed by Li et al. (2014), who reported no significant differences in these parameters as mice aged. The present study demonstrated a significant decrease in LV wall thickness at week 16, whereas no significant changes were observed by (Abdel-Hamid & Firgany, 2015; A. Daniels et al., 2010). Taken together, the measurement of mitral flow data enabled us to confirm the establishment of diastolic dysfunction as early as week 9 and to confirm that the db/db mouse model is a suitable model to study DCM pathology.

Liver pathology and analysis of serum liver markers as a risk predictor of DCM

HF patients are reported to have 15-65% of liver injury cases, with diabetic individuals displaying increased hepatic fat with high transaminase levels having a higher CVD risk (Maleki et al., 2011). Studies demonstrated a complex but strong association linking increased diabetes-induced fatty liver injury to CVD development (Targher et al., 2005). Increased liver enzymes (AST and ALT) indicate liver injury associated with cardiac dysfunction and T2DM (Maleki et al., 2011). In the present study, both AST and ALT levels were increased, thus showing liver injury linked with cardiac dysfunction. Similarly, McCullough and colleagues (2004) showed increased ALT levels which could be associated with CVD outcomes (McCullough, 2004). Furthermore, through histology analysis of liver sections using H&E

staining, micro-and macro-vesicle formation were observed, which correlate with NAFLD establishment (Xanthopoulos et al., 2019). Together, these results suggest the liver has been affected by the T2DM phenotype alluded to above as a result of both lipid accumulation and changes in AST and ALT profiles.

Cardiac hypertrophy and fibrosis markers

During disease progression, increased levels of NPPA are usually associated with changes in cardiac output. The exact mechanism of NPPA in the diagnosis of HF is unclear. However, it is known that this protein is released in response to atrial stress and thus, plays an essential role in vascular remodeling and energy metabolism (Jujić et al., 2014). Furthermore, during hypertrophy and heart failure, NPPA is highly expressed, and as such, it has been identified as a highly conserved marker in CVD. In the present study, an increase in NPPA mRNA expression was observed at week 6. Similar observations were made by Hou and co-workers (2019) at 13-14 weeks (Hou et al., 2019). Therefore, these studies confirm our findings suggesting a possible early onset of cardiac injury.

Cardiac fibrosis is a prominent DCM feature characterized by the overproduction of ECM proteins (Gilca et al., 2017; Maya & Villarreal, 2010). Additionally, cardiac fibrosis is one of the main contributing factors to diastolic dysfunction, with increased expression and activity of pro-fibrotic signaling molecules such as CTGF causing augmented ECM protein deposition (Sakai et al., 2017; Dirk Westermann et al., 2007). We observed an increase in CTGF (associated with myocardial fibrosis) expression as early as week 6 of age in db/db mice. Likewise, Way et al. (2002) and Zhao et al. (2019) observed increased CTGF expression in protein kinase C beta 2 (PKCß2) transgenic rats (2, 4, 8 weeks) and streptozotocin-induced diabetic rats (16 weeks), respectively, when they were compared to their control counterparts, thus demonstrating increased fibrosis (Way et al., 2002; Yunyue Zhao et al., 2019).

Myocyte cell death occurs due to necrosis and apoptosis, which have been shown to increase in diabetic individuals. As such, differential expressions of BAX and BCL2 were investigated. In the current study, an increase in BAX (pro-apoptotic) and a significant decrease in BCL2 (anti-apoptotic) were observed in db/db mice compared to their db/+ counterparts. Similarly, Hasnan and colleagues (2010) observed an increase in BAX and a significant decrease in BCL2 in T2DM patients compared to their non-diabetic counterparts (Hasnan et al., 2010).

Cardiomyocyte apoptosis has been correlated to DCM pathogenesis, with increased cardiomyocyte apoptosis being proportional to loss in cardiac contractility, remodelling and finally culminating in cardiac dysfunction (Ren et al., 2016).

Differentially expressed genes of potential biomarkers

The mRNA levels of the genes ZKSCAN4, IGF1, USP34, ETFβ, and LOXL2 were tested in myocardial tissues. The results obtained for ZKSCAN4 showed significantly increased expression at weeks 6 and 16. The increased expression of this gene at week six could explain why no hypertrophy was observed in the myocardium since it suppresses the expression of the SRF, AP-1 and NF-KB which all play an essential role in cardiac hypertrophy development (C. J. Yu et al., 2017). However, in contrast to the observations made in our study, Yu and colleagues (2017) observed a proportional relationship between ZKSCAN4 expression levels and hypertrophy, with increased levels of this gene associated with cardiac hypertrophy in diabetic mice hearts when compared to their control counterparts (C. J. Yu et al., 2017). In the present study, normal heart weights were observed in the db/db mice compared to their db/+ counterparts, confirming the results observed by Yu et al. (2017).

IGF has been reported to play a role in cardiac contractility; increasing IGF gene expression is linked to improved cardiac output and ejection fraction (Chisalita et al., 2011; Friedrich et al., 2012). In our study, an age-dependent non-significant decrease in IGF-1 expression was observed. This decreased IGF-1 expression was confirmed by Andreassen et al. (2009), who reported an age-dependent reduction in IGF-1 expression in an elderly population with increased CVD risk (Andreassen et al., 2009). Previous studies showed that IGF-1 overexpression ameliorates contractile dysfunction and simultaneously halts oxidative stress-induced protein damage. Furthermore, it normalizes calcium homeostasis and reverses age-dependent changes in pro-and anti-apoptotic proteins (Andreassen et al., 2009; Ungvari & Csiszar, 2012). These functions confirm its potential role as a prospective biomarker detecting cardiac dysfunction.

Next, USP34 expression in cardiac tissue was investigated as a potential biomarker for cardiac hypertrophy. To date, a lack of data exists related to USP34 expression and cardiac disease pathology. However, USP34 contains an E3 ligase, which has been linked to cardiac hypertrophy (Lui et al., 2011; Powell et al., 2012; Sy et al., 2013), thus suggesting that it may

contribute to the development of DCM. In the current study, USP34 expression remained unchanged throughout all time points, and we were unable to highlight its potential role in the development of DCM.

Interestingly, although the mRNA expression of ETFβ was only significantly different at week 11, a peak was also observed at week 9, and a decreased expression of this gene is associated with a shift in myocardial substrate preference. After the substrate shift from FA oxidation to glucose oxidation, a cascade of events occurs, including defective oxidative phosphorylation, increased ROS generation and mitochondrial oxygen consumption with no increase in ATP production, leading to reduced energy efficiency in the heart (Borghetti et al., 2018). In T2DM patients, reduced glucose uptake (increased FAO due to substrate preference shift) is associated with impaired glucose oxidation and decreased ejection fraction, which was also observed in our study (Nirengi et al., 2020). Moreover, our study showed that LOXL2 increased expression is associated with increased myocardial fibrosis as this gene was significantly increased at 11-16 weeks. Our data are consistent with studies conducted in both cardiac and renal tissues (Cosgrove et al., 2018; Yang et al., 2016).

Serum expression of biomarkers

cTn-T and NT-proBNP are biomarkers currently used to diagnose CVD. However, Niizuma et al. (2019) and followed by Johnson et al. (2020), highlighted that the reported biomarkers are not sensitive enough to detect DCM at its asymptomatic stage Niizuma et al (2019) and Johnson et al (2020). Although studies conducted in pre-diabetic rats have shown that serum NT-proBNP levels are elevated in response to myocardial infarction, unstable angina and pressure overload, its use in DCM remains inconclusive (Nunes et al., 2013). Of note, high plasma levels of cTn-T have been shown to be high in T2DM experimental rat models with HF (Korkmaz-Icöz et al., 2016). Thus, predictive markers that would enable corrective treatment are still needed.

In the present study, the following serum biomarkers UPS34, ZKSCAN4 and IGF1, showed no differential expression, which shows no hypertrophy was measured in db/db mice compared to their db/+ counterparts. Therefore, although the mRNA levels of these genes were differentially expressed, serum levels of these proved to be unchanged. Interestingly, Oh and co-workers (2017) reported that downregulation of USP34 induces transcription factor β (TGFβ) and WNT signalling in epithelial-mesenchymal, which are involved in fibrosis and

cancer/embryogenesis signalling, respectively, fibrosis and hypertrophy are prominent features of DCM (Oh et al., 2017). Yu and colleagues (2017) observed increased expression of ZKSCAN4 at protein level, which is contrary to our findings since serum ZKSCAN4 remain constant (C. J. Yu et al., 2017). However, they used a cardiac-specific zinc finger protein, 307 transgenic and knockout mice, which were more specific than db/db mice model used in the present study. While the results obtained for serum IGF1 levels in this study showed no differential expression, Barroso et al. (2016) showed that decreased levels of IGF1 in conjunction with Insulin-like growth factor binding protein-7 (IGFBP-7) could be used to determine diastolic dysfunction in patients with DCM/HFpEF (Barroso et al., 2016). However, unlike the present study, which was conducted in a rodent model. Barroso et al. (2016) worked with serum samples from human patients. Although they had both male and female participants, male volunteers made up 51% of the study.

Differentially increased LOXL2 serum levels were consistent with observations made by Yang and co-authors (2016), as well as Zhao and co-authors (2017), who linked increased LOXL2 levels with atrial fibrillation (Yang et al., 2016; Yingming Zhao et al., 2017). Lastly, serum ETFβ was differently decreased, suggesting a reduced capacity of the mitochondria to perform FAO and provide sufficient energy for the heart to perform at its peak. Similarly, Ruiz-Pinto and co-workers (2018) observed reduced expression of ETFβ in doxorubicin-treated adult rat cardiomyocytes as well as changes in oxidative capacities through proteomics analysis (Ruiz-Pinto et al., 2018). Taken together, both serum and mRNA expression levels of these genes (LOXL2 and ETFβ) showed interesting results pointing to their possible use in detecting DCM at its asymptomatic stage. As such, further analyses were conducted to characterise better whether both of these genes may potentially be useful to detect DCM at an early stage.

Correlation of ETFβ, LOXL2 and NT-pro BNP mitral E: A ratio

Pandey et al. (2021) recently showed that NT-pro BNP could detect asymptomatic diabetic cardiomyopathy patients in T2DM patients between 30-60 years old, while the E: A ratio is used to assess the measure of heart functionality (Pandey et al., 2021). In the present study, NT-pro BNP could only detect DCM at the late stage (14 weeks) and was thus inversely correlated with E: A, which could detect DCM at its asymptomatic stage. Both ETFβ (11 weeks) and LOXL2 (9 weeks) were correlated positively with E: A (9 weeks) in our study, which suggests that these biomarkers might be more sensitive biomarkers than NT-proBNP in

detecting DCM at its asymptomatic stage, especially taking into consideration that NT-proBNP may not be specific to DCM according to our findings.

Histological analysis and immunostaining

No disease pathology was detected when H&E and Masson's Trichrome stain were used to assess cardiac morphology and fibrosis, respectively. Unlike our findings, several studies using the same model observed significant changes when db/db mice cardiac sections were stained with either H&E and/or Masson's trichrome stain (Huynh et al., 2012; Plante et al., 2015; J. Zhao et al., 2016). However, when anti-LOXL2 immunostaining was used in the sections, notable changes were observed suggesting the establishment of DCM. Thus, our data are in line with other studies that have also reported that LOXL2 expression could be linked to the presence of DCM, although their observations were made in humans and not in db/db mice like the present study (Yang et al., 2016). Similarly, immunostaining of cardiac slices with anti-ETFβ revealed a trend towards increase from week 6, compared to no changes that were observed with H&E as well as Masson's Trichrome stain. This was supported by Zhao et al. (2016), who also reported a significant increase in ETFβ expression using western blot techniques in db/db mice at 8 and 9 weeks, an effect associated with alterations of the mitochondrial energy metabolism.

Phase 3: Functional confirmation of LOXL2 and ETFβ in the pathogenesis of diabetic cardiomyopathy

The ECM supports cellular components while conveying contractile force and comprises about 85% fibrillar type I collagen (Rodríguez & Martínez-González, 2019). Collagen deposition is essential for wound healing and tissue remodelling; however, unregulated collagen deposition causes cardiac tissue scarring and fibrosis. Synergistically, collagen accumulation impairs myocardial contractility, reducing the heart's compliance and diastolic function (Erasmus et al., 2020). In this study, upon both LOXL2 and ETFβ knockdown, Col1a1 levels were significantly reduced. These findings are similar to those obtained by Yang and colleagues (2016) on Col1a1, who showed decreased expression of this gene upon silencing LOXL2 and overexpression when LOXL2 was increased.

Similarly, ETFβ expression was previously shown to be proportional to Col1a1 levels in collagen gel cultures (Hirokawa et al., 2011). The TGFβ superfamily regulates fibrotic

responses in the heart. Interestingly, it was previously shown by Yang et al. (2016) that LOXL2 was essential for TGFβ2 secretion and that LOXL2 was proportional to TGFβ2 production. Surprisingly, TGFβ2 expression was not attenuated by silencing LOXL2 in our study and was actually significantly upregulated. This could be explained by another observation made by Yang et al. (2016), which showed an alternative pathway in which LOXL2 stimulated TGFβ through the phosphatidylinositol-3-kinase (PI3K)/ /protein kinase B (AKT)/mechanistic target of rapamycin (mTOR) pathway, that controls translation and facilitates HF. An *in vitro* knockdown of PI3Kα caused a low expression of LOXL2 through AKT/ mTORC1, signaling a subsequent decrease in TGFβ2 expression.

Phase 4: Sensitivity and specificity

The present study further interrogated whether ETFβ and LOXL2 proteins may detect the presence of DCM and may represent a quantifiable index of DCM as the disease progresses. Although not specific, results suggest these biomarkers are sensitive enough to detect early-onset (subclinical) of DCM. A similar study was recently conducted by Abdelrahman et al. (2021), showing a panel of biomarkers (IL-6, TNF-α and AGEs). However, contrary to the present study, which used db/db mice, they used echocardiography to place patients with diabetes mellitus into three groups, namely; diabetes mellitus with normal cardiac function (DM-N), diabetes mellitus diastolic dysfunction (DM-DD), diabetes mellitus systolic dysfunction (DM-SD) while the non-diabetic, which was used as a control group was dived into two the non-diabetic with diastolic dysfunction and non-diabetic with normal echocardiography. Additionally, they used different algorithms to determine the probability of patients having DCM.

Limitations

Although our data led to new knowledge in the field, we acknowledge some limitations in our study:

- Only the top 5 genes were used in this study, although 228 were discovered, some of which may be relevant as possible biomarkers to detect early cardiomyopathy in diabetic study. As an example, phosphodiesterase 2A (PDE2A) hydrolyses cyclic adenosine monophosphate (cAMP) and is involved in mouse development. Its absence was shown to cause congenital heart defects (Assenza et al., 2018). This is important

since, in DCM, the heart reverts to foetal metabolism, and elevated cytosolic cAMP is known to stimulate insulin secretion (Borghetti et al., 2018; Stanley et al., 2005).

- It would be important to conduct an *in silico* prediction of functional significance using other non-public software since no results were obtained using STRING, KEGG and DAVID.

- Even though numerous animal models to induce hyperglycaemia exist (Lee & Kim, 2021), they only manifest certain aspects of clinical T2DM; thus, a model that would mimic the development of the disease pathology is still required. Additionally, *in vivo* knock-out experiments to better understand the pathways connected to ETFβ and LOXL2 are still required to confirm their role in the development of DCM. Future experiments, similar to the experiments conducted by Yang et al. (2016) that allowed them to highlight the role of LOXL2 in developing fibrosis in HF using knocking out LOXL2, will be key to confirm our findings.

- It is widely known that diabetic women are more likely to develop CVD complications than their male counterparts (Fourny et al., 2021). However, most experimental studies, including the present study, have used male mouse models. Our findings will therefore need to be confirmed in female animals. Several mouse models manifesting T2DM and/or obesity have given invaluable insight regarding molecular mechanisms resulting from the pathological complications of either of these. Albeit, the complications following these are observed from leptin receptor deficient mice (db/db), or leptin deficient (ob/ob) mice originate from single-gene mutations (Cruz-Topete et al., 2011). Both T2DM and obesity are polygenic, and using a single altered gene limits the effects to the pathway associated with the genetic mutation. Additionally, since obesity, T2DM and CVD are correlated with poor nutrition, single mutation gene models do not cater for alterations induced by environmental factors (Cruz-Topete et al., 2011). Thus, a model that closely mimics the disease pathophysiology is required.

- As a result of the above limitations with animal models, using human subjects' samples is desirable in the future. The biomarkers levels should be compared between healthy individuals, diabetic, CAD, and DCM patients in these subjects.

- Apoptosis is one of the main features of DCM (Cai et al., 2002). Although this study analysed mRNA levels of BAX and BCL2 to show its occurrence in the myocardium, confirmation of apoptosis will be to be confirmed using alternative methods such as the terminal deoxynucleotidyl transferase-mediated dUTP nick-end labelling (TUNEL) assay.

Future studies

Although there is a certain level of similarity and reproducibility in db/db mice vs human studies of T2DM, db/db mice do not possess the pancreatic amyloid deposition and never develop the full extent of T2DM (Asghar et al., 2009; Cefalu, 2006). In light of this, future studies will be needed with proof of concept studies in humans. Since the ROC analysis results obtained in this study suggest that the combined use of the biomarkers would aid in early detection of DCM, the biomarkers should be measured in prediabetic individuals, T2DM and individuals without T2DM (control group), keeping in mind the aim to implement corrective treatment at the inception of the disease. Additionally, a close look at the expression of these genes in female vs male patients would also be interesting.

A link between LOXL2 and collagen production and a pathway was previously elucidated in the study by Yang et al. (2016). Hirokawa et al. (2011) showed its involvement in mechano-regulation of fibroblast cell numbers an ETFβ pathway analysis to understand the interception between ETFβ's role in mitochondrial energy metabolism and changes in the ECM observed in the present study.

Conclusions

This is the first study to associate serum ETFβ and LOXL2 with asymptomatic detection of DCM. An in silico pipeline of both diabetic and cardiac biomarkers was used to identify a biomarker profile that can be used to identify DCM in its subclinical stage. A candidate gene list with 228 biomarkers was identified, and a Wilcoxon score (p value $< 6 \times 10^{-6}$) was used to select the first five genes (USP34, ETFβ, LOXL2, ZKSCAN4 and IGF1) for downstream analysis. These genes were validated in an *in vivo* db/db mouse model in which diabetes was observed as early as 6 weeks as seen with an increased body weight, liver weight and HR when the db/db mice were compared to their db/+ counterparts. In addition, the E: A ratio (at week 16) and ejection fractions (week 14 and 16) were reduced thus, showing cardiac dysfunction. Serum LOXL2 levels were negatively associated with ejection fraction and E: A ratio. Immunostaining with anti- ETFβ and anti-LOXL2 showed fibrotic tissue, which was not observed with Masson's Trichrome stain. Knockdown of LOXL2 showed reduced expression of Col1a1, while TGFβ and NT-pro BNP were increased. In ETFβ knocked down cells, Acadm was reduced, although not significantly.

Additionally, Col1a1 mRNA expression was significantly reduced. Our data highlight that the linear model did not detect significant differences between the NT-pro BNP and LOXL2. However, there were significant differences observed for ETFβ. The ROC curve analysis showed ETFβ to be sensitive in determining DCM presence, while combined use of LOXL2 and ETFβ was shown to have a higher predictive value than when ETFβ was used on its own. Thus, a lateral flow device that would house both genes that would enable rapid subclinical DCM would be made available in resource-poor settings where TDI is not available to every prediabetic and/or diabetic patient for early corrective treatment to be implemented.

References

Abdel-Hamid, A. A. M., & Firgany, A. E. D. L. (2015). Atorvastatin alleviates experimental diabetic cardiomyopathy by suppressing apoptosis and oxidative stress. *Journal of Molecular Histology*, *46*(4–5), 337–345. https://doi.org/10.1007/s10735-015-9625-4

Abdul-Ghani, M., Suen, C., Jiang, B., Deng, Y., Weldrick, J. J., Putinski, C., Brunette, S., Fernando, P., Lee, T. T., Flynn, P., Leenen, F. H. H., Burgon, P. G., Stewart, D. J., & Megeney, L. A. (2017). Cardiotrophin 1 stimulates beneficial myogenic and vascular remodeling of the heart. *Cell Research*, *27*(10), 1195–1215. https://doi.org/10.1038/cr.2017.87

Abel, E. D., O'Shea, K. M., & Ramasamy, R. (2012). Insulin Resistance: Metabolic Mechanisms and Consequences in the Heart. *Arteriosclerosis, Thrombosis, and Vascular Biology*, *32*(9), 2068–2076. https://doi.org/10.1161/ATVBAHA.111.241984

Adela, R., & Banerjee, S. K. (2015). GDF-15 as a target and biomarker for diabetes and cardiovascular diseases: A translational prospective. *Journal of Diabetes Research*, *2015*. https://doi.org/10.1155/2015/490842

Aimo, A., Vergaro, G., Passino, C., Ripoli, A., Ky, B., Miller, W. L., Bayes-Genis, A., Anand, I., Januzzi, J. L., & Emdin, M. (2017). Prognostic Value of Soluble Suppression of Tumorigenicity-2 in Chronic Heart Failure: A Meta-Analysis. *JACC: Heart Failure*, *5*(4), 280–286. https://doi.org/https://doi.org/10.1016/j.jchf.2016.09.010

Akahori, H., Tsujino, T., Naito, Y., Matsumoto, M., Sasaki, N., Iwasaku, T., Eguchi, A., Sawada, H., Hirotani, S., & Masuyama, T. (2014). Atorvastatin ameliorates cardiac fibrosis and improves left ventricular diastolic function in hypertensive diastolic heart failure model rats. *Journal of Hypertension*, *32*(7), 1534–1541; discussion 1541. https://doi.org/10.1097/HJH.0000000000000184

Al-Rasheed, N. M., Al-Rasheed, N. M., Hasan, I. H., Al-Amin, M. A., Al-Ajmi, H. N., Mohamad, R. A., & Mahmoud, A. M. (2017). Simvastatin Ameliorates Diabetic Cardiomyopathy by Attenuating Oxidative Stress and Inflammation in Rats. *Oxidative Medicine and Cellular Longevity*, *2017*, 1092015. https://doi.org/10.1155/2017/1092015

An, D., & Rodrigues, B. (2006). Role of changes in cardiac metabolism in development of diabetic cardiomyopathy. *American Journal of Physiology - Heart and Circulatory Physiology*, *291*(4). https://doi.org/10.1152/ajpheart.00278.2006

Anderson, R. M. (1993). *The gross physiology of the cardiovascular system* (Second Edi). Racquet Press.

Andreassen, M., Raymond, I., Kistorp, C., Hildebrandt, P., Eaber, J., & Kristensen, L. Ø. (2009). IGF1 as predictor of all cause mortality and cardiovascular disease in an elderly population. *European Journal of Endocrinology*, *160*(1), 25–31. https://doi.org/10.1530/EJE-08-0452

Aneja, A., Tang, W. H. W., Bansilal, S., Garcia, M. J., & Farkouh, M. E. (2008). Diabetic Cardiomyopathy: Insights into Pathogenesis, Diagnostic Challenges, and Therapeutic Options. *The American Journal of Medicine*, *121*(9), 748–757. https://doi.org/10.1016/j.amjmed.2008.03.046

Anthony, S., Guarnieri, A., Gozdiff, A., Helsley, R., Owens III, A., & Tranter, M. (2019). Mehanisms linking adipose tissue inflammation to cardic hypertrophy and fibrosis.

Clinical Science, *133*(22), 2329–2344. https://doi.org/10.1042/CS20190578.Mechanisms

Antonopoulos, A. S., Margaritis, M., Lee, R., Channon, K., & Antoniades, C. (2012). Statins as anti-inflammatory agents in atherogenesis: molecular mechanisms and lessons from the recent clinical trials. *Current Pharmaceutical Design*, *18*(11), 1519–1530. https://doi.org/10.2174/138161212799504803

Ares-Carrasco, S., Picatoste, B., Benito-Martín, A., Zubiri, I., Sanz, A. B., Sánchez-Niño, M. D., Ortiz, A., Egido, J., Tuñón, J., & Lorenzo, O. (2009). Myocardial fibrosis and apoptosis, but not inflammation, are present in long-term experimental diabetes. *American Journal of Physiology - Heart and Circulatory Physiology*, *297*(6), 2109–2119. https://doi.org/10.1152/ajpheart.00157.2009

Aronow, W. S., Ahn, C., & Kronzon, I. (1999). Comparison of incidences of congestive heart failure in older African-Americans, Hispanics, and whites. *The American Journal of Cardiology*, *84*(5), 611–612, A9. https://doi.org/10.1016/s0002-9149(99)00392-6

Arow, M., Waldman, M., Yadin, D., Nudelman, V., Shainberg, A., Abraham, N. G., Freimark, D., Kornowski, R., Aravot, D., Hochhauser, E., & Arad, M. (2020). Sodium–glucose cotransporter 2 inhibitor Dapagliflozin attenuates diabetic cardiomyopathy. *Cardiovascular Diabetology*, *19*(1), 7. https://doi.org/10.1186/s12933-019-0980-4

Asbun, J., & Villarreal, F. J. (2006). The Pathogenesis of Myocardial Fibrosis in the Setting of Diabetic Cardiomyopathy. *Journal of the American College of Cardiology*, *47*(4), 693–700. https://doi.org/https://doi.org/10.1016/j.jacc.2005.09.050

Asghar, O., Al-Sunni, A., Khavandi, K., Khavandi, A., Withers, S., Greenstein, A., Heagerty, A. M., & Malik, R. A. (2009). Diabetic cardiomyopathy. *Clinical Science*, *116*(10), 741–760. https://doi.org/10.1042/CS20080500

Assenza, M. R., Barbagallo, F., Barrios, F., Cornacchione, M., Campolo, F., Vivarelli, E., Gianfrilli, D., Auletta, L., Soricelli, A., Isidori, A. M., Lenzi, A., Pellegrini, M., & Naro, F. (2018). Critical role of phosphodiesterase 2A in mouse congenital heart defects. *Cardiovascular Research*, *114*(6), 830–845. https://doi.org/10.1093/cvr/cvy030

Association, A. H. (2019). *Heart Disease and Stroke Statistics-2019 At-a-Glance Heart Disease, Stroke and other Cardiovascular Diseases*. https://healthmetrics.heart.org/wp-content/uploads/2019/02/At-A-Glance-Heart-Disease-and-Stroke-Statistics-–-2019.pdf

Athéa, Y., Garnier, A., Fortin, D., Bahi, L., Veksler, V., & Ventura-Clapier, R. (2007). Mitochondrial and energetic cardiac phenotype in hypothyroid rat. Relevance to heart failure. *Pflugers Archiv European Journal of Physiology*, *455*(3), 431–442. https://doi.org/10.1007/s00424-007-0307-2

Atlas, I. D. [Jul; 2019]. (2019). *Diabetes atlas 2019*.

Barroso, M. C., Kramer, F., Greene, S. J., Scheyer, D., Köhler, T., Karoff, M., Seyfarth, M., Gheorghiade, M., & Dinh, W. (2016). Serum insulin-like growth factor-1 and its binding protein-7: Potential novel biomarkers for heart failure with preserved ejection fraction. *BMC Cardiovascular Disorders*, *16*(1), 1–9. https://doi.org/10.1186/s12872-016-0376-2

Barsanti, C., Lenzarini, F., & Kusmic, C. (2015). Diagnostic and prognostic utility of non-invasive imaging in diabetes management. *World Journal of Diabetes*, *6*(6), 792–806. https://doi.org/10.4239/wjd.v6.i6.792

Battiprolu, P. K., Gillette, T. G., Wang, Z. V., Lavandero, S., & Hill, J. A. (2010). Diabetic cardiomyopathy: Mechanisms and therapeutic targets. *Drug Discovery Today: Disease Mechanisms*, *7*(2), 1–15. https://doi.org/10.1016/j.ddmec.2010.08.001

Bax, J. J., Inzucchi, S. E., Bonow, R. O., Schuijf, J. D., Freeman, M. R., & Barrett, E. J. (2007). Cardiac Imaging for Risk Stratification in Diabetes. *Diabetes Care*, *30*(5), 1295 LP – 1304. https://doi.org/10.2337/dc06-2094

Bayeva, M., Sawicki, K. T., & Ardehali, H. (2013). Taking diabetes to heart--deregulation of myocardial lipid metabolism in diabetic cardiomyopathy. *Journal of the American Heart Association*, *2*(6), 1–17. https://doi.org/10.1161/JAHA.113.000433

Belke, D. D., Betuing, S., Tuttle, M. J., Graveleau, C., Young, M. E., Pham, M., Zhang, D., Cooksey, R. C., McClain, D. A., Litwin, S. E., Taegtmeyer, H., Severson, D., Kahn, C. R., & Abel, E. D. (2002). Insulin signaling coordinately regulates cardiac size, metabolism, and contractile protein isoform expression. *Journal of Clinical Investigation*, *109*(5), 629–639. https://doi.org/10.1172/JCI13946

Belke, D. D., & Dillmann, W. H. (2004). Altered cardiac calcium handling in diabetes. *Current Hypertension Reports*, *6*(6), 424–429. https://doi.org/10.1007/s11906-004-0035-3

Bell, D. S. H., & Goncalves, E. (2019). Heart failure in the patient with diabetes: Epidemiology, aetiology, prognosis, therapy and the effect of glucose-lowering medications. *Diabetes, Obesity and Metabolism*, *21*(6), 1277–1290. https://doi.org/10.1111/dom.13652

Berthiaume, J. M., Kurdys, J. G., Muntean, D. M., & Rosca, M. G. (2019). Mitochondrial NAD+/NADH redox state and diabetic cardiomyopathy. *Antioxidants & Redox Signaling*, *30*(3), 375–398.

Bertoni, A. G., Tsai, A., Kasper, E. K., & Brancati, F. L. (2003). Diabetes and idiopatihic cardiomyopathy: A nationwide case-control study. *Diabetes Care*, *26*(10), 2791–2795. https://doi.org/10.2337/diacare.26.10.2791

Blanco, A., & Blanco, G. (2017). *Chapter 32 - Apoptosis* (A. Blanco & G. B. T.-M. B. Blanco (eds.); pp. 791–796). Academic Press. https://doi.org/https://doi.org/10.1016/B978-0-12-803550-4.00032-X

Borghetti, G., von Lewinski, D., Eaton, D. M., Sourij, H., Houser, S. R., & Wallner, M. (2018). Diabetic Cardiomyopathy: Current and Future Therapies. Beyond Glycemic Control . *Frontiers in Physiology* , *9*(OCT), 1514. https://doi.org/10.3389/fphys.2018.01514

Borlaug, B. A., & Paulus, W. J. (2011). Heart failure with preserved ejection fraction: Pathophysiology, diagnosis, and treatment. *European Heart Journal*, *32*(6), 670–679. https://doi.org/10.1093/eurheartj/ehq426

Boudina, S., & Abel, E. D. (2010). Diabetic cardiomyopathy, causes and effects. *Reviews in Endocrine and Metabolic Disorders*, *11*(1), 31–39. https://doi.org/10.1007/s11154-010-9131-7

Boudina, S., Boudina, S., Sena, S., Sena, S., Hu, X. X., Hu, X. X., Aziz, S., Aziz, S., Theobald, H., Theobald, H., Johnson, J. I., Johnson, J. I., Sheng, X., Sheng, X., Bugger, H., Bugger, H., Vlad G. Zaha, 1, Vlad G. Zaha, 1, Abel, E. D., & Abel, E. D. (2007).

Direct Evidence for Increased Uncoupled Respiration and Activation of Uncoupling Proteins. *October*, *56*(October), 2457–2466. https://doi.org/10.2337/db07-0481.Additional

Brar, B. K., Stephanou, A., Liao, Z., O'Leary, R. M., Pennica, D., Yellon, D. M., & Latchman, D. S. (2001). Cardiotrophin-1 can protect cardiac myocytes from injury when added both prior to simulated ischaemia and at reoxygenation. *Cardiovascular Research*, *51*(2), 265–274. https://doi.org/10.1016/s0008-6363(01)00294-2

Bratulic, S., Gatto, F., & Nielsen, J. (2019). The Translational Status of Cancer Liquid Biopsies. *Regenerative Engineering and Translational Medicine*, 1–41.

Bugger, H. (2015). Diabetic cardiomyopathy, does it exist? *Heart and Metabolism*, *68*, 35–38.

Bugger, H., & Abel, E. D. (2010). Mitochondria in the diabetic heart. *Cardiovascular Research*, *88*(2), 229–240.

Bursi, F., Weston, S. A., Redfield, M. M., Jacobsen, S. J., Pakhomov, S., Nkomo, V. T., Ryan A. Meverden, & Roger, V. L. (2017). Systolic and Diastolic Heart Failure. *Emergency Medicine Reports*, *38*(13), 141–155.

Cai, L., & Kang, Y. J. (2001). Oxidative stress and diabetic cardiomyopathy: A brief review. *Cardiovascular Toxicology*, *1*(3), 181–193. https://doi.org/10.1385/CT:1:3:181

Cai, L., Li, W., Wang, G., Guo, L., Jiang, Y., & James Kang, Y. (2002). Hyperglycemia-induced apoptosis in mouse myocardium: Mitochondrial cytochrome c-mediated caspase-3 activation pathway. *Diabetes*, *51*(6), 1938–1948. https://doi.org/10.2337/diabetes.51.6.1938

Cefalu, W. T. (2006). Animal models of type 2 diabetes: Clinical presentation and pathophysiological relevance to the human condition. *ILAR Journal*, *47*(3), 186–198. https://doi.org/10.1093/ilar.47.3.186

Centers for Disease Control. (2022). *National Diabetes Statistics Report*. Centers for Disease Control and Prevention. https://www.cdc.gov/diabetes/data/statistics-report/index.html.

Chavali, V., Tyagi, S. C., & Mishra, P. K. (2013). Predictors and prevention of diabetic cardiomyopathy. *Diabetes, Metabolic Syndrome and Obesity: Targets and Therapy*, *6*, 151–160. https://doi.org/10.2147/DMSO.S30968

Chisalita, S. I., Dahlstrom¨, U., Arnqvist, H. J., & Alehagen, U. (2011). Increased IGF1 levels in relation to heart failure and cardiovascular mortality in an elderly population: Impact of ACE inhibitors. *European Journal of Endocrinology*, *165*(6), 891–898. https://doi.org/10.1530/EJE-11-0584

Chogtu, B. (2015). Statin use and risk of diabetes mellitus. *World Journal of Diabetes*, *6*(2), 352. https://doi.org/10.4239/wjd.v6.i2.352

Chong, C. R., Clarke, K., & Levelt, E. (2017). Metabolic remodelling in diabetic cardiomyopathy. *Cardiovascular Research*, *113*(4), 422–430. https://doi.org/10.1093/cvr/cvx018

Cosgrove, D., Dufek, B., Meehan, D. T., Delimont, D., Hartnett, M., Samuelson, G., Gratton, M. A., Phillips, G., MacKenna, D. A., & Bain, G. (2018). Lysyl oxidase like-2 contributes to renal fibrosis in Col4α3/Alport mice. *Kidney International*, *94*(2), 303–

314. https://doi.org/10.1016/j.kint.2018.02.024

Cotter, G., Voors, A. A., Prescott, M. F., Felker, G. M., Filippatos, G., Greenberg, B. H., Pang, P. S., Ponikowski, P., Milo, O., Hua, T. A., Qian, M., Severin, T. M., Teerlink, J. R., Metra, M., & Davison, B. A. (2015). Growth differentiation factor 15 (GDF-15) in patients admitted for acute heart failure: Results from the RELAX-AHF study. *European Journal of Heart Failure*, *17*(11), 1133–1143. https://doi.org/10.1002/ejhf.331

Cruz-Topete, D., List, E. O., Okada, S., Kelder, B., & Kopchick, J. J. (2011). Proteomic changes in the heart of diet-induced pre-diabetic mice. *Journal of Proteomics*, *74*(5), 716–727. https://doi.org/10.1016/j.jprot.2011.02.018

Dahlström, U. (2004). Can natriuretic peptides be used for the diagnosis of diastolic heart failure? *European Journal of Heart Failure*, *6*(3), 281–287. https://doi.org/10.1016/j.ejheart.2004.01.005

Dalbøge, L. S., Almholt, D. L. C., Neerup, T. S. R., Vassiliadis, E., Vrang, N., Pedersen, L., Fosgerau, K., & Jelsing, J. (2013). Characterisation of age-dependent beta cell dynamics in the male db/db mice. *PLoS ONE*, *8*(12), 1–10. https://doi.org/10.1371/journal.pone.0082813

Daniels, A., van Bilsen, M., Janssen, B. J. A., Brouns, A. E., Cleutjens, J. P. M., Roemen, T. H. M., Schaart, G., van der Velden, J., van der Vusse, G. J., & van Nieuwenhoven, F. A. (2010). Impaired cardiac functional reserve in type 2 diabetic db/db mice is associated with metabolic, but not structural, remodelling. *Acta Physiologica*, *200*(1), 11–22. https://doi.org/10.1111/j.1748-1716.2010.02102.x

Daniels, L., Clopton, P., Laughlin, G., Maisel, A., & Barrett-Connor, E. (2011). Growth-Differentiation Factor-15 is a Robust, Independent Predictor of 11-Year Mortality Risk in Community-Dwelling Older Adults: The Rancho Bernardo Study. *National Institute of Health*, *123*(19), 2101–2110. https://doi.org/10.1161/CIRCULATIONAHA.110.979740.Growth-Differentiation

Davia, K., Bernobich, E., Ranu, H. K., del Monte, F., Terracciano, C. M. N., MacLeod, K. T., Adamson, D. L., Chaudhri, B., Hajjar, R. J., & Harding, S. E. (2001). SERCA2A overexpression decreases the incidence of aftercontractions in adult rabbit ventricular myocytes. *Journal of Molecular and Cellular Cardiology*, *33*(5), 1005–1015.

De Boer, R. A., Lok, D. J. A., Jaarsma, T., Van Der Meer, P., Voors, A. A., Hillege, H. L., & Van Veldhuisen, D. J. (2011). Predictive value of plasma galectin-3 levels in heart failure with reduced and preserved ejection fraction. *Annals of Medicine*, *43*(1), 60–68. https://doi.org/10.3109/07853890.2010.538080

De Boer, R. A., Yu, L., & Van Veldhuisen, D. J. (2010). Galectin-3 in cardiac remodeling and heart failure. *Current Heart Failure Reports*, *7*(1), 1–8. https://doi.org/10.1007/s11897-010-0004-x

DeLeon-Pennell, K. Y., Meschiari, C. A., Jung, M., & Lindsey, M. L. (2017). Matrix Metalloproteinases in Myocardial Infarction and Heart Failure. *Progress in Molecular Biology and Translational Science*, *147*, 75–100. https://doi.org/10.1016/bs.pmbts.2017.02.001

Di Bonito, P., Moio, N., Cavuto, L., Covino, G., Murena, E., Scilla, C., Turco, S., Capaldo, B., & Sibilio, G. (2005). Early detection of diabetic cardiomyopathy: usefulness of tissue Doppler imaging. *Diabetic Medicine : A Journal of the British Diabetic*

Association, *22*(12), 1720–1725. https://doi.org/10.1111/j.1464-5491.2005.01685.x

Dludla, P. V., Essop, M. F., Gabuza, K. B., Muller, C. J. F., Louw, J., & Johnson, R. (2017). Age-dependent development of left ventricular wall thickness in type 2 diabetic (db/db) mice is associated with elevated low-density lipoprotein and triglyceride serum levels. *Heart and Vessels*, *32*(8), 1025–1031. https://doi.org/10.1007/s00380-017-0978-3

Doerstling, S., Hedberg, P., Öhrvik, J., Leppert, J., & Henriksen, E. (2018). Growth differentiation factor 15 in a community-based sample: age-dependent reference limits and prognostic impact. *Upsala Journal of Medical Sciences*, *123*(2), 86–93. https://doi.org/10.1080/03009734.2018.1460427

Dorn II, G. (2016). Mitochondrial fission/fusion and cardiomyopathy. *Current Opinion in Genetics & Development*, *38*, 38–44. https://doi.org/10.1016/j.gde.2016.03.001

Duncan, J. G. (2011). Mitochondrial dysfunction in diabetic cardiomyopathy. *Biochimica et Biophysica Acta (BBA)-Molecular Cell Research*, *1813*(7), 1351–1359.

Ecker, K., Lorenz, A., Wolf, F., Ploner, C., Böck, G., Duncan, T., Galey, S., & Helmberg, A. (2009). A RAS recruitment screen identifies ZKSCAN4 as a glucocorticoid receptor-interacting protein. *Journal of Molecular Endocrinology*, *42*(2), 105–117. https://doi.org/10.1677/JME-08-0087

Eguchi, K., & Manabe, I. (2014). Toll-like receptor, lipotoxicity and chronic inflammation: The pathological link between obesity and cardiometabolic disease. *Journal of Atherosclerosis and Thrombosis*, *21*(7), 629–639. https://doi.org/10.5551/jat.22533

Erasmus, M., Samodien, E., Lecour, S., Cour, M., Lorenzo, O., Dludla, P., Pheiffer, C., & Johnson, R. (2020). Linking LOXL2 to Cardiac Interstitial Fibrosis. *International Journal of Molecular Sciences*, *21*(16), 5913. https://doi.org/10.3390/ijms21165913

Evdokimova, V., Tognon, C. E., Benatar, T., Yang, W., Krutikov, K., Pollak, M., Sorensen, P. H. B., & Seth, A. (2012). IGFBP7 binds to the IGF-1 receptor and blocks its activation by insulin-like growth factors. *Science Signaling*, *5*(255), ra92. https://doi.org/10.1126/scisignal.2003184

Faita, F., Di Lascio, N., Rossi, C., Kusmic, C., & Solini, A. (2018). Ultrasonographic characterization of the db/db mouse: An animal model of metabolic abnormalities. *Journal of Diabetes Research*, *2018*. https://doi.org/10.1155/2018/4561309

Falcão-Pires, I., & Leite-Moreira, A. F. (2012). Diabetic cardiomyopathy: Understanding the molecular and cellular basis to progress in diagnosis and treatment. *Heart Failure Reviews*, *17*(3), 325–344. https://doi.org/10.1007/s10741-011-9257-z

Fan, D., Takawale, A., Lee, J., & Kassiri, Z. (2012). Cardiac fibroblasts, fibrosis and extracellular matrix remodeling in heart disease. *Fibrogenesis and Tissue Repair*, *5*(1), 1. https://doi.org/10.1186/1755-1536-5-15

Feng, W., Wu, X., Li, S., Zhai, C., Wang, J., Shi, W., & Li, M. (2017). Association of Serum Galectin-3 with the Acute Exacerbation of Chronic Obstructive Pulmonary Disease. *Medical Science Monitor : International Medical Journal of Experimental and Clinical Research*, *23*, 4612–4618. https://doi.org/10.12659/msm.903472

Ferreira, P. F., Gatehouse, P. D., Mohiaddin, R. H., & Firmin, D. N. (2013). Cardiovascular magnetic resonance artefacts. *Journal of Cardiovascular Magnetic Resonance : Official Journal of the Society for Cardiovascular Magnetic Resonance*, *15*(1), 41.

https://doi.org/10.1186/1532-429X-15-41

Filipe, M. D., Meijers, W. C., Rogier van der Velde, A., & de Boer, R. A. (2015). Galectin-3 and heart failure: prognosis, prediction & clinical utility. *Clinica Chimica Acta; International Journal of Clinical Chemistry*, *443*, 48–56. https://doi.org/10.1016/j.cca.2014.10.009

Fitzpatrick, E., Johnson, M. P., Dyer, T. D., Forrest, S., Elliott, K., Blangero, J., Brennecke, S. P., & Moses, E. K. (2009). Genetic association of the activin A receptor gene (ACVR2A) and pre-eclampsia. *Molecular Human Reproduction*, *15*(3), 195–204. https://doi.org/10.1093/molehr/gap001

Fourny, N., Beauloye, C., Bernard, M., Horman, S., Desrois, M., & Bertrand, L. (2021). Sex Differences of the Diabetic Heart . In *Frontiers in Physiology* (Vol. 12, p. 619). https://www.frontiersin.org/article/10.3389/fphys.2021.661297

Fralick, M., Redelmeier, D. A., Patorno, E., Franklin, J. M., Razak, F., Gomes, T., & Schneeweiss, S. (2021). Identifying Risk Factors for Diabetic Ketoacidosis Associated with SGLT2 Inhibitors: a Nationwide Cohort Study in the USA. *Journal of General Internal Medicine*, *36*(9), 2601–2607. https://doi.org/10.1007/s11606-020-06561-z

Friedrich, N., Thuesen, B., Jrøgensen, T., Juul, A., Spielhagen, C., Wallaschofksi, H., & Linneberg, A. (2012). The association between IGF-I and insulin resistance: A general population study in Danish adults. *Diabetes Care*, *35*(4), 768–773. https://doi.org/10.2337/dc11-1833

Fuentes-Antrás, J., Picatoste, B., Ramírez, E., Egido, J., Tuñón, J., & Lorenzo, Ó. (2015). Targeting metabolic disturbance in the diabetic heart. *Cardiovascular Diabetology*, *14*(1). https://doi.org/10.1186/s12933-015-0173-8

Fuster, J., Ouchi, N., Gokce, N., & Walsh, K. (2016). Obesity-induced Changes in Adipose Tissue Microenvironment and Their Impact on Cardiovascular Disease. *Circulation Research*, *118*(11), 1786–1807. https://doi.org/10.1016/s0172-2190(97)82761-5

Galloway, C. A., & Yoon, Y. (2015). Mitochondrial dynamics in diabetic cardiomyopathy. *Antioxidants & Redox Signaling*, *22*(17), 1545–1562.

Gao, S., Ho, D., Vatner, D. E., & Vatner, S. F. (2011). Echocardiography in Mice. *Current Protocols in Mouse Biology*, *1*, 71–83. https://doi.org/10.1002/9780470942390.mo100130.Echocardiography

Gilca, G.-E., Stefanescu, G., Badulescu, O., Tanase, D.-M., Bararu, I., & Ciocoiu, M. (2017). Diabetic Cardiomyopathy: Current Approach and Potential Diagnostic and Therapeutic Targets. *Journal of Diabetes Research*, *2017*, 1310265. https://doi.org/10.1155/2017/1310265

Godinho, R., Mega, C., Teixeira-De-Lemos, E., Carvalho, E., Teixeira, F., Fernandes, R., & Reis, F. (2015). The Place of Dipeptidyl Peptidase-4 Inhibitors in Type 2 Diabetes Therapeutics: A "Me Too" or "the Special One" Antidiabetic Class? *Journal of Diabetes Research*, *2015*. https://doi.org/10.1155/2015/806979

Gordillo-Moscoso, A., Ruiz, E., Carnero, M., Reguillo, F., Rodriguez, E., Tejerina, T., & Redondo, S. (2013). Relationship between serum levels of triglycerides and vascular inflammation, measured as COX-2, in arteries from diabetic patients: a translational study. *Lipids in Health and Disease*, *12*, 62. https://doi.org/10.1186/1476-511X-12-62

Gül, İ., Yücel, O., Zararsız, A., Demirpençe, Ö., Yücel, H., Zorlu, A., & Yılmaz, M. B. (2017). Prognostic role of soluble suppression of tumorigenicity-2 on cardiovascular mortality in outpatients with heart failure. *Anatolian Journal of Cardiology*, *18*(3), 200–205. https://doi.org/10.14744/AnatolJCardiol.2017.7741

Gundewar, S., Calvert, J. W., Jha, S., Toedt-Pingel, I., Ji, S. Y., Nunez, D., Ramachandran, A., Anaya-Cisneros, M., Tian, R., & Lefer, D. J. (2009). Activation of AMP-activated protein kinase by metformin improves left ventricular function and survival in heart failure. *Circulation Research*, *104*(3), 403–411. https://doi.org/10.1161/CIRCRESAHA.108.190918

Gupta, V. (2013). Glucagon-like peptide-1 analogues: An overview. *Indian Journal of Endocrinology and Metabolism*, *17*(3), 413–421. https://doi.org/10.4103/2230-8210.111625

Gupta, V., & Kalra, S. (2011). Choosing a gliptin. *Indian Journal of Endocrinology and Metabolism*, *15*(4), 298–308. https://doi.org/10.4103/2230-8210.85583

Hage, C., Bjerre, M., Frystyk, J., Gu, H. F., Brismar, K., Donal, E., Daubert, J. C., Linde, C., & Lund, L. H. (2018). Comparison of Prognostic Usefulness of Serum Insulin-Like Growth Factor-Binding Protein 7 in Patients With Heart Failure and Preserved Versus Reduced Left Ventricular Ejection Fraction. *American Journal of Cardiology*, *121*(12), 1558–1566. https://doi.org/10.1016/j.amjcard.2018.02.041

Hampel, H., O'Bryant, S. E., Molinuevo, J. L., Zetterberg, H., Masters, C. L., Lista, S., Kiddle, S. J., Batrla, R., & Blennow, K. (2018). Blood-based biomarkers for Alzheimer disease: mapping the road to the clinic. *Nature Reviews. Neurology*, *14*(11), 639–652. https://doi.org/10.1038/s41582-018-0079-7

Hasnan, J., Yusof, M. I., Damitri, T. D., Faridah, A. R., Adenan, A. S., & Norbaini, T. H. (2010). Relationship between apoptotic markers (Bax and bcl-2) and biochemical markers in type 2 diabetes mellitus. *Singapore Medical Journal*, *51*(1), 50–55.

Hernandez-Presa, M., Bustos, C., Ortego, M., Tunon, J., Renedo, G., Ruiz-Ortega, M., & Egido, J. (1997). Angiotensin-converting enzyme inhibition prevents arterial nuclear factor-kappa B activation, monocyte chemoattractant protein-1 expression, and macrophage infiltration in a rabbit model of early accelerated atherosclerosis. *Circulation*, *95*(6), 1532–1541. https://doi.org/10.1161/01.cir.95.6.1532

Hirokawa, S., Shimanuki, T., Kitajima, H., Nishimori, Y., & Shimosaka, M. (2011). Identification of ETFB as a candidate protein that participates in the mechanoregulation of fibroblast cell number in collagen gel culture. *Journal of Dermatological Science*, *64*(2), 119–126. https://doi.org/10.1016/j.jdermsci.2011.08.003

Hishinuma, S., Funamoto, M., Fujio, Y., Kunisada, K., & Yamauchi-Takihara, K. (1999). Hypoxic stress induces cardiotrophin-1 expression in cardiac myocytes. *Biochemical and Biophysical Research Communications*, *264*(2), 436–440. https://doi.org/10.1006/bbrc.1999.1535

Ho, S. K., Wu, Y. W., Tseng, W. K., Leu, H. B., Yin, W. H., Lin, T. H., Chang, K. C., Wang, J. H., Yeh, H. I., Wu, C. C., & Chen, J. W. (2018). The prognostic significance of heart-type fatty acid binding protein in patients with stable coronary heart disease. *Scientific Reports*, *8*(1), 1–7. https://doi.org/10.1038/s41598-018-32210-x

Hou, N., Mai, Y., Qiu, X., Yuan, W., Li, Y., Luo, C., Liu, Y., Zhang, G., Zhao, G., & Luo, J.

D. (2019). Carvacrol attenuates diabetic cardiomyopathy by modulating the PI3K/Akt/GLUT4 pathway in diabetic mice. *Frontiers in Pharmacology*, *10*. https://doi.org/10.3389/fphar.2019.00998

Hu, P., Zhang, D., Swenson, L., Chakrabarti, G., Dale Abel, E., Litwin, S. E., Litwin Min, S. E., & Litwin, S. E. (2003). Minimally invasive aortic banding in mice: effects of altered cardiomyocyte insulin signaling during pressure overload. *Am J Physiol Heart Circ Physiol*, *285*, 1261–1269. https://doi.org/10.1152/ajpheart.00108

Huson, M. A. M., Kaminstein, D., Kahn, D., Belard, S., Ganesh, P., Kandoole-Kabwere, V., Wallrauch, C., Phiri, S., Kreuels, B., & Heller, T. (2019). Cardiac ultrasound in resource-limited settings (CURLS): towards a wider use of basic echo applications in Africa. *The Ultrasound Journal*, *11*(1), 34. https://doi.org/10.1186/s13089-019-0149-0

Huynh, K., Kiriazis, H., Du, X. J., Love, J. E., Jandeleit-Dahm, K. A., Forbes, J. M., McMullen, J. R., & Ritchie, R. H. (2012). Coenzyme Q 10 attenuates diastolic dysfunction, cardiomyocyte hypertrophy and cardiac fibrosis in the db/db mouse model of type 2 diabetes. *Diabetologia*, *55*(5), 1544–1553. https://doi.org/10.1007/s00125-012-2495-3

Hwang, S. J., Lee, H. W., Kim, H. R., Lee, H., Shin, C. H., Yun, S. Il, Lee, D. H., Kim, D. H., Kim, K. K., Joo, K. M., & Kim, H. H. (2016). Ubiquitin-specific protease 4 controls metastatic potential through β-catenin stabilization in brain metastatic lung adenocarcinoma. *Scientific Reports*, *6*(October 2015), 1–13. https://doi.org/10.1038/srep21596

Ingelsson, E., Langenberg, C., Hivert, M. F., Prokopenko, I., Lyssenko, V., Dupuis, J., Mägi, R., Sharp, S., Jackson, A. U., Assimes, T. L., Shrader, P., Knowles, J. W., Zethelius, B., Abbasi, F. A., Bergman, R. N., Bergmann, A., Berne, C., Boehnke, M., Bonnycastle, L. L., … Florez, J. C. (2010). Detailed physiologic characterization reveals diverse mechanisms for novel genetic loci regulating glucose and insulin mefile:///C:/Users/BrandC/Downloads/daniels2010.pdftabolism in humans. *Diabetes*, *59*(5), 1266–1275. https://doi.org/10.2337/db09-1568

Innao, P., Pothisuwan, M., & Pengsa, P. (2016). Does Human Epididymis Protein 4 (HE4) Have a Role in Prediction of Recurrent Epithelial Ovarian Cancer. *Asian Pacific Journal of Cancer Prevention : APJCP*, *17*(9), 4483–4486.

Inzucchi, S. E. (2005). Metformin and Heart Failure. *Diabetes Care*, *28*(10), 2585 LP – 2587. https://doi.org/10.2337/diacare.28.10.2585

Jia, G., Whaley-Connell, A., & Sowers, J. R. (2018). Diabetic cardiomyopathy: a hyperglycaemia- and insulin-resistance-induced heart disease. *Diabetologia*, *61*(1), 21–28. https://doi.org/10.1007/s00125-017-4390-4

Johnson, R., Nxele, X., Cour, M., Sangweni, N., & Jooste, T. (2020). Identification of potential biomarkers for predicting the early onset of diabetic cardiomyopathy in a mouse model. *Nature.Com*. https://www.nature.com/articles/s41598-020-69254-x

Johnston, J. R., Chase, P. B., & Pinto, J. R. (2017). Troponin through the looking-glass: emerging roles beyond regulation of striated muscle contraction. *Oncotarget*, *9*(1), 1461–1482. https://doi.org/10.18632/oncotarget.22879

Jørgensen, P. G., Jensen, M. T., Biering-Sørensen, T., Mogelvang, R., Galatius, S., Fritz-Hansen, T., Rossing, P., Vilsbøll, T., & Jensen, J. S. (2016). Cholesterol remnants and

triglycerides are associated with decreased myocardial function in patients with type 2 diabetes. *Cardiovascular Diabetology*, *15*(1), 137. https://doi.org/10.1186/s12933-016-0454-x

Jørgensen, P. G., Jensen, M. T., Mogelvang, R., von Scholten, B. J., Bech, J., Fritz-Hansen, T., Galatius, S., Biering-Sørensen, T., Andersen, H. U., Vilsbøll, T., Rossing, P., & Jensen, J. S. (2016). Abnormal echocardiography in patients with type 2 diabetes and relation to symptoms and clinical characteristics. *Diabetes & Vascular Disease Research*, *13*(5), 321–330. https://doi.org/10.1177/1479164116645583

Jujić, A., Nilsson, P. M., Engström, G., Hedblad, B., Melander, O., & Magnusson, M. (2014). Atrial natriuretic peptide and type 2 diabetes development - Biomarker and genotype association study. *PLoS ONE*, *9*(2), 1–6. https://doi.org/10.1371/journal.pone.0089201

Kalisz, K., & Rajiah, P. (2017). Computed tomography of cardiomyopathies. *Cardiovascular Diagnosis and Therapy*, *7*(5), 539–556. https://doi.org/10.21037/cdt.2017.09.07

Kaneto, H., Nakatani, Y., Kawamori, D., Miyatsuka, T., & Matsuoka, T. (2004). Involvement of Oxidative Stress and the JNK Pathway in Glucose Toxicity. *The Review of Diabetic Studies*, *1*(4), 165–165. https://doi.org/10.1900/rds.2004.1.165

Kannel, W. B., Hjortland, M., & Castelli, W. P. (1974). Role of diabetes in congestive heart failure: The Framingham study. *The American Journal of Cardiology*, *34*(1), 29–34. https://doi.org/https://doi.org/10.1016/0002-9149(74)90089-7

Kanwar, M., Walter, C., Clarke, M., & Patarroyo-Aponte, M. (2016). Targeting heart failure with preserved ejection fraction: current status and future prospects. *Vascular Health and Risk Management*, *12*, 129. https://doi.org/10.2147/VHRM.S83662

Kaplan, A., Abidi, E., El-Yazbi, A., Eid, A., Booz, G. W., & Zouein, F. A. (2018). Direct cardiovascular impact of SGLT2 inhibitors: mechanisms and effects. *Heart Failure Reviews*, *23*(3), 419–437. https://doi.org/10.1007/s10741-017-9665-9

Karlsson, S. A., Franzén, S., Svensson, A. M., Miftaraj, M., Eliasson, B., & Andersson Sundell, K. (2018). Prescription of lipid-lowering medications for patients with type 2 diabetes mellitus and risk-associated LDL cholesterol: A nationwide study of guideline adherence from the Swedish National Diabetes Register 11 Medical and Health Sciences 1117 Public Hea. *BMC Health Services Research*, *18*(1), 1–10. https://doi.org/10.1186/s12913-018-3707-4

Katholi, R. E., & Couri, D. M. (2011). Left ventricular hypertrophy: major risk factor in patients with hypertension: update and practical clinical applications. *International Journal of Hypertension*, *2011*, 495349. https://doi.org/10.4061/2011/495349

Kemps, H., Kränkel, N., Dörr, M., Moholdt, T., Wilhelm, M., Paneni, F., Serratosa, L., Ekker Solberg, E., Hansen, D., Halle, M., & Guazzi, M. (2019). Exercise training for patients with type 2 diabetes and cardiovascular disease: What to pursue and how to do it. A Position Paper of the European Association of Preventive Cardiology (EAPC). *European Journal of Preventive Cardiology*, *26*(7), 709–727. https://doi.org/10.1177/2047487318820420

Kim, A. H., Jang, J. E., & Han, J. (2022). Current status on the therapeutic strategies for heart failure and diabetic cardiomyopathy. *Biomedicine and Pharmacotherapy*, *145*(September 2021), 112463. https://doi.org/10.1016/j.biopha.2021.112463

Kim, H. Y., & Han, S.-H. (2006). Matrix Metalloproteinases in Cerebral Ischemia. *Journal of Clinical Neurology*, *2*(3), 163. https://doi.org/10.3988/jcn.2006.2.3.163

Kim, M. K., Kim, G., Jang, E. H., Kwon, H. S., Baek, K. H., Oh, K. W., Lee, J. H., Yoon, K.-H., Lee, W. C., & Lee, K. W. (2010). Altered calcium homeostasis is correlated with the presence of metabolic syndrome and diabetes in middle-aged and elderly Korean subjects: the Chungju Metabolic Disease Cohort study (CMC study). *Atherosclerosis*, *212*(2), 674–681.

Kim, Y., Xia, K., Tao, R., Giusti-Rodriguez, P., Vladimirov, V., van den Oord, E., & Sullivan, P. F. (2014). A meta-analysis of gene expression quantitative trait loci in brain. *Translational Psychiatry*, *4*(10), e459. https://doi.org/10.1038/tp.2014.96

King, A. J. F. (2012). The use of animal models in diabetes research. *British Journal of Pharmacology*, *166*(3), 877–894. https://doi.org/10.1111/j.1476-5381.2012.01911.x

Kleinert, M., Clemmensen, C., Hofmann, S. M., Moore, M. C., Renner, S., Woods, S. C., Huypens, P., Beckers, J., De Angelis, M. H., Schürmann, A., Bakhti, M., Klingenspor, M., Heiman, M., Cherrington, A. D., Ristow, M., Lickert, H., Wolf, E., Havel, P. J., Müller, T. D., & Tschöp, M. H. (2018). Animal models of obesity and diabetes mellitus. *Nature Reviews Endocrinology*, *14*(3), 140–162. https://doi.org/10.1038/nrendo.2017.161

Kobayashi, K., Forte, T. M., Taniguchi, S., Ishida, B. Y., Oka, K., & Chan, L. (2000). The db/db mouse, a model for diabetic dyslipidemia: Molecular characterization and effects of western diet feeding. *Metabolism: Clinical and Experimental*, *49*(1), 22–31. https://doi.org/10.1016/S0026-0495(00)90588-2

Kober, K. I., Cano, A., Géraud, C., Sipila, K., Mobasseri, S. A., Philippeos, C., Pisco, A. O., Stannard, A., Martin, A., Salvador, F., Santos, V., Boutros, M., Rognoni, E., & Watt, F. M. (2018). Loxl2 is dispensable for dermal development, homeostasis and tumour stroma formation. *PLoS ONE*, *13*(6), 1–18. https://doi.org/10.1371/journal.pone.0199679

Korkmaz-Icöz, S., Lehner, A., Li, S., Vater, A., Radovits, T., Brune, M., Ruppert, M., Sun, X., Brlecic, P., Zorn, M., Karck, M., & Szabó, G. (2016). Left ventricular pressure-volume measurements and myocardial gene expression profile in type 2 diabetic Goto-Kakizaki rats. *American Journal of Physiology - Heart and Circulatory Physiology*, *311*(4), H958–H971. https://doi.org/10.1152/ajpheart.00956.2015

Korosoglou, G., & Humpert, P. M. (2007). Non-invasive diagnostic imaging techniques as a window into the diabetic heart: a review of experimental and clinical data. *Experimental and Clinical Endocrinology & Diabetes : Official Journal, German Society of Endocrinology [and] German Diabetes Association*, *115*(4), 211–220. https://doi.org/10.1055/s-2007-973083

Koussounadis, A., Langdon, S. P., Um, I. H., Harrison, D. J., & Smith, V. A. (2015). Relationship between differentially expressed mRNA and mRNA-protein correlations in a xenograft model system. *Scientific Reports*, *5*(May), 1–9. https://doi.org/10.1038/srep10775

Kumric, M., Ticinovic Kurir, T., Borovac, J. A., & Bozic, J. (2021). Role of novel biomarkers in diabetic cardiomyopathy. *World Journal of Diabetes*, *12*(6), 685–705. https://doi.org/10.4239/wjd.v12.i6.685

Lee, W.-S., & Kim, J. (2017). Diabetic cardiomyopathy: where we are and where we are going. *The Korean Journal of Internal Medicine*, *32*(3), 404–421. https://doi.org/10.3904/kjim.2016.208

Lee, W.-S., & Kim, J. (2021). Application of Animal Models in Diabetic Cardiomyopathy. *Diabetes & Metabolism Journal*, *45*(2), 129–145. https://doi.org/10.4093/dmj.2020.0285

León, L. E., Rani, S., Fernandez, M., Larico, M., & Calligaris, S. D. (2016). Subclinical detection of diabetic cardiomyopathy with MicroRNAs: Challenges and perspectives. *Journal of Diabetes Research*, *2016*. https://doi.org/10.1155/2016/6143129

Leroith, D. (2002). *B-Cell Dysfunction and Insulin Resistance in Type 2 Diabetes.Pdf*.

Levy, D., Larson, M. G., Vasan, R. S., Kannel, W. B., & Ho, K. K. L. (1996). The Progression From Hypertension to Congestive Heart Failure. *JAMA*, *275*(20), 1557–1562. https://doi.org/10.1001/jama.1996.03530440037034

Li, C. jun, Lv, L., Li, H., & Yu, D. min. (2012). Cardiac fibrosis and dysfunction in experimental diabetic cardiomyopathy are ameliorated by alpha-lipoic acid. *Cardiovascular Diabetology*, *11*, 1–10. https://doi.org/10.1186/1475-2840-11-73

Li, N., Wu, H., Geng, R., & Tang, Q. (2018). Identification of Core Gene Biomarkers in Patients with Diabetic Cardiomyopathy. *Disease Markers*, *2018*. https://doi.org/10.1155/2018/6025061

Li, R., Yang, J., Yang, Y., Ma, N., Jiang, B., Sun, Q., & Li, Y. (2014). Speckle tracking echocardiography in the diagnosis of early left ventricular systolic dysfunction in type II diabetic mice. *BMC Cardiovascular Disorders*, *14*, 141. https://doi.org/10.1186/1471-2261-14-141

Li, Y., & Rosenblit, P. D. (2018). Glucagon-Like Peptide-1 Receptor Agonists and Cardiovascular Risk Reduction in Type 2 Diabetes Mellitus: Is It a Class Effect? *Current Cardiology Reports*, *20*(11), 1–13. https://doi.org/10.1007/s11886-018-1051-2

Lin, J. F., Hsu, S. Y., Teng, M. S., Wu, S., Hsieh, C. A., Jang, S. J., Liu, C. J., Huang, H. L., & Ko, Y. L. (2016). Activin a predicts left ventricular remodeling and mortality in patients with ST-Elevation myocardial infarction. *Acta Cardiologica Sinica*, *32*(4), 420–427. https://doi.org/10.6515/ACS20150415A

Liu, M., He, A., Chu, J., Chen, C., Zhang, S., He, Y., Tao, W., Lu, M., Hua, M., Ju, W., & Fang, Z. (2018). Serum N1-methylnicotinamide is Associated with Left Ventricular Systolic Dysfunction in Chinese. *Scientific Reports*, *8*(1), 1–6. https://doi.org/10.1038/s41598-018-26956-7

Lloyd, D., Vara, R., & Mathur, S. (2017). The Cardiac Manifestations of Inherited Metabolic Diseases in Children. *Wiley Online Library*, *59*(5), 525–529. https://doi.org/10.1111/ped.13272

Loncarevic, B., Trifunovic, D., Soldatovic, I., & Vujisic-Tesic, B. (2016). Silent diabetic cardiomyopathy in everyday practice: a clinical and echocardiographic study. *BMC Cardiovascular Disorders*, *16*(1), 242. https://doi.org/10.1186/s12872-016-0395-z

Lopaschuk, G. D., Ussher, J. R., Folmes, C. D. L., Jaswal, J. S., & Stanley, W. C. (2018). *Myocardial Fatty Acid Metabolism in Health and Disease*. 207–258. https://doi.org/10.1152/physrev.00015.2009.

Lopez-Izquierdo, A., Pereira, R. O., Wende, A. R., Punske, B. B., Dale Abel, E., & Tristani-Firouzi, M. (2014). The absence of insulin signaling in the heart induces changes in potassium channel expression and ventricular repolarization. *American Journal of Physiology - Heart and Circulatory Physiology*, *306*(5), 747–754. https://doi.org/10.1152/AJPHEART.00849.2013/ASSET/IMAGES/LARGE/ZH400514 10450008.JPEG

Lorenzo-Almorós, A., Tuñón, J., Orejas, M., Cortés, M., Egido, J., & Lorenzo. (2017). Diagnostic approaches for diabetic cardiomyopathy. *Cardiovascular Diabetology*, *16*(1), 1–14. https://doi.org/10.1186/s12933-017-0506-x

Lorenzo, O., Ramírez, E., Picatoste, B., Egido, J., & Tuñón, J. (2013). Alteration of energy substrates and ROS production in diabetic cardiomyopathy. *Mediators of Inflammation*, *2013*. https://doi.org/10.1155/2013/461967

Lui, T. T. H., Lacroix, C., Ahmed, S. M., Goldenberg, S. J., Leach, C. A., Daulat, A. M., & Angers, S. (2011). The Ubiquitin-Specific Protease USP34 Regulates Axin Stability and Wnt/ -Catenin Signaling. *Molecular and Cellular Biology*, *31*(10), 2053–2065. https://doi.org/10.1128/mcb.01094-10

Maleki, M., Vakilian, F., & Amin, A. (2011). Liver diseases in heart failure. *Heart Asia*, *3*(1), 143–149. https://doi.org/10.1136/heartasia-2011-010023

Maric, C. (2010). Risk factors for cardiovascular disease in women with diabetes. *Gender Medicine*, *7*(6), 551–556. https://doi.org/10.1016/j.genm.2010.11.007

Marín-García, J. (2016). Cell death in the pathogenesis and progression of heart failure. *Heart Failure Reviews*, *21*(2), 117–121. https://doi.org/10.1007/s10741-016-9538-7

Masiha, S., Sundström, J., & Lind, L. (2013). Inflammatory markers are associated with left ventricular hypertrophy and diastolic dysfunction in a population-based sample of elderly men and women. *Journal of Human Hypertension*, *27*(1), 13–17. https://doi.org/10.1038/jhh.2011.113

Maya, L., & Villarreal, F. J. (2010). Diagnostic approaches for diabetic cardiomyopathy and myocardial fibrosis. *Journal of Molecular and Cellular Cardiology*, *48*(3), 524–529. https://doi.org/10.1016/j.yjmcc.2009.06.021

McCullough, A. J. (2004). The clinical features, diagnosis and natural history of nonalcoholic fatty liver disease. *Clinics in Liver Disease*, *8*(3), 521–533, viii. https://doi.org/10.1016/j.cld.2004.04.004

Meijers, W. C., van der Velde, A. R., & de Boer, R. A. (2016). Biomarkers in heart failure with preserved ejection fraction. *Netherlands Heart Journal : Monthly Journal of the Netherlands Society of Cardiology and the Netherlands Heart Foundation*, *24*(4), 252–258. https://doi.org/10.1007/s12471-016-0817-7

Mercer, T., Chang, A. C., Fischer, L., Gardner, A., Kerubo, I., Tran, D. N., Laktabai, J., & Pastakia, S. (2019). Mitigating The Burden Of Diabetes In Sub-Saharan Africa Through An Integrated Diagonal Health Systems Approach. *Diabetes, Metabolic Syndrome and Obesity : Targets and Therapy*, *12*, 2261–2272. https://doi.org/10.2147/DMSO.S207427

Moore, C. C., McVeigh, E. R., & Zerhouni, E. A. (2000). Quantitative tagged magnetic resonance imaging of the normal human left ventricle. *Topics in Magnetic Resonance Imaging : TMRI*, *11*(6), 359–371. https://doi.org/10.1097/00002142-200012000-00005

Mori, J., Patel, V. B., Alrob, O. A., Basu, R., Altamimi, T., DesAulniers, J., Wagg, C. S., Kassiri, Z., Lopaschuk, G. D., & Oudit, G. Y. (2014). Angiotensin 1-7 ameliorates diabetic cardiomyopathy and diastolic dysfunction in db/db mice by reducing lipotoxicity and inflammation. *Circulation: Heart Failure*, *7*(2), 327–339. https://doi.org/10.1161/CIRCHEARTFAILURE.113.000672

Mudunuri, U., Che, A., Yi, M., & Stephens, R. M. (2009). bioDBnet: The biological database network. *Bioinformatics*, *25*(4), 555–556. https://doi.org/10.1093/bioinformatics/btn654

Murarka, S., & Movahed, M. R. (2010). Diabetic cardiomyopathy. *Journal of Cardiac Failure*, *16*(12), 971–979. https://doi.org/10.1016/j.cardfail.2010.07.249

Nagy, B. J., Krasznai, Z. T., Balla, H., Csobán, M., Antal-Szalmás, P., Hernádi, Z., & Kappelmayer, J. (2012). Elevated human epididymis protein 4 concentrations in chronic kidney disease. *Annals of Clinical Biochemistry*, *49*(Pt 4), 377–380. https://doi.org/10.1258/acb.2011.011258

Naito, Y., Tsujino, T., Lee-Kawabata, M., Matsumoto, M., Ezumi, A., Nakao, S., Goda, A., Ohyanagi, M., & Masuyama, T. (2009). Matrix metalloproteinase-1 and -2 levels are differently regulated in acute exacerbation of heart failure in patients with and without left ventricular systolic dysfunction. *Heart and Vessels*, *24*(3), 181–186. https://doi.org/10.1007/s00380-008-1100-7

Nakagawa, Y., Nishikimi, T., & Kuwahara, K. (2018). Peptides Atrial and brain natriuretic peptides : Hormones secreted from the heart. *Peptides*, *February*, 1–8. https://doi.org/10.1016/j.peptides.2018.05.012

Neumann, P., Jaé, N., Knau, A., Glaser, S. F., Fouani, Y., Rossbach, O., Krüger, M., John, D., Bindereif, A., Grote, P., Boon, R. A., & Dimmeler, S. (2018). The lncRNA GATA6-AS epigenetically regulates endothelial gene expression via interaction with LOXL2. *Nature Communications*, *9*(1). https://doi.org/10.1038/s41467-017-02431-1

Nirengi, S., Peres Valgas da Silva, C., & Stanford, K. I. (2020). Disruption of energy utilization in diabetic cardiomyopathy; a mini review. *Current Opinion in Pharmacology*, *54*, 82–90. https://doi.org/https://doi.org/10.1016/j.coph.2020.08.015

Nishida, K., & Otsu, K. (2017). Inflammation andmetabolic cardiomyopathy. *Cardiovascular Research*, *113*(4), 389–398. https://doi.org/10.1093/cvr/cvx012

Nishikimi, T., Maeda, N., & Matsuoka, H. (2006). The role of natriuretic peptides in cardioprotection. *Cardiovascular Research*, *69*(2), 318–328. https://doi.org/10.1016/j.cardiores.2005.10.001

Nishimura, R. A., & Tajik, A. J. (1997). Evaluation of diastolic filling of left ventricle in health and disease: Doppler echocardiography is the clinician's Rosetta Stone. *Journal of the American College of Cardiology*, *30*(1), 8–18. https://doi.org/10.1016/s0735-1097(97)00144-7

Nkum, B. C., Micah, F. B., Ankrah, T. C., & Nyan, O. (2014). Left Ventricular Hypertrophy and Insulin Resistance in Adults from an Urban Community in the Gambia: Cross-Sectional Study. *PLOS ONE*, *9*(4), e93606. https://doi.org/10.1371/journal.pone.0093606

Nunes, S., Soares, E., Fernandes, J., Viana, S., Carvalho, E., Pereira, F. C., & Reis, F. (2013). Early cardiac changes in a rat model of prediabetes: Brain natriuretic peptide

overexpression seems to be the best marker. *Cardiovascular Diabetology*, *12*(1), 44. https://doi.org/10.1186/1475-2840-12-44

Nunes, S., Soares, E., Pereira, F., & Reis, F. (2012). The role of inflammation in diabetic cardiomyopathy. *International Journal of Interferon, Cytokine and Mediator Research*, *4*(1), 59–73. https://doi.org/10.2147/IJICMR.S21679

Oh, E., Kim, J. Y., Sung, D., Cho, Y., Lee, N., An, H., Kim, Y. J., Cho, T. M., & Seo, J. H. (2017). Inhibition of ubiquitin-specific protease 34 (USP34) induces epithelial-mesenchymal transition and promotes stemness in mammary epithelial cells. *Cellular Signalling*, *36*(January), 230–239. https://doi.org/10.1016/j.cellsig.2017.05.009

Oktay, A. A., Rich, J. D., & Shah, S. J. (2013). The emerging epidemic of heart failure with preserved ejection fraction. *Current Heart Failure Reports*, *10*(4), 401–410. https://doi.org/10.1007/s11897-013-0155-7

Olejarz, W., Łacheta, D., & Kubiak-Tomaszewska, G. (2020). Matrix Metalloproteinases as Biomarkers of Atherosclerotic Plaque Instability. *International Journal of Molecular Sciences*, *21*(11), 3946.

Ota, T., Suzuki, Y., Nishikawa, T., Otsuki, T., Sugiyama, T., Irie, R., Wakamatsu, A., Hayashi, K., Sato, H., Nagai, K., Kimura, K., Makita, H., Sekine, M., Obayashi, M., Nishi, T., Shibahara, T., Tanaka, T., Ishii, S., Yamamoto, J. ichi, … Sugano, S. (2004). Complete sequencing and characterization of 21,243 full-length human cDNAs. *Nature Genetics*, *36*(1), 40–45. https://doi.org/10.1038/ng1285

Ottolia, M., Torres, N., Bridge, J. H. B., Philipson, K. D., & Goldhaber, J. I. (2013). Na/Ca exchange and contraction of the heart. *Journal of Molecular and Cellular Cardiology*, *61*, 28–33. https://doi.org/10.1016/j.yjmcc.2013.06.001

Owan, T. E., Hodge, D. O., Herges, R. M., Jacobsen, S. J., Roger, V. L., & Redfield, M. M. (2006). Trends in Prevalence and Outcome of Heart Failure with Preserved Ejection Fraction. *New England Journal of Medicine*, *355*(3), 251–259. https://doi.org/10.1056/nejmoa052256

Packer, M. (2020). SGLT2 inhibitors produce cardiorenal benefits by promoting adaptive cellular reprogramming to induce a state of fasting mimicry: a paradigm shift in understanding their mechanism of action. *Diabetes Care*, *43*(3), 508–511.

Pandey, N. K., Karki, P., Shah, P., & Lamsal, M. (2021). Role of NT-proBNP in Detection of Left Ventricular Diastolic Dysfunction in Asymptomatic Type 2 Diabetes Patients with Preserved Ejection Fraction: A Cross-sectional Study. *Journal of BP Koirala Institute of Health Sciences*, *4*(1), 20–25.

Papazafiropoulou, A., & Tentolouris, N. (2009). Matrix metalloproteinases and cardiovascular diseases. *Hippokratia*, *13*(2), 76–82. https://pubmed.ncbi.nlm.nih.gov/19561775

Pappachan, J. M., Varughese, G. I., Sriraman, R., & Arunagirinathan, G. (2013). Diabetic cardiomyopathy: Pathophysiology, diagnostic evaluation and management. *World Journal of Diabetes*, *4*(5), 177–189. https://doi.org/10.4239/wjd.v4.i5.177

Paulus, W. J., & Dal Canto, E. (2018). Distinct Myocardial Targets for Diabetes Therapy in Heart Failure With Preserved or Reduced Ejection Fraction. *JACC: Heart Failure*, *6*(1), 1–7. https://doi.org/10.1016/j.jchf.2017.07.012

Perl, K., Ushakov, K., Pozniak, Y., Yizhar-Barnea, O., Bhonker, Y., Shivatzki, S., Geiger, T., Avraham, K. B., & Shamir, R. (2017). Reduced changes in protein compared to mRNA levels across non-proliferating tissues. *BMC Genomics*, *18*(1), 1–14. https://doi.org/10.1186/s12864-017-3683-9

Philis-Tsimikas, A., Chang, A., & Miller, L. (2011). Precision, accuracy, and user acceptance of the OneTouch SelectSimple blood glucose monitoring system. *Journal of Diabetes Science and Technology*, *5*(6), 1602–1609. https://doi.org/10.1177/193229681100500638

Phillip, J. M., Aifuwa, I., Walston, J., & Wirtz, D. (2015). The Mechanobiology of Aging. *Annual Review of Biomedical Engineering*, *17*(1), 113–141. https://doi.org/10.1146/annurev-bioeng-071114-040829

Piek, A., Du, W., de Boer, R. A., & Silljé, H. H. W. (2018). Novel heart failure biomarkers: why do we fail to exploit their potential? *Critical Reviews in Clinical Laboratory Sciences*, *55*(4), 246–263. https://doi.org/10.1080/10408363.2018.1460576

Piek, A., Meijers, W. C., Schroten, N. F., Gansevoort, R. T., de Boer, R. A., & Silljé, H. H. W. (2017). HE4 Serum Levels Are Associated with Heart Failure Severity in Patients With Chronic Heart Failure. *Journal of Cardiac Failure*, *23*(1), 12–19. https://doi.org/https://doi.org/10.1016/j.cardfail.2016.05.002

Plante, E., Menaouar, A., Danalache, B. A., Yip, D., Broderick, T. L., Chiasson, J. L., Jankowski, M., & Gutkowska, J. (2015). Oxytocin treatment prevents the cardiomyopathy observed in obese diabetic male db/db mice. *Endocrinology*, *156*(4), 1416–1428. https://doi.org/10.1210/en.2014-1718

Powell, S. R., Herrmann, J., Lerman, A., Patterson, C., & Wang, X. (2012). The ubiquitin-proteasome system and cardiovascular disease. In *Progress in Molecular Biology and Translational Science* (Vol. 109). https://doi.org/10.1016/B978-0-12-397863-9.00009-2

Przybytkowski, E., Davis, T., Hosny, A., Eismann, J., Matulonis, U. A., Wulf, G. M., & Nabavi, S. (2020). An immune-centric exploration of BRCA1 and BRCA2 germline mutation related breast and ovarian cancers. *BMC Cancer*, *20*(1), 197. https://doi.org/10.1186/s12885-020-6605-1

Rainer, J., Sanchez-cabo, F., Stocker, G., Sturn, A., & Trajanoski, Z. (2006). *CARMAweb : comprehensive R- and bioconductor- based web service for microarray data analysis*. *34*, 498–503. https://doi.org/10.1093/nar/gkl038

Raizada, A., Bhandari, S., Khan, M. A., Singh, H. V., Thomas, S., Sarabhai, V., Singh, N., & Trehan, N. (2007). Brain type natriuretic peptide (BNP)—A marker of new millennium in diagnosis of congestive heart failure. *Indian Journal of Clinical Biochemistry*, *22*(1), 4–9. https://doi.org/10.1007/BF02912873

Ren, X. M., Zuo, G. F., Wu, W., Luo, J., Ye, P., Chen, S. L., & Hu, Z. (2016). Atorvastatin alleviates experimental diabetic cardiomyopathy by regulating the GSK-3β-PP2Ac-NF-κB signaling axis. *PLoS ONE*, *11*(11), 1–22. https://doi.org/10.1371/journal.pone.0166740

Riehle, C., & Bauersachs, J. (2019). Of mice and men: models and mechanisms of diabetic cardiomyopathy. *Basic Research in Cardiology*, *114*(1), 1–22. https://doi.org/10.1007/s00395-018-0711-0

Rigden, D. J., & Fernández, X. M. (2018). The 2018 Nucleic Acids Research database issue and the online molecular biology database collection. *Nucleic Acids Research*, *46*(D1), D1–D7. https://doi.org/10.1093/nar/gkx1235

Rodeheffer, R. J., & Chen, H. H. (2008). *The Prevalence of Diabetic Cardiomyopathy: A Population Based Study in Olmsted County, MN*. *42*(2), 157–162. https://doi.org/10.1037/a0030561.Striving

Rodríguez, C., & Martínez-González, J. (2019). The Role of Lysyl Oxidase Enzymes in Cardiac Function and Remodeling. *Cells*, *8*(12). https://doi.org/10.3390/cells8121483

Rosano, G. M., Vitale, C., & Seferovic, P. (2017). Heart Failure in Patients with Diabetes Mellitus. *Cardiac Failure Review*, *3*(1), 52. https://doi.org/10.15420/CFR.2016:20:2

Ruiz-Pinto, S., Pita, G., Martín, M., Alonso-Gordoa, T., Barnes, D. R., Alonso, M. R., Herraez, B., García-Miguel, P., Alonso, J., Pérez-Martínez, A., Cartón, A. J., Gutiérrez-Larraya, F., García-Sáenz, J. A., Benítez, J., Easton, D. F., Patiño-García, A., & González-Neira, A. (2018). Exome array analysis identifies ETFB as a novel susceptibility gene for anthracycline-induced cardiotoxicity in cancer patients. *Breast Cancer Research and Treatment*, *167*(1), 249–256. https://doi.org/10.1007/s10549-017-4497-9

Rustici, G., Kolesnikov, N., Brandizi, M., Burdett, T., Dylag, M., Emam, I., Farne, A., Hastings, E., Ison, J., Keays, M., Kurbatova, N., Malone, J., Mani, R., Mupo, A., Pereira, R. P., Pilicheva, E., Rung, J., Sharma, A., Tang, Y. A., … Sarkans, U. (2013). ArrayExpress update-trends in database growth and links to data analysis tools. *Nucleic Acids Research*, *41*(D1), 987–990. https://doi.org/10.1093/nar/gks1174

Sághy, É., Vörös, I., Ágg, B., Kiss, B., Koncsos, G., Varga, Z. V., Görbe, A., Giricz, Z., Schulz, R., & Ferdinandy, P. (2020). Cardiac miRNA expression and their mRNA targets in a rat model of prediabetes. *International Journal of Molecular Sciences*, *21*(6). https://doi.org/10.3390/ijms21062128

Sakai, N., Nakamura, M., Lipson, K. E., Miyake, T., Kamikawa, Y., Sagara, A., Shinozaki, Y., Kitajima, S., Toyama, T., Hara, A., Iwata, Y., Shimizu, M., Furuichi, K., Kaneko, S., Tager, A. M., & Wada, T. (2017). Inhibition of CTGF ameliorates peritoneal fibrosis through suppression of fibroblast and myofibroblast accumulation and angiogenesis. *Scientific Reports*, *7*(1), 1–13. https://doi.org/10.1038/s41598-017-05624-2

Saunders, J., Mathewkutty, S., Drazner, M. H., & McGuire, D. K. (2008). Cardiomyopathy in type 2 diabetes: Update on pathophysiological mechanisms. *Herz*, *33*(3), 184–190. https://doi.org/10.1007/s00059-008-3115-3

Savarese, G., & Lund, L. H. (2017). Global Public Health Burden of Heart Failure. *Cardiac Failure Review*, *03*(01), 7. https://doi.org/10.15420/cfr.2016:25:2

Schieffer, B., Luchtefeld, M., Braun, S., Hilfiker, A., Hilfiker-Kleiner, D., & Drexler, H. (2000). Role of NAD(P)H oxidase in angiotensin II-induced JAK/STAT signaling and cytokine induction. *Circulation Research*, *87*(12), 1195–1201. https://doi.org/10.1161/01.res.87.12.1195

Schilling, J. D., & Mann, D. L. (2012). Diabetic Cardiomyopathy: Bench to Bedside. *Heart Failure Clinics*, *8*(4), 619–631. https://doi.org/10.1016/j.hfc.2012.06.007

Schillinger, W., Fiolet, J. W., Schlotthauer, K., & Hasenfuss, G. (2003). Relevance of Na+–

Ca2+ exchange in heart failure. *Cardiovascular Research*, *57*(4), 921–933. https://doi.org/10.1016/S0008-6363(02)00826-X

Semeniuk, L. M., Kryski, A. J., & Severson, D. L. (2002). Echocardiographic assessment of cardiac function in diabetic db/db and transgenic db/db-hGLUT4 mice. *American Journal of Physiology - Heart and Circulatory Physiology*, *283*(3 52-3), 976–982. https://doi.org/10.1152/ajpheart.00088.2002

Semizarov, D., Frost, L., Sarthy, A., Kroeger, P., Halbert, D. N., & Fesik, S. W. (2003). Specificity of short interfering RNA determined through gene expression signatures. *Proceedings of the National Academy of Sciences of the United States of America*, *100*(11), 6347–6352. https://doi.org/10.1073/pnas.1131959100

Sena, S., Rasmussen, I. R., Wende, A. R., McQueen, A. P., Theobald, H. A., Wilde, N., Pereira, R. O., Litwin, S. E., Berger, J. P., & Abel, E. D. (2007). Cardiac hypertrophy caused by peroxisome proliferator-activated receptor-γ agonist treatment occurs independently of changes in myocardial insulin signaling. *Endocrinology*, *148*(12), 6047–6053. https://doi.org/10.1210/en.2006-1559

Shah, R. V, Abbasi, S. A., & Kwong, R. Y. (2014). Role of cardiac MRI in diabetes. *Current Cardiology Reports*, *16*(2), 449. https://doi.org/10.1007/s11886-013-0449-0

Shaver, A., Nichols, A., Thompson, E., Mallick, A., Payne, K., Jones, C., Manne, N. D. P. K., Sundaram, S., Shapiro, J. I., & Sodhi, K. (2016). Role of serum biomarkers in early detection of diabetic cardiomyopathy in the West Virginian population. *International Journal of Medical Sciences*, *13*(3), 161–168. https://doi.org/10.7150/ijms.14141

Shida, T., Nozawa, T., Sobajima, M., Ihori, H., Matsuki, A., & Inoue, H. (2014). Fluvastatin-induced reduction of oxidative stress ameliorates diabetic cardiomyopathy in association with improving coronary microvasculature. *Heart and Vessels*, *29*(4), 532–541. https://doi.org/10.1007/s00380-013-0402-6

Silverman, D. N., Plante, T. B., Infeld, M., Callas, P. W., Juraschek, S. P., Dougherty, G. B., & Meyer, M. (2019). Association of β-Blocker Use With Heart Failure Hospitalizations and Cardiovascular Disease Mortality Among Patients With Heart Failure With a Preserved Ejection Fraction: A Secondary Analysis of the TOPCAT Trial. *JAMA Network Open*, *2*(12), e1916598–e1916598. https://doi.org/10.1001/JAMANETWORKOPEN.2019.16598

Sivitz, W. I., & Yorek, M. A. (2010). Mitochondrial dysfunction in diabetes: From molecular mechanisms to functional significance and therapeutic opportunities. *Antioxidants and Redox Signaling*, *12*(4), 537–577. https://doi.org/10.1089/ars.2009.2531

Solomon, S. D., McMurray, J. J. V., Anand, I. S., Ge, J., Lam, C. S. P., Maggioni, A. P., Martinez, F., Packer, M., Pfeffer, M. A., Pieske, B., Redfield, M. M., Rouleau, J. L., van Veldhuisen, D. J., Zannad, F., Zile, M. R., Desai, A. S., Claggett, B., Jhund, P. S., Boytsov, S. A., … Lefkowitz, M. P. (2019). Angiotensin–Neprilysin Inhibition in Heart Failure with Preserved Ejection Fraction. *New England Journal of Medicine*, *381*(17), 1609–1620. https://doi.org/10.1056/nejmoa1908655

Solskov, L., Løfgren, B., Kristiansen, S. B., Jessen, N., Pold, R., Nielsen, T. T., Bøtker, H. E., Schmitz, O., & Lund, S. (2008). Metformin induces cardioprotection against ischaemia/reperfusion injury in the rat heart 24 hours after administration. *Basic & Clinical Pharmacology & Toxicology*, *103*(1), 82–87.

Stanley, W. C., Recchia, F. A., & Lopaschuk, G. D. (2005). Myocardial substrate metabolism in the normal and failing heart. *Physiological Reviews*, *85*(3), 1093–1129. https://doi.org/10.1152/physrev.00006.2004

Stepanova, M., & Younossi, Z. M. (2012). Independent Association Between Nonalcoholic Fatty Liver Disease and Cardiovascular Disease in the US Population. *Clinical Gastroenterology and Hepatology*, *10*(6), 646–650. https://doi.org/10.1016/j.cgh.2011.12.039

Steppan, J., Wang, H., Bergman, Y., Rauer, M. J., Tan, S., Jandu, S., Nandakumar, K., Barreto-Ortiz, S., Cole, R. N., Boronina, T. N., Zhu, W., Halushka, M. K., An, S. S., Berkowitz, D. E., & Santhanam, L. (2019). Lysyl oxidase-like 2 depletion is protective in age-associated vascular stiffening. *American Journal of Physiology - Heart and Circulatory Physiology*, *317*(1), H49–H59. https://doi.org/10.1152/ajpheart.00670.2018

Strawbridge, R. J., & van Zuydam, N. R. (2018). Shared Genetic Contribution of Type 2 Diabetes and Cardiovascular Disease: Implications for Prognosis and Treatment. *Current Diabetes Reports*, *18*(8), 7–10. https://doi.org/10.1007/s11892-018-1021-5

Striepe, K., Jumar, A., Ott, C., Karg, M. V, Schneider, M. P., Kannenkeril, D., & Schmieder, R. E. (2017). Effects of the Selective Sodium-Glucose Cotransporter 2 Inhibitor Empagliflozin on Vascular Function and Central Hemodynamics in Patients With Type 2 Diabetes Mellitus. In *Circulation* (Vol. 136, Issue 12, pp. 1167–1169). https://doi.org/10.1161/CIRCULATIONAHA.117.029529

Strimbu, K., & Tavel, J. A. (2010). What are biomarkers? *Current Opinion in HIV and AIDS*, *5*(6), 463–466. https://doi.org/10.1097/COH.0b013e32833ed177

Sudo, Y., Sasaki, A., Wakabayashi, T., Numakura, C., & Hayasaka, K. (2015). DATA REPORT A novel ETFB mutation in a patient with glutaric aciduria type II. *Nature Publishing Group*. https://doi.org/10.1038/hgv.2015.16

Suresh, K., Abarna Devi, S., Badrinath, A. K., Suresh Babu, S., & Nagalingam, S. (2018). Diagnostic utility of heart type fatty acid binding protein (H-FABP) versus cardiac troponin I in myocardial infarction. *Int J Adv Med*, *5*, 514–519.

Suthahar, N., Meijers, W. C., Brouwers, F. P., Heerspink, H. J. L., Gansevoort, R. T., van der Harst, P., Bakker, S. J. L., & de Boer, R. A. (2018). Heart failure and inflammation-related biomarkers as predictors of new-onset diabetes in the general population. *International Journal of Cardiology*, *250*, 188–194. https://doi.org/10.1016/j.ijcard.2017.10.035

Sy, S. M. H., Jiang, J., O, W. S., Deng, Y., & Huen, M. S. Y. (2013). The ubiquitin specific protease USP34 promotes ubiquitin signaling at DNA double-strand breaks. *Nucleic Acids Research*, *41*(18), 8572–8580. https://doi.org/10.1093/nar/gkt622

Szot, J. O., Cuny, H., Blue, G. M., Humphreys, D. T., Ip, E., Harrison, K., Sholler, G. F., Giannoulatou, E., Leo, P., Duncan, E. L., Sparrow, D. B., Ho, J. W. K., Graham, R. M., Pachter, N., Chapman, G., Winlaw, D. S., & Dunwoodie, S. L. (2018). A Screening Approach to Identify Clinically Actionable Variants Causing Congenital Heart Disease in Exome Data. *Circulation. Genomic and Precision Medicine*, *11*(3), e001978. https://doi.org/10.1161/CIRCGEN.117.001978

Takahashi, Y., Soejima, Y., Fukusato, T., & Profes-Sor, A. (2012). Animal models of nonalcoholic fatty liver disease/ nonalcoholic steatohepatitis. *World J Gastroenterol*, *18*.

https://doi.org/10.3748/wjg.v18.i19.2300

Targher, G., Bertolini, L., Padovani, R., Rodella, S., Tessari, R., Zenari, L., Day, C., & Arcaro, G. (2007). Prevalence of nonalcoholic fatty liver disease and its association with cardiovascular disease among type 2 diabetic patients. *Diabetes Care*, *30*(5), 1212–1218. https://doi.org/10.2337/dc06-2247

Targher, G., Bertolini, L., Poli, F., Rodella, S., Scala, L., Tessari, R., Zenari, L., & Falezza, G. (2005). Nonalcoholic Fatty Liver Disease and Risk of Future Cardiovascular Events Among Type 2 Diabetic Patients. *Diabetes*, *54*(12), 3541 LP – 3546. https://doi.org/10.2337/diabetes.54.12.3541

Tate, M., Prakoso, D., Willis, A. M., Peng, C., Deo, M., Qin, C. X., Walsh, J. L., Nash, D. M., Cohen, C. D., Rofe, A. K., Sharma, A., Kiriazis, H., Donner, D. G., De Haan, J. B., Watson, A. M. D., De Blasio, M. J., & Ritchie, R. H. (2019). Characterising an Alternative Murine Model of Diabetic Cardiomyopathy . *Frontiers in Physiology* , *10*, 1395. https://doi.org/10.3389/fphys.2019.01395

Toedebusch, R., Belenchia, A., & Pulakat, L. (2018). Diabetic Cardiomyopathy: Impact of Biological Sex on Disease Development and Molecular Signatures. *Frontiers in Physiology*, *9*(MAY), 453. https://doi.org/10.3389/fphys.2018.00453

Torun, D., Ozelsancak, R., Yiğit, F., & Micozkadıoğlu, H. (2012). Increased inflammatory markers are associated with obesity and not with target organ damage in newly diagnosed untreated essential hypertensive patients. *Clinical and Experimental Hypertension (New York, N.Y. : 1993)*, *34*(3), 171–175. https://doi.org/10.3109/10641963.2011.577489

Tsuchida, S., Satoh, M., Takiwaki, M., & Nomura, F. (2018). Current Status of Proteomic Technologies for Discovering and Identifying Gingival Crevicular Fluid Biomarkers for Periodontal Disease. *International Journal of Molecular Sciences*, *20*(1), 86. https://doi.org/10.3390/ijms20010086

Tsujimoto, T., Sugiyama, T., Shapiro, M. F., Noda, M., & Kajio, H. (2017). Risk of Cardiovascular Events in Patients with Diabetes Mellitus on β-Blockers. *Hypertension*, *70*(1), 103–110. https://doi.org/10.1161/HYPERTENSIONAHA.117.09259

Ungvari, Z., & Csiszar, A. (2012). The emerging role of IGF-1 deficiency in cardiovascular aging: Recent advances. *Journals of Gerontology - Series A Biological Sciences and Medical Sciences*, *67 A*(6), 599–610. https://doi.org/10.1093/gerona/gls072

Van De Weijer, T., Schrauwen-Hinderling, V. B., & Schrauwen, P. (2011). Lipotoxicity in type 2 diabetic cardiomyopathy. *Cardiovascular Research*, *92*(1), 10–18. https://doi.org/10.1093/cvr/cvr212

Varughese, J. F., Chalovich, J. M., & Lit, Y. (2010). Molecular Dynamics Studies on Troponin (Tnl-TnT-TnC) Complexes: Insight into the Regulation of Muscle Contraction. *Journal of Biomolecular Structure and Dynamics*, *28*(2), 159–173. https://doi.org/10.1080/07391102.2010.10507350

Venardos, K., De Jong, K. A., Elkamie, M., Connor, T., & McGee, S. L. (2015). The PKD inhibitor CID755673 enhances cardiac function in diabetic db/db mice. *PLoS ONE*, *10*(3), 1–14. https://doi.org/10.1371/journal.pone.0120934

Ventura-Clapier, R., Garnier, A., & Veksler, V. (2008). Transcriptional control of

mitochondrial biogenesis: The central role of PGC-1α. *Cardiovascular Research*, *79*(2), 208–217. https://doi.org/10.1093/cvr/cvn098

Verhagen, H. J., de Leeuw, D. C., Roemer, M. G., Denkers, F., Pouwels, W., Rutten, A., Celie, P. H., Ossenkoppele, G. J., Schuurhuis, G. J., & Smit, L. (2014). IGFBP7 induces apoptosis of acute myeloid leukemia cells and synergizes with chemotherapy in suppression of leukemia cell survival. *Cell Death & Disease*, *5*(6), e1300. https://doi.org/10.1038/cddis.2014.268

Verma, S., & McMurray, J. J. V. (2018). SGLT2 inhibitors and mechanisms of cardiovascular benefit: a state-of-the-art review. *Diabetologia*, *61*(10), 2108–2117. https://doi.org/10.1007/s00125-018-4670-7

Vettor, R., & Conci, S. (2017). Obesity Pathogenesis. In P. Sbraccia & N. Finer (Eds.), *Obesity: Pathogenesis, Diagnosis, and Treatment* (pp. 1–21). Springer International Publishing. https://doi.org/10.1007/978-3-319-47685-8_14-1

Vikhorev, P. G., & Vikhoreva, N. N. (2018). Cardiomyopathies and Related Changes in Contractility of Human Heart Muscle. *International Journal of Molecular Sciences*, *19*(8). https://doi.org/10.3390/ijms19082234

Wachter, R., Shah, S. J., Cowie, M. R., Szecsödy, P., Shi, V., Ibram, G., Zhao, Z., Gong, J., Klebs, S., & Pieske, B. (2020). Angiotensin receptor neprilysin inhibition versus individualized RAAS blockade: design and rationale of the PARALLAX trial. *ESC Heart Failure*, *7*(3), 856–864. https://doi.org/10.1002/EHF2.12694

Walsh, M. F., Nathanson, K. L., Couch, F. J., & Offit, K. (2016). Genomic Biomarkers for Breast Cancer Risk. *Advances in Experimental Medicine and Biology*, *882*, 1–32. https://doi.org/10.1007/978-3-319-22909-6_1

Wang, B., Chandrasekera, P. C., & Pippin, J. J. (2014). Leptin-and Leptin Receptor-Deficient Rodent Models: Relevance for Human Type 2 Diabetes. *Current Diabetes Reviews*, *10*(2), 131–144.

Wang, C. Y., Li, X. D., Hao, Z. H., & Xu, D. (2016). Insulin-like growth factor-1 improves diabetic cardiomyopathy through antioxidative and anti-inflammatory processes along with modulation of Akt/GSK-3β signaling in rats. *The Korean Journal of Physiology & Pharmacology : Official Journal of the Korean Physiological Society and the Korean Society of Pharmacology*, *20*(6), 613–619. https://doi.org/10.4196/kjpp.2016.20.6.613

Wang, S., Wang, B., Wang, Y., Tong, Q., Liu, Q., Sun, J., Zheng, Y., & Cai, L. (2017). Zinc prevents the development of diabetic cardiomyopathy in db/db mice. *International Journal of Molecular Sciences*, *18*(3). https://doi.org/10.3390/ijms18030580

Wang, Y., Zhou, R., Lu, C., Chen, Q., Xu, T., & Li, D. (2019). Effects of the angiotensin-receptor neprilysin inhibitor on cardiac reverse remodeling: Meta-analysis. *Journal of the American Heart Association*, *8*(13). https://doi.org/10.1161/JAHA.119.012272

Watanabe, T., Konii, H., & Sato, K. (2018). Emerging Roles of Cardiotrophin-1 in the Pathogenesis and Biomarker of Atherosclerosis. *J—Multidisciplinary Scientific Journal*, *1*(1), 94–105.

Way, K. J., Isshiki, K., Suzuma, K., Yokota, T., Zvagelsky, D., Schoen, F. J., Sandusky, G. E., Pechous, P. A., Vlahos, C. J., Wakasaki, H., & King, G. L. (2002). Expression of connective tissue growth factor is increased in injured myocardium associated with

protein kinase C β2 activation and diabetes. *Diabetes*, *51*(9), 2709–2718. https://doi.org/10.2337/diabetes.51.9.2709

Webber, S. (2021). International Diabetes Federation. In *Diabetes Research and Clinical Practice* (Vol. 102, Issue 2). https://doi.org/10.1016/j.diabres.2013.10.013

Westermann, D., Rutschow, S., Van Linthout, S., Linderer, A., Bücker-Gärtner, C., Sobirey, M., Riad, A., Pauschinger, M., Schultheiss, H. P., & Tschöpe, C. (2006). Inhibition of p38 mitogen-activated protein kinase attenuates left ventricular dysfunction by mediating pro-inflammatory cardiac cytokine levels in a mouse model of diabetes mellitus. *Diabetologia*, *49*(10), 2507–2513. https://doi.org/10.1007/s00125-006-0385-2

Westermann, Dirk, Rutschow, S., Jäger, S., Linderer, A., Anker, S., Riad, A., Unger, T., Schultheiss, H. P., Pauschinger, M., & Tschöpe, C. (2007). Contributions of inflammation and cardiac matrix metalloproteinase activity to cardiac failure in diabetic cardiomyopathy: The role of angiotensin type 1 receptor antagonism. *Diabetes*, *56*(3), 641–646. https://doi.org/10.2337/db06-1163

Whittington, H. J., Hall, A. R., McLaughlin, C. P., Hausenloy, D. J., Yellon, D. M., & Mocanu, M. M. (2013). Chronic Metformin Associated Cardioprotection Against Infarction: Not Just a Glucose Lowering Phenomenon. *Cardiovascular Drugs and Therapy*, *27*(1), 5–16. https://doi.org/10.1007/s10557-012-6425-x

Wichi, R., Malfitano, C., Rosa, K., De Souza, S. B., Salemi, V., Mostarda, C., De Angelis, K., & Irigoyen, M. C. (2007). Noninvasive and invasive evaluation of cardiac dysfunction in experimental diabetes in rodents. *Cardiovascular Diabetology*, *6*, 14. https://doi.org/10.1186/1475-2840-6-14

Widya, R. L., van der Meer, R. W., Smit, J. W. A., Rijzewijk, L. J., Diamant, M., Bax, J. J., de Roos, A., & Lamb, H. J. (2013). Right ventricular involvement in diabetic cardiomyopathy. *Diabetes Care*, *36*(2), 457–462. https://doi.org/10.2337/dc12-0474

World Health Organisation. (2021). *Cardiovascular diseases (CVDs)*. World Health Organisation. https://www.who.int/news-room/fact-sheets/detail/cardiovascular-diseases-(cvds)

Wu, H., Wu, M., Chen, Y., Allan, C. A., Phillips, D. J., & Hedger, M. P. (2012). Correlation between blood activin levels and clinical parameters of type 2 diabetes. *Experimental Diabetes Research*, *2012*, 410579. https://doi.org/10.1155/2012/410579

Xanthopoulos, A., Starling, R. C., Kitai, T., & Triposkiadis, F. (2019). Heart Failure and Liver Disease: Cardiohepatic Interactions. In *JACC: Heart Failure* (Vol. 7, Issue 2, pp. 87–97). Elsevier Inc. https://doi.org/10.1016/j.jchf.2018.10.007

Xu, J., Nie, H., Zhang, X., Tian, Y., & Yu, B. (n.d.). Down-regulated energy metabolism genes associated with mitochondria oxidative phosphorylation and fatty acid metabolism in viral cardiomyopathy mouse heart. *Molecular Biology Reports*. Retrieved September 12, 2020, from https://link.springer.com/content/pdf/10.1007/s11033-010-0519-y.pdf

Yamamoto, D., & Takai, S. (2009). Pharmacological implications of MMP-9 inhibition by ACE inhibitors. *Current Medicinal Chemistry*, *16*(11), 1349–1354. https://doi.org/10.2174/092986709787846514

Yan, L. J. (2014). Pathogenesis of chronic hyperglycemia: From reductive stress to oxidative stress. *Journal of Diabetes Research*, *2014*. https://doi.org/10.1155/2014/137919

Yang, J., Savvatis, K., Kang, J. S., Fan, P., Zhong, H., Schwartz, K., Barry, V., Mikels-Vigdal, A., Karpinski, S., Kornyeyev, D., Adamkewicz, J., Feng, X., Zhou, Q., Shang, C., Kumar, P., Phan, D., Kasner, M., López, B., Diez, J., … Chang, C. P. (2016). Targeting LOXL2 for cardiac interstitial fibrosis and heart failure treatment. *Nature Communications*, *7*. https://doi.org/10.1038/ncomms13710

Yu, C. J., Liang, C., Li, Y. X., Hu, Q. Q., Zheng, W. W., Niu, N., Yang, X., Wang, Z. R., Yu, X. Di, Zhang, B. L., Song, B. L., & Zhang, Z. R. (2017). ZNF307 (Zinc Finger Protein 307) Acts as a Negative Regulator of Pressure Overload-Induced Cardiac Hypertrophy. *Hypertension*, *69*(4), 615–624. https://doi.org/10.1161/HYPERTENSIONAHA.116.08500

Yu, T., Sheu, S.-S., Robotham, J. L., & Yoon, Y. (2008). Mitochondrial fission mediates high glucose-induced cell death through elevated production of reactive oxygen species. *Cardiovascular Research*, *79*(2), 341–351. https://doi.org/10.1093/cvr/cvn104

Yu, X. Y., Chen, H. M., Liang, J. L., Lin, Q. X., Tan, H. H., Fu, Y. H., Liu, X. Y., Shan, Z. X., Li, X. H., Yang, H. Z., Yang, M., Li, Y., & Lin, S. G. (2011). Hyperglycemic myocardial damage is mediated by proinflammatory cytokine: Macrophage migration inhibitory factor. *PLoS ONE*, *6*(1). https://doi.org/10.1371/journal.pone.0016239

Yusuf, S., Pfeffer, M. A., Swedberg, K., Granger, C. B., Held, P., McMurray, J. J. V., Michelson, E. L., Olofsson, B., & Östergren, J. (2003). Effects of candesartan in patients with chronic heart failure and preserved left-ventricular ejection fraction: The CHARM-preserved trial. *Lancet*, *362*(9386), 777–781. https://doi.org/10.1016/S0140-6736(03)14285-7

Yuyun, M. F., Sliwa, K., Kengne, A. P., Mocumbi, A. O., & Bukhman, G. (2020). Cardiovascular Diseases in Sub-Saharan Africa Compared to High-Income Countries: An Epidemiological Perspective. *Global Heart*, *15*(1), 15. https://doi.org/10.5334/gh.403

Zhan, X. H., Jiao, J. W., Zhang, H. F., Li, C. Q., Zhao, J. M., Liao, L. Di, Wu, J. Y., Wu, B. L., Wu, Z. Y., Wang, S. H., Du, Z. P., Shen, J. H., Zou, H. Y., Neufeld, G., Xu, L. Y., & Li, E. M. (2017). A three-gene signature from protein–protein interaction network of LOXL2- and actin-related proteins for esophageal squamous cell carcinoma prognosis. *Cancer Medicine*, *6*(7), 1707–1719. https://doi.org/10.1002/cam4.1096

Zhang, M., Yuan, L., Yao, F., Cao, P., Rong, J., Zhang, B., & Su, J. (2018). Human epididymis protein 4 concentration is not associated with liver fibrosis and cirrhosis in a case control study. *Clinica Chimica Acta; International Journal of Clinical Chemistry*, *484*, 213–217. https://doi.org/10.1016/j.cca.2018.05.051

Zhao, J., Cao, T. T., Tian, J., Chen, H. H., Zhang, C., Wei, H. C., Guo, W., & Lu, R. (2016). Shengmai San Ameliorates Myocardial Dysfunction and Fibrosis in Diabetic db/db Mice. *Evidence-Based Complementary and Alternative Medicine*, *2016*. https://doi.org/10.1155/2016/4621235

Zhao, Q., Yang, Y., Wang, C., Hou, Y., & Chen, H. (2016). ATP5B and ETFB metabolic markers in children with congenital hydronephrosis. *Molecular Medicine Reports*, *14*(6), 5111–5115. https://doi.org/10.3892/mmr.2016.5914

Zhao, S., Tian, Y., Zhang, W., Xing, X., Li, T., Liu, H., Huang, T., Ning, Y., Zhao, H., & Chen, Z. J. (2015). An association study between USP34 and polycystic ovary

syndrome. *Journal of Ovarian Research*, *8*(1), 1–5. https://doi.org/10.1186/s13048-015-0158-y

Zhao, Yingming, Tang, K., Tianbao, X., Wang, J., Yang, J., & Li, D. (2017). Increased serum lysyl oxidase-like 2 levels correlate with the degree of left atrial fibrosis in patients with atrial fibrillation. *Bioscience Reports*, *37*(6). https://doi.org/10.1042/BSR20171332

Zhao, Yunyue, Li, S., Quan, E., Zhang, H., Wu, Y., Luo, Y., Peng, L., Wang, J., Zhu, J., & Liu, J. (2019). Trimetazidine inhibits cardiac fibrosis by reducing reactive oxygen species and downregulating connective tissue growth factor in streptozotocin-induced diabetic rats. *Experimental and Therapeutic Medicine*, *18*(2), 1477. https://doi.org/10.3892/etm.2019.7705

Zheng, Y., Ley, S. H., & Hu, F. B. (2018). Global aetiology and epidemiology of type 2 diabetes mellitus and its complications. *Nature Reviews Endocrinology*, *14*(2), 88–98. https://doi.org/10.1038/nrendo.2017.151

Zhou, Y. T., Grayburn, P., Karim, A., Shimabukuro, M., Higa, M., Baetens, D., Orci, L., & Unger, R. H. (2000). Lipotoxic heart disease in obese rats: Implications for human obesity. *Proceedings of the National Academy of Sciences of the United States of America*, *97*(4), 1784–1789. https://doi.org/10.1073/pnas.97.4.1784

Zile, M. R., & Brutsaert, D. L. (2002). New concepts in diastolic dysfunction and diastolic heart failure: Part I: diagnosis, prognosis, and measurements of diastolic function. *Circulation*, *105*(11), 1387–1393. https://doi.org/10.1161/hc1102.105289

Appendix

Table A1: Reagents and Chemicals

Chemical/Reagent	Catalogue number	Company
ATP ViaLight assay kit	LT27-008	Lonza, Walkersville, MD, USA
Cell counting chamber slides	C10228	Life Technologies Corporation, Carlsbad, CA, USA
Cell lysis Buffer	FNN0011	Life Technologies Corporation, Carlsbad, CA, USA
Chloroform	136112-00-0	Sigma-Aldrich, St Louis, MO, USA
Palmitic acid ≥99%	P0500-10G	Sigma-Aldrich, St Louis, MO, USA
Coomassie blue stain	161-0437	Bio-Rad, Hercules, CA, USA
Insulin solution human	SLBH1094	Sigma-Aldrich, St Louis, MO, USA
Cryotubes	430659	Corning, MA, USA
DeadEnd coulometric TUNEL system	PRG3250	Promega, Madison, Wilsconsin, USA
Dimethyl sulfoxide (DMSO)	276855	Sigma-Aldrich, St Louis, MO, USA
Dulbecco`s modified Eagle`s medium (DMEM) with phenol red	B12-604F	Lonza, Walkersville, MD, USA
Dulbecco`s modified Eagle`s medium (DMEM) without phenol red	B12-917F	Lonza, Walkersville, MD, USA
Dulbecco's phosphate buffered saline (DPBS)	B17-513F	Lonza, Walkersville, MD, USA
Ethanol	2875	Sigma-Aldrich , St Louis, MO, USA

Foetal bovine serum	BC/S0615-HI	Lonza, Walkersville, MD, USA
Hybond-P PVDF Membrane	RNP1416F	Amersham
Iso-propanol	I9516	Sigma-Aldrich , St Louis, MO, USA
Methanol	1070182511	Merck, Whitehouse Station, NJ, USA
Fat-free milk powder	N/A	Clover, Johannesburg, SA
Paraformaldehyde	158127	Sigma-Aldrich , St Louis, MO, USA
Penicillin-streptomycin mixture	DE17-602E	Lonza, Walkersville, MD, USA
Phenylmethanesulfonylfluoride fluoride (PMSF)	11206893001	Roche, Basel, Switzerland
Ponceau S Stain	P23295	Sigma-Aldrich, St Louis, MO, USA
Propidium iodide	P4170	Sigma-Aldrich , St Louis, MO, USA
Protease Inhibitors	11206893001	Roche, Basel, Switzerland
Qiazol	79306	Qiagen, Hilden, Germany
RNase free water	Am9937	Ambion, Austin, TX, USA
Running buffer SDS	161-0772	Bio-Rad, Hercules, CA, USA
SDS-PAGE gels	161-0993	Bio-Rad, Hercules, CA, USA
Sodium bicarbonate (NaHCO3)	M2645	Sigma-Aldrich , St Louis, MO, USA
Sodium hydroxide (NaOH)	109140	Merck, Whitehouse Station, NJ, USA
Stainless steel beads 5mm	69989	Qiagen, Hilden, Germany
Sterile TC water	59900C	Lonza, Walkersville, MD, USA
SYBR Green mix	4385612	Applied Biosystems, Foster City, CA, USA

Tris-base	93352	Sigma-Aldrich , St Louis, MO, USA
Trypan blue	15050-065	Invitrogen, Carlsbad, CA, USA
Trypsin	17-161F	Lonza, Walkersville, MD, USA
Tween 20	58980C	Sigma-Aldrich , St Louis, MO, USA
Restore plus Western blot stripping buffer	46430	Thermo Fisher Scientific, Waltham, MA, USA

Table A2: Consumables

Consumables	**Catalogue number**	**Company**
0. 2 PCR tubes, flat cap	AX/PCR-02-C/S	Axgyen, Corning, NY
0.5 mL Eppendorf safe-lock tubes	0030 123.301	Eppendorf, Hamburg, Germany
1.5 mL Eppendorf safe- lock tubes	0030 123.328	Eppendorf, Hamburg, Germany
2 mL Eppendorf safe- lock tubes	0030 123. 344	Eppendorf, Hamburg, Germany
15 mL centrifuge tubes	602072	NEST Biotechnology, Jiangsu China Wuxi
50 mL centrifuge tubes	601001	NEST Biotechnology, Jiangsu China Wuxi
CELLBIND 24- well plates	3337	Corning, MA, USA
CELLBIND 6- well plates	3335	Corning, MA, USA
CELLBIND 96-well clear plates	3300	Corning, MA, USA
Cryotubes	430659	Corning, MA, USA
Filter Pads	23385	Sigma-Aldrich , St Louis, MO, USA
T75 Flasks	658975	Greiner bio-one, Frickenhausen, Germany

Table A3: Experimental kits

Experimental kits	Catalogue no	Company
ViaLight ATP assay kit	LT27-008	Lonza, Walkersville, MD, USA
Bio-Rad RC DC protein kit	500-0201	Bio-Rad, Hercules, CA, USA
DeadEnd Fluorometric TUNEL system	G3250	Promega, Madison, Wilsconsin, USA
High Capacity cDNA kit	PN 4375575	Applied biosystem, Foster City, CA, USA
Turbo DNase kit	AM1907	Ambion, Austin, TX, USA
RNeasy mini kit	74106	Qiagen, Hilden, Germany
Clarity Western ECL substrate	1705060	Bio-Rad, Hercules, CA, USA

Table A4 List of antibodies

Antibody	Dilution	% Gel	Cat #	Company
Primary				
LOXL2	1: 500	10	AB96233	Biocom Africa
ETFβ	1:500	10	AB104944	Biocom Africa
β-Actin	1: 1 000	10	Sc-47778	Santa Cruz
Secondary				
Donkey anti-mouse IgG-HRP	1: 4 000	-	Sc-23181	Santa Cruz
Donkey anti-rabbit IgG-HRP	1: 4 000	-	Sc-2012	Santa Cruz

Table A5: Equipment

Equipment	Product Number	Supplier
Agilent Bioanalyzer	G2946-90004	Agilent Technologies, Santa Clara, California
CountessTM Automated Cell Counter	C10227	Invitrogen, Carlsbad, CA, USA
D1200-230V Heating block	S62927099	Labnet, Adison,NJ,USA

IKA® MS 3 digital shakers	IKA 331900X	Sigma-Aldrich , St Louis, MO, USA
Benchtop Centrifuge	SL16R	Thermo Fisher Scientific, Waltham, MA, USA
Micro-centrifuge	001977	Eppendorf, Hamburg, Germany
Mini Protean casting frame	165-3304	Bio-Rad, Hercules, CA, USA
Mini Protean casting stand	165-3303	Bio-Rad, Hercules, CA, USA
Mini Protein tetra cell	165-8030	Bio-Rad, Hercules, CA, USA
Mini Trans-blot cell	170-4070	Bio-Rad, Hercules, CA, USA
NanoDrop™1000 Spectrophotometer	A984	Thermo Fisher Scientific, Waltham, MA, USA
Orbital shaker ITPSIC 10	20197	Torrey pines Scientific
PowerPac HC	165-8025	Bio-Rad, Hercules, CA, USA
TissueLyser	85300	Qiagen, Hilden, Germany
ABI 7500 Real time PCR system	4351104	Applied Biosystem, Foster City, CA, USA
2720 Thermal cycler	4413750	Applied Biosystem, Foster City, CA, USA
Nikon Eclipse Ti inverted microscope	Ti inverted	Nikon, Tokyo, Japan
Biotek® FLX 800 plate reader	FLX 800	BioTek Instruments Inc., Winooski, VT, USA
BioTek® ELX800 plate reader	ELX800	BioTek Instruments Inc., Winooski, VT, USA
Orbital shaker	20197	Stoval life Science

Table A6: Platforms and search-terms used within ArrayExpress to identify datasets related to T2DM and CVD

	T2DM	CVD
Search terms used	"diabetic cardiomyopathy", "diabetic heart", "left ventricular hypertrophy", "diabetes mellitus" and "type 2 diabetes mellitus"	"heart", "heart failure", "heart left ventricle", "diastolic dysfunction", "left ventricular dysfunction"
Datasets	GSE23561, GSE40234, GSE29231, GSE13760, GSE38642, GSE29221, GSE21340, E-CBIL-28, E-MEXP1270, E-MEXP2559, E-MTAB2854	GSE 26887, GSE1869, GSE5406, GSE43435, GSE21125, GSE9128, E-TABM-480
Platforms	Affymetrix: E-CBIL-28, E-MEXP1270, E-MEXP2559, E-MTAB2854 Agilent: GSE23561, GSE40234, GSE29231, GSE13760, GSE38642, GSE29221, GSE21340	Affymetrix: E-TABM-480 Agilent: GSE 26887, GSE1869, GSE5406, GSE43435, GSE21125, GSE9128

Table A7: Gene list

Gene name	Abbreviation	Wilcoxon score
ubiquitin specific peptidase 34	Usp34	4.22E-07
zinc finger with KRAB and SCAN domains 4	Zkscan4	1.30E-06
Lysyl oxidase like 2	LoxL2	3.26E-06
insulin like growth factor 1	Igf1	5.08E-06

electron transfer flavoprotein subunit beta	Etfβ	5.65E-06
amyloid beta precursor protein binding family A member 3	Apba3	7.73E-06
BCL2 like 1	Bcl2l1	8.25E-06
REV1, DNA directed polymerase	Rev1	1.09E-05
diphthamide biosynthesis 1	Dph1	1.16E-05
ATP binding cassette subfamily D member 4	Abcd4	1.63E-05
phosphodiesterase 2A	Pde2a	1.88E-05
protein O-glucosyltransferase 1	Poglut1	2.38E-05
coatomer protein complex subunit zeta 2	Copz2	2.75E-05
collectin subfamily member 11	Colec11	3.08E-05
proteasome 26S subunit, non-ATPase 7	Psmd7	3.43E-05
solute carrier family 35-member E1	Slc35e1	6.61E-05
dystrophin	Dmd	7.14E-05
neuronal vesicle trafficking associated 1	Nsg1	8.62E-05
sphingosine-1-phosphate receptor 5	S1pr5	8.91E-05
solute carrier family 16 member 1	Slc16a1	9.89E-05
family with sequence similarity 13-member B	Fam13b	1.05E-04
FK506 binding protein 9 pseudogene 1	Fkbp9p1	1.25E-04
malignant fibrous histiocytoma amplified sequence 1	Mfhas1	1.50E-04
C-X-C motif chemokine ligand 12	Cxcl12	1.79E-04
proteasome 26S subunit, non-ATPase 1	Psmd1	1.80E-04
beta-1,4-galactosyltransferase 5	B4galt5	1.92E-04
OS9, endoplasmic reticulum lectin	Os9	1.97E-04
coiled-coil domain containing 177	Ccdc177	2.05E-04
pleiotrophin	Ptn	2.09E-04
thrombospondin 4	Thbs4	2.21E-04
SPT16 homolog, facilitates chromatin remodelling subunit	Supt16h	2.62E-04
fatty acid desaturase 2	Fads2	2.65E-04

glycosyltransferase like domain containing 1	Gtdc1	2.68E-04
ecto-NOX disulphide-thiol exchanger 1	Enox1	2.72E-04
MCTS1, re-initiation and release factor	Mcts1	2.74E-04
stathmin 1	Stmn1	2.77E-04
regucalcin	Rgn	2.87E-04
immunoglobulin superfamily containing leucine rich repeat	Islr	3.28E-04
von Willebrand factor A domain containing 1	Vwa1	3.30E-04
CDC42 binding protein kinase beta	Cdc42bpb	3.37E-04
mercaptopyruvate sulfurtransferase	Mpst	3.57E-04
sirtuin 5	Sirt5	3.74E-04
PERP, TP53 apoptosis effector	Perp	3.97E-04
ATP binding cassette subfamily C member 4	Abcc4	4.32E-04
zinc finger protein 688	Znf688	4.32E-04
RIO kinase 3	Riok3	5.46E-04
fibroblast growth factor 5	Fgf5	5.52E-04
engrailed homeobox 2	En2	5.88E-04
VPS26 endosomal protein sorting factor C	Vps26c	5.94E-04
vinculin	Vcl	6.35E-04
SURP and G-patch domain containing 2	Sugp2	6.45E-04
isochorismatase domain containing 2	Isoc2	6.80E-04
kelch like family member 20	Klhl20	6.80E-04
cyclin dependent kinase 12	Cdk12	7.31E-04
La ribonucleoprotein domain family member 7	Larp7	7.38E-04
carboxypeptidase A3	Cpa3	7.54E-04
ATM serine/threonine kinase	Atm	8.79E-04
heterogeneous nuclear ribonucleoprotein D like	Hnrnpdl	9.31E-04
glycosylphosphatidylinositol anchored molecule like	Gml	9.31E-04
epoxide hydrolase 2	Ephx2	9.60E-04

lipoprotein lipase	Lpl	1.03E-03
growth arrest specific 2	Gas2	1.08E-03
polo like kinase 2	Plk2	1.22E-03
ribosomal protein L14	Rpl14	1.26E-03
GTP binding protein 1	Gtpbp1	1.44E-03
metadherin	Mtdh	1.45E-03
IQ motif and Sec7 domain 2	Iqsec2	1.46E-03
alcohol dehydrogenase 6 (class V)	Adh6	1.51E-03
VPS53, GARP complex subunit	Vps53	1.51E-03
vesicle associated membrane protein 1	Vamp1	1.63E-03
CCR4-NOT transcription complex subunit 6	Cnot6	1.63E-03
serine and arginine rich splicing factor 8	Srsf8	1.68E-03
NLR family member X1	Nlrx1	1.74E-03
latent transforming growth factor beta binding protein 4	Ltbp4	1.85E-03
cysteine rich C-terminal 1	Crct1	1.94E-03
golgi SNAP receptor complex member 2	Gosr2	2.01E-03
breast cancer metastasis suppressor 1	Brms1	2.11E-03
CDV3 homolog	Cdv3	2.12E-03
carbonic anhydrase 2	Ca2	2.13E-03
EH domain containing 2	Ehd2	2.18E-03
cryptochrome circadian regulator 2	Cry2	2.29E-03
mex-3 RNA binding family member D	Mex3d	2.45E-03
SFT2 domain containing 2	Sft2d2	2.68E-03
dedicator of cytokinesis 4	Dock4	2.79E-03
widely interspaced zinc finger motifs	Wiz	3.17E-03
CYLD lysine 63 deubiquitinase	Cyld	3.17E-03
tubulin beta 4A class IVa	Tubb4a	3.41E-03
glucocorticoid modulatory element binding protein 2	Gmeb2	3.56E-03

DEAD-box helicase 18	Ddx18	4.11E-03
lysophosphatidylcholine acyltransferase 1	Lpcat1	4.40E-03
DNA methyltransferase 1	Dnmt1	4.42E-03
integrator complex subunit 1	Ints1	4.44E-03
checkpoint with forkhead and ring finger domains	Chfr	4.46E-03
poly(A) specific ribonuclease subunit PAN2	Pan2	4.64E-03
family with sequence similarity 45-member A	Fam45a	4.64E-03
terminal nucleotidyltransferase 5C	Tent5c	4.73E-03
sphingosine-1-phosphate lyase 1	Sgpl1	4.82E-03
perilipin 3	Plin3	4.94E-03
formin binding protein 1	Fnbp1	4.99E-03
inhibitor of DNA binding 1, HLH protein	Id1	5.01E-03
zinc finger homeobox 4	Zfhx4	5.21E-03
Rho guanine nucleotide exchange factor 15	Arhgef15	5.57E-03
growth differentiation factor 10	Gdf10	5.63E-03
vascular endothelial growth factor D	Vegfd	5.79E-03
phosphatidylethanolamine binding protein 1	Pebp1	5.87E-03
tyrosyl-tRNA synthetase	Yars	5.96E-03
retrotransposon Gag like 10	Rtl10	6.37E-03
tRNA methyltransferase 13 homolog	Trmt13	6.40E-03
proline rich and Gla domain 4	Prrg4	6.43E-03
regulator of microtubule dynamics 1	Rmdn1	6.59E-03
ATP synthase mitochondrial F1 complex assembly factor 2	Atpaf2	6.78E-03
cyclin dependent kinase inhibitor 2A	Cdkn2a	7.01E-03
NIMA related kinase 9	Nek9	7.15E-03
H2A histone family member Z	H2afz	7.18E-03
OTU deubiquitinase 4	Otud4	7.50E-03
yrdC N6-threonylcarbamoyltransferase domain containing	Yrdc	7.60E-03

glycophorin A (MNS blood group)	Gypa	7.75E-03
MCF.2 cell line derived transforming sequence like	Mcf2l	7.79E-03
CREB/ATF bZIP transcription factor	Crebzf	8.09E-03
protein phosphatase 4 regulatory subunit 3A	Ppp4r3a	8.13E-03
tumor suppressor candidate 3	Tusc3	8.17E-03
karyopherin subunit beta 1	Kpnb1	8.28E-03
solute carrier family 26 member 6	Slc26a6	8.40E-03
TTK protein kinase	Ttk	8.44E-03
butyrophilin subfamily 3 member A1	Btn3a1	8.44E-03
LSM3 homolog, U6 small nuclear RNA and mRNA degradation associated	Lsm3	8.60E-03
beta-secretase 1	Bace1	8.69E-03
ras homolog family member T1	Rhot1	8.81E-03
ciliary neurotrophic factor receptor	Cntfr	8.81E-03
G3BP stress granule assembly factor 2	G3bp2	8.89E-03
H2A histone family member X	H2afx	9.50E-03
ST3 beta-galactoside alpha-2,3-sialyltransferase 1	St3gal1	9.59E-03
DEAH-box helicase 40	Dhx40	9.68E-03
TP73 antisense RNA 1	Tp73-as1	9.77E-03
cyclase associated actin cytoskeleton regulatory protein 1	Cap1	9.82E-03
EWS RNA binding protein 1	Ewsr1	1.02E-02
solute carrier family 14 member 2	Slc14a2	1.03E-02
ribosomal protein S6 kinase B1	Rps6kb1	1.04E-02
fibrillin 1	Fbn1	1.04E-02
Fc fragment of IgM receptor	Fcmr	1.06E-02
transglutaminase 1	Tgm1	1.07E-02
cyclin T1	Ccnt1	1.08E-02
zinc finger protein 646	Znf646	1.16E-02

cell division cycle 25B	Cdc25b	1.20E-02
A-kinase anchoring protein 8	Akap8	1.22E-02
tetratricopeptide repeat domain 13	Ttc13	1.24E-02
oxytocin/neurophysin I prepropeptide	Oxt	1.25E-02
granulin precursor	Grn	1.27E-02
CREB regulated transcription coactivator 1	Crtc1	1.30E-02
armadillo repeat containing X-linked 4	Armcx4	1.36E-02
paired like homeobox 2a	Phox2a	1.37E-02
nucleolar protein 3	Nol3	1.38E-02
TRAF3 interacting protein 2	Traf3ip2	1.41E-02
teneurin transmembrane protein 4	Tenm4	1.43E-02
hes related family bHLH transcription factor with YRPW motif 1	Hey1	1.52E-02
cilia and flagella associated protein 298	Cfap298	1.52E-02
peptidylprolyl isomerase C	Ppic	1.54E-02
androgen receptor	Ar	1.59E-02
glutaredoxin	Glrx	1.61E-02
WD repeat domain 33	Wdr33	1.61E-02
KAT8 regulatory NSL complex subunit 2	Kansl2	1.63E-02
homeodomain interacting protein kinase 1	Hipk1	1.63E-02
ADP ribosylation factor like GTPase 3	Arl3	1.65E-02
regulation of nuclear pre-mRNA domain containing 2	Rprd2	1.67E-02
replication timing regulatory factor 1	Rif1	1.77E-02
POM121 transmembrane nucleoporin	Pom121	1.78E-02
fibromodulin	Fmod	1.82E-02
CDC like kinase 4	Clk4	1.86E-02
tumor protein D52 like 1	Tpd52l1	1.89E-02
malic enzyme 3	Me3	2.00E-02
glycolipid transfer protein	Gltp	2.01E-02

solute carrier family 47 member 1	Slc47a1	2.03E-02
mitochondrial ribosomal protein L58	Mrpl58	2.06E-02
RAN guanine nucleotide release factor	Rangrf	2.10E-02
AFDN divergent transcript	Afdn-dt	2.15E-02
tripartite motif containing 23	Trim23	2.20E-02
protein inhibitor of activated STAT 4	Pias4	2.39E-02
early growth response 3	Egr3	2.44E-02
SERTA domain containing 2	Sertad2	2.45E-02
mitochondrial ribosomal protein L16	Mrpl16	2.49E-02
nitric oxide synthase 2	Nos2	2.51E-02
down-regulator of transcription 1	Dr1	2.58E-02
serine and arginine rich splicing factor 1	Srsf1	2.70E-02
zinc finger protein 250	Znf250	2.71E-02
asporin	Aspn	2.74E-02
NADH:ubiquinone oxidoreductase complex assembly factor 3	Ndufaf3	2.75E-02
bone morphogenetic protein 4	Bmp4	2.75E-02
PDZ domain containing 7	Pdzd7	2.80E-02
muscle RAS oncogene homolog	Mras	2.82E-02
promyelocytic leukaemia	Pml	2.82E-02
LDL receptor related protein associated protein 1	Lrpap1	2.93E-02
ALG8, alpha-1,3-glucosyltransferase	Alg8	2.95E-02
stromal cell derived factor 4	Sdf4	3.05E-02
tectonic family member 3	Tctn3	3.06E-02
CD320 molecule	Cd320	3.06E-02
G protein-coupled receptor 4	Gpr4	3.13E-02
ribosomal oxygenase 2	Riox2	3.19E-02
copine 3	Cpne3	3.20E-02
coiled-coil domain containing 85B	Ccdc85b	3.23E-02

ring finger protein 130	Rnf130	3.28E-02
leucine rich repeat containing 20	Lrrc20	3.35E-02
mannose phosphate isomerase	Mpi	3.37E-02
nucleolar protein 7	Nol7	3.52E-02
proteasome 26S subunit, non-ATPase 3	Psmd3	3.54E-02
ubiquitin specific peptidase 9 X-linked	Usp9x	3.55E-02
G protein subunit beta 1	Gnb1	3.62E-02
dedicator of cytokinesis 5	Dock5	3.63E-02
ARP2 actin related protein 2 homolog	Actr2	3.68E-02
glycerophosphodiester phosphodiesterase domain containing 5	Gdpd5	3.68E-02
NMDA receptor synaptonuclear signaling and neuronal migration factor	Nsmf	3.70E-02
poly(ADP-ribose) polymerase family member 8	Parp8	3.70E-02
Rac/Cdc42 guanine nucleotide exchange factor 6	Arhgef6	3.87E-02
PHD finger protein 20 like 1	Phf20l1	3.87E-02
ATPase phospholipid transporting 11B (putative)	Atp11b	3.97E-02
ring finger and WD repeat domain 3	Rfwd3	3.97E-02
ribosomal L24 domain containing 1	Rsl24d1	3.99E-02
RNA polymerase II subunit L	Polr2l	4.08E-02
paired box 8	Pax8	4.19E-02
putative homeodomain transcription factor 1	Phtf1	4.28E-02
leucine rich repeats and immunoglobulin like domains 2	Lrig2	4.34E-02
tRNA methyltransferase 12 homolog	Trmt12	4.36E-02
nicotinamide nucleotide adenylyltransferase 2	Nmnat2	4.42E-02
NADH:ubiquinone oxidoreductase core subunit S1	Ndufs1	4.48E-02
frataxin	Fxn	4.66E-02
UPF2, regulator of nonsense mediated mRNA decay	Upf2	4.66E-02
forkhead box D3	Foxd3	4.80E-02
transcription factor AP-2 alpha	Tfap2a	5.00E-02

nucleoporin 210	Nup210	5.00E-02

APPENDIX B PREPARATION OF REAGENTS

I. Preparation of DMEM: Stored at 4°C in 50 mL tubes

500mL of DMEM with phenol red and glutamate was supplemented with;

- 50 mL of FBS (Final FBS concentration of 10%)
- 5.5mL of pen-strep (Final concentration of 1%)

II. Preparation of treatment media: Stored at 4°C in 50 mL tubes

- 33 mM glucose containing; 1000 mg/L DMEM powder and 1 % BSA
- 5.5 mM glucose containing: 1000 mg/L DMEM powder and 1 % BSA

III. Preparation of 10x Tris-buffered saline (TBS) wash buffer: Stored at 4°C

The 10x TBS wash buffer was prepared by dissolving:

- 200 mM of Tris (24.22 g)
- 1.37 mM NaCl (80.06 g)
- Topped up with distilled to a total volume of 1L.

IV. 1X TBS and Tween 20 (1X TBST-20): Stored at 4°C

1X TBST-20 was prepared by added:

- 100 mL of 10 x TBST
- 900 mL of distilled water (v/v)
- 1 mL Tween 20

V. Transfer buffer for Western Blot

The buffer was prepared by adding:

- 25 mM of Tris (3.03 g)
- 192 mM glycine (14.4 g)
- 800 mL of distilled water,
- 200mL of methanol to make up a total volume of 1L.